2024

Extensions Of The Standard Model With Improved Ultraviolet Behavior

Mikayla Anderson
College of William and Mary - Arts & Sciences, mikkieranderson@gmail.com

Follow this and additional works at: https://scholarworks.wm.edu/etd

Part of the Physics Commons

Extensions of the Standard Model with Improved Ultraviolet Behavior

Mikayla Roumayne Anderson

Anchorage, Alaska

Master of Science, William & Mary, 2022
Bachelor of Science, University of Washington, 2019

A Dissertation presented to the Graduate Faculty of
The College of William and Mary in Virginia in Candidacy for the Degree of
Doctor of Philosophy

Department of Physics

The College of William and Mary in Virginia
August, 2024

APPROVAL PAGE
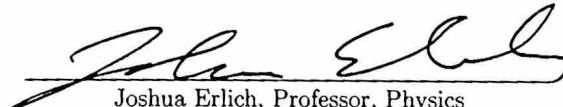
This Dissertation is submitted in partial fulfillment of
the requirements for the degree of

Doctor of Philosophy

Mikayla R Anderson

Mikayla Roumayne Anderson

Approved by the Committee, August 2024

Committee Chair
Christopher Carone, Professor, Physics
College of William & Mary

Joshua Erlich, Professor, Physics
College of William & Mary

Justin Stevens, Associate Professor, Physics
College of William & Mary

Andrew Jackura, Assistant Professor, Physics
College of William & Mary

Jose Goity, Professor, Physics
Hampton University

ABSTRACT

Although general relativity and the standard model have proved incredibly consistent at all currently accessible energy scales, they are not expected to accurately describe natu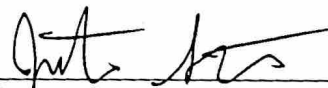re at all scales; we know there is new physics to be discovered at higher energy scales (shorter distances). The nonrenormalizability of gravity prohibits a predictive quantum field theory description, unless the infinite parameter space needed to absorb divergences can be constrained. An asymptotically safe theory is one in which all of the couplings in the theory run to either zero or a nonzero ultraviolet fixed point. Requiring that a coupling reach an ultraviolet fixed point constrains it to live on an ultraviolet critical surface that is of smaller dimension than the original parameter space. We study a theory with gauged baryon number, and require that it is asymptotically safe by introducing gravitational corrections above the Planck scale. This constrains the parameter space of the theory, giving a relationship between the baryon number gauge coupling and a coupling that gives the kinetic mixing between baryon number and hypercharge, effectively removing a free parameter.

We then introduce a TeV-scale, fermionic dark matter candidate into the theory, with the baryon number gauge boson acting as a portal between the visible and dark sectors. The dark matter relic density for our candidate is determined and compared to direct detection bounds. We then examine the problem of the enormous fine-tuning required to keep the Higgs boson mass light despite contributions from large quadratic divergences, called the hierarchy problem. Higher derivative theories are one class of theories that offer a solution to this problem. Infinite-derivative nonlocal theories and finite-derivative Lee-Wick theories each have strengths in this regard, but they also each have weaknesses (for instance, Lee-Wick particles cancel quadratic divergences, but we would have ideally expected to detect them by now at current collider sensitivities). Asymptotically nonlocal theories interpolate between the two and behave differently from either, although they appear nonlocal in the low-energy limit. In asymptotic nonlocality, an emergent nonlocal scale arises that regulates quadratic divergences and that is hierarchically smaller than the mass of the lightest new particle, suggesting a solution to the hierarchy problem. We examine the center-of-mass energy dependence of the cross section in an asymptotically nonlocal theory and demonstrate that the behavior is different from either a nonlocal or Lee-Wick theory. We then derive the Feynman rules in an asymptotically nonlocal extension of QCD, which are needed for the study of strong interaction processes at hadron colliders. We examine the basic process of dijet production from two-into-two parton scattering, calculating the relevant parton-level cross sections. An experimental bound on the nonlocal scale is determined by comparing the predicted dijet invariant mass spectrum in our model with data from the Large Hadron Collider.

TABLE OF CONTENTS

ACKNOWLEDGMENTS

I would like to dedicate this dissertation to my husband, Trey, who has given me tremendous support throughout this whole process.

LIST OF TABLES

LIST OF FIGURES

Chapter 1

Introduction

The energy scales relevant in particle physics span an incredibly wide range. From atoms to black holes, from the hot, dense early universe to today and well into the future, we expect a fundamental theory of physics to explain it all. It takes the highest of energies to study the things that happen at the smallest distances. The Planck scale, $M_{Pl} \equiv \sqrt{\frac{\hbar c}{G}} \sim 10^{19}$ GeV[1], is the scale at which gravitational interactions between particles become strong, and general relativity and the standard model no longer hold. A theory of quantum gravity is required to describe interactions above that scale. We can also think of this scale in terms of length, $l_{Pl} \sim 10^{-35}$ m. Gravitational interactions have only been measured down to ~ 50 μm [1], many orders of magnitude larger than the Planck length, while the standard model has been probed to $\sim (10 \text{ TeV})^{-1} \sim 10^{-20}$ m [2].

Studying smaller and smaller distance scales has historically led to great discoveries and a better understanding of the relationships between fields and interactions. Before the quark model was proposed in the mid-1960s independently by Gell-Mann and Zweig [3,4], mesons and baryons were thought to be elementary particles. The eightfold way was the main organizing theory of the time, grouping mesons and baryons into separate multiplets. Each hadron was categorized by charge and strangeness, with charges $Q = -1, 0, +1$ and

---

[1]In this dissertation we use the convention $\hbar = c = 1$, so that mass and energy have the same units. As a consequence, the Planck mass, $M_{Pl} = \sqrt{\frac{\hbar c}{G}}$, is equivalent to the Planck energy, $E_{Pl} = M_{Pl} \ c^2$. We use energy and mass interchangeably throughout the remainder of this dissertation.

strangeness numbers $S = 0, 1, 2$ for the baryon octet and $S = -1, 0, +1$ for the meson octet (For a more thorough discussion of the eightfold way see Ref. [3]). There were still questions, for instance why the observed ranges of strangeness varied between baryons and mesons. Looking down to smaller distances led to the solution. The quark model defined the simplest baryons as bound states of three quarks, and mesons as bound states of a quark and an antiquark. The electric charges of hadrons were a sum of the charges of the constituent quarks and the strangeness of hadrons was determined by the number of strange quarks they contained. Of course, we now know the picture was incomplete: only the up, down, and strange quarks were theorized, which are the only quarks appearing in the hadrons summarized in the eightfold way. There are many more hadrons that the eightfold way did not predict, but that can be understood with the inclusion of additional flavors of quarks.

Beginning around the same time, as physicists pondered even higher energy scales, the success of QED led to searches for additional gauge field theories. There was also interest in unification of theories, especially after the successful unification of electricity and magnetism. The understanding of weak interactions at the time was characterized by the Fermi Model, which was not a gauge theory and did not include a mediator for the interaction [5]. A number of parallels were found between the electromagnetic and weak interactions, leading to the question of whether the two theories could be combined in a gauge theory. A theory was proposed, $\mathrm{SU(2)_L} \times \mathrm{U(1)}$ in which there were four force carriers, one massless (the photon) and the other three massive ($W^\pm$, Z) [6]. The large masses required of the force carriers of the weak interaction were unexplained; mediators in gauge theories were expected to be massless like the photon, and no mechanism was yet known that could give them mass. This problem would not be solved until the application of the Higgs mechanism in 1967 [7, 8] led to a complete gauge theory description of the weak force and unification of the electromagnetic and weak interactions at the electroweak scale, $M_{EW} \sim 246$ GeV.

The discoveries mentioned above, along with many others, have led to the standard

model, an SU(2)×U(1) gauge theory which has survived all experimental tests within available sensitivities. It does not, however, describe the fundamental parameters of the theory, prompting the exploration of even smaller distance scales, referred to as the ultraviolet (UV) henceforth.

1.1   Challenges of UV physics

Similar to the desire in the mid-20th century to unite the electromagnetic and weak interactions, we now question whether there is an opportunity for a more comprehensive unification. It seems only natural to probe the physics of smaller scales, searching for further unification, this time of all the fundamental forces. Grand unified theories (GUTs) specifically look at unification of the electroweak and strong interactions. Examining the renormalization group flow (discussed in Sec. 1.2.1) of the U(1), SU(2), and SU(3) gauge couplings, one finds that the three interactions nearly meet at around $\sim 10^{14}$ GeV [9]. This seems to suggest that some form of new physics could make the interactions meet at that energy scale, thus the scale is referred to as M_{GUT}[2]. One of the popular theories that leads to grand unification (at $M_{\mathrm{GUT}} \sim 10^{16}$ TeV) is the minimal supersymmetric standard model (MSSM), though the theory contains additional particles that have not been found (see Ref. [10–12] for an overview and additional references on GUTs including MSSM). Searches continue with many ideas looking to unite the standard model interactions with the discovery of new physics at smaller distance scales, yet so far there has been no conclusive evidence that grand unification will occur. Beyond M_{GUT}, an even more intriguing prospect than GUTs exists: a complete theory that describes all forces including gravity. As discussed above, the standard model is only consistent up to the Planck scale, the scale at which gravitational interactions become strong. A Theory of Everything (TOE) should describe all interactions, with general relativity and the standard model functioning as the low-energy effective field theory.

---

[2]The renormalization group equations, discussed later on, tell us about the energy dependence of the couplings in a theory. This allows us to investigate processes at high energy scales, such as M_{GUT}.

The standard model has been highly effective at describing particle physics at experimental energies, as high as those probed at the LHC, but even so some things are missing. We know that dark matter makes up about 85% of the matter in the universe [13], and yet the standard model offers us no clues as to what dark matter actually is. Additionally, we know that there is vastly more matter than antimatter in the universe. The standard model has allowances for differences in the amount of matter and antimatter (such as CP violation in weak interactions), but not nearly enough to explain the observed matter-antimatter asymmetry. Neutrino oscillations are another area where the standard model falls short, it has no prediction that neutrinos will oscillate between flavors, and yet experiments have shown they do [10]. More generally, the existence of three generations of fermions and the hierarchy of their masses is unexplained. The heaviest of the fermions is the top quark, whose mass is $\sim 10^5$ times larger than the mass of the electron, the lightest fermion. Each generation becomes increasingly heavier, yet there is no explanation for this to be so. These gaps in our understanding motivate exploration of higher energies and shorter lengths, looking for new discoveries that lead us to a simpler description of elementary particles and their interactions.

1.1.1 The difficulty of quantizing gravity

A quantum theory of gravity has long been a goal of physics. As discussed above, it is clear that there exists a scale (the Planck scale) above which the current theories of gravity and standard model physics must break down. At that scale, a theory that describes the interactions of particles must account for strong gravitational effects. Much consideration in the literature has gone into theories that attempt to predict physics at the Planck scale. Some of the more popular options are string theory, loop quantum gravity, and quantum field theories of gravity. Of the first two theories, string theory is a candidate for a TOE [14], while loop quantum gravity is consistent with but does not explain the origin of ordinary matter [15]. Loop quantum gravity begins with a geometrical construction and posits a discrete structure of spacetime at the Planck scale, cutting off the possibility

of any physics below the Planck length. String theory requires both supersymmetry and extra dimensions to provide a quantum theory of gravity, and is not inconsistent with the particle physics of the standard model. The major drawback of string theory is that, while it is able to fit well with experimental observations in many areas, it lacks predictivity due to the large number of string vacuum states, of order 10^{500}. In this dissertation, we are interested in gravity as a quantum field theory.

One of the primary issues in developing a quantum field theory of gravity is that gravity is inherently nonrenormalizable. Following the many discussions on renormalizability of gravity (See [16–19]), the superficial degree of divergence, D, of a Feynman diagram in general relativity is $D = 2 + 2L$, where L is the number of loops in the diagram. Since the superficial degree of divergence increases with the number of loops, every amplitude is divergent. This means that an infinite number of counterterms are required to absorb divergences. A theory with an infinite number of counterterms is not predictive, since an infinite number of constraints determined by experiments are needed to make predictions in the theory. However, we will see later there is a framework in which physical observables may be predicted by a finite dimensional subspace of the parameter space of the theory.

1.1.2 Naturalness and the hierarchy problem

Naturalness in physical theories refers to the stability of a theory in regard to small, $\mathcal{O}(1)$ changes in its parameters. If a prediction in the theory requires extreme fine-tuning, for example to cancel large divergences due to loop contributions, the theory will not be stable, and therefore not natural.

The cosmological constant problem is an extreme example of a naturalness problem. The cosmological constant in general relativity is the simplest explanation for dark energy, which comprises $\sim 72\%$ of the universe [13]. The observed cosmological constant can be written as $\Lambda_{\text{eff}} = \Lambda_0 + \kappa \, \rho_{\text{vac}}$, where Λ_0 is the bare value of the cosmological constant, $\kappa = M_{Pl}^{-2}$, and ρ_{vac} is the vacuum energy density of the universe. Cosmological constraints place an upper bound, $\Lambda_{\text{eff}} < 10^{-56}$ cm^{-2}, corresponding to an upper bound on the vacuum

energy density of $\rho_{\text{vac}}^{\text{obs.}} < 10^{-9}$ erg/cm^3 [20]. Predictions of the vacuum energy density from QFT yield $\rho_{\text{vac}}^{\text{QFT}} \sim 10^{35}-10^{114}$ erg/cm^3, depending heavily on the cut-off scale above which one expects new physics to emerge [20]. Any value of the vacuum energy density in this range constitutes a considerable amount of fine-tuning in Λ_0 to cancel its contribution. The cancellation would have to be nearly exact in order to get the observed cosmological constant.

The smallness of the cosmological constant is not the only naturalness problem in the standard model. An additional naturalness problem comes from measurements of the electric dipole moment of the neutron. Experimental bounds place a constraint on the value of the vacuum angle, $\overline{\theta} \leq 10^{-9}$ [21]. The smallness of this bound is referred to as the strong CP problem. A different type of naturalness problem is given by the small masses of the electron and light quarks in the standard model. With $M_{\text{EW}} \sim 246$ GeV the heaviest of the fermions, the top quark, with $m_t \sim 173$ GeV fits reasonably with expectations. When we get down to the up quark mass $m_u \sim 2$ MeV and the electron mass $m_e \sim 0.5$ MeV, we find these lightest fermions are $\sim 10^{-5}$ times lighter than symmetry breaking at the electroweak scale would suggest. The fermion masses do not require fine tuning, yet the fact that they do not all have masses $\sim M_{\text{EW}}$ is not explained.

The above examples demonstrate the large range of unnaturalness in theories. For the purpose of this dissertation, our interest lies in one particular naturalness problem: the gauge hierarchy problem, or just the hierarchy problem. This problem has received a considerable amount of attention in the literature, as will be discussed throughout this section. The hierarchy problem deals with corrections to the mass of the Higgs field. It stems from the fact that the scale of electroweak symmetry breaking, $M_{EW} \sim 10^2$ GeV, is 17 orders of magnitude below the Planck scale, $M_{Pl} \sim 10^{19}$ GeV. The physical mass of the Higgs that has been determined experimentally, $m_{H,\text{phys}} \approx 125$ GeV [10], is related to the bare mass by

$$m_{H,\text{phys}}^2 = m_{H,0}^2 + \mathcal{O}\left(\frac{\Lambda^2}{16\pi^2}\right) \,, \tag{1.1}$$

where $m_{H,0}$ is the bare mass and the second term represents the 1-loop corrections to the Higgs self-energy, with Λ an ultraviolet cut-off. As shown in Fig. 1.1, the leading part of each of the self-energy contributions is proportional to the square of the cut-off scale, Λ, making the corrections quadratically divergent. Our cut-off scale is the highest energy scale where the theoretical description is valid, and in this case we would expect the theory should be applicable all the way up to the Planck scale, $\Lambda \sim 10^{19}$ GeV. With the cut-off scale so high, the bare mass would have to be exactly $m_{H,0}^2 = -10^{36}$ GeV$^2 + (125$ GeV$)^2$. The bare mass must be this value exactly, to the 32nd decimal place, in order to cancel the contribution from the loop corrections and give the correct physical mass; this implies an awful lot of fine-tuning and doesn't seem very natural at all.

$$= \frac{1}{16\pi^2} \lambda \left[\Lambda^2 - m_H^2 \ln \left(\frac{\Lambda^2}{m_H^2} \right) \right]$$

$$= -\frac{3}{8\pi^2} \lambda_t^2 \left[\Lambda^2 - 3m_t^2 \ln \left(\frac{\Lambda^2}{m_t^2} \right) \right]$$

Figure 1.1: Diagrams contributing to the Higgs self energy (Adapted from [5] and [22]). The couplings λ and λ_t denote self-couplings to the Higgs and the coupling to the top quark, respectively, and m_H and m_t are the masses of the Higgs and the top quark.

With all of this, one may question whether the hierarchy problem is actually a problem at all. Even though it seems unnatural for the fine-tuning necessary to cancel quadratic divergences to occur, it is not at all impossible. A common school of thought is to dismiss the issue as just a feature of our universe. This reasoning relates to the anthropic principle, the idea that, in simple terms, we can only ask the question because all the conditions of the universe are exactly right to produce intelligent life forms. This reasoning seems poorly motivated since under such a principle one could question the value of seeking any information about the universe at all. Such a concept seems to go against the very purpose of science. Although fine-tuning may in fact be the way the universe really works,

we currently have no way of knowing. In the absence of any concrete answers, the logical track is to keep looking for one. In its essence, the hierarchy problem is not so much a problem that demands solving, but a puzzle that invites further thought and inspires investigation. We know the standard model is not complete, so a puzzle seems like a great place to focus investigations of new physics.

A considerable amount of work has been devoted over the years to proposing solutions to the hierarchy problem. We outline a few of the common ideas here for context, although only one of these ideas (higher derivative theories) is important to this dissertation. For the other areas, the reader will be referred to more complete discussions in the literature.

One of the most popular proposals to solve the hierarchy problem has been supersymmetry. In supersymmetry, each particle in the standard model has a superpartner with the same color and charge but opposite spin statistics. Bosons have fermionic superpartners and fermions have bosonic superpartners. Note that in Fig. 1.1 the contributions from diagrams involving bosons are positive, while the contributions from diagrams involving fermions are negative. In the standard model, there are unequal numbers of bosons and fermions so their contributions to the Higgs mass do not cancel; in supersymmetry, there are by definition partners to cancel the quadratic contributions from every standard model particle. Still, while we wouldn't have the quadratic contributions shown in Fig. 1.1, we would still have the logarithmic contributions. To keep the logarithmic terms from becoming too large to supply a convincing solution to the hierarchy problem, the masses of the superpartners can't be much larger than the electroweak scale. The lack of evidence of any such particles in experimental searches constitutes a problem for minimal models of supersymmetry. For a more detailed examination of supersymmetry, see Refs. [10, 23, 24].

Another common idea is Little Higgs in which the Higgs takes the form of a pseudo Nambu-Goldstone boson produced by the breaking of a global symmetry [22, 25]. This theory includes new particles at the $\sim$ TeV scale that have loop contributions which cancel quadratic divergences from loops of standard model particles [26]. In this way, they share similarities with supersymmetry and Lee-Wick theories, which will be discussed in

Sec. 1.2.2.

Extra dimensions have also been considered as a solution to the hierarchy problem. In this theory, below the size of the extra dimensions, gravitational effects are altered by their presence. Since the gravitational constant is different in extra dimensions, this serves to effectively lower the Planck scale to the TeV-scale, resolving the hierarchy problem. This solution is unique in that it suggests new physics that lowers the scale at which general relativity ceases to describe gravitational interactions. Instead of breaking down at $M_{Pl} \sim 10^{19}$ GeV, our current understanding of the theory of gravity could start to break down at much lower scales, perhaps even just beyond our current experimental sensitivities.

Higher derivative theories constitute another potential solution to the hierarchy problem, and they will be discussed in detail below in Sec. 1.2.2.

1.2 Meeting the challenges of the UV

In this section we introduce ideas that can provide solutions to the nonpredictivity of a quantum field theory of gravity and the fine-tuning required to cancel quadratic divergences to the Higgs mass. These ideas are the major concepts that motivate the beyond-the-standard-model physics that will be discussed throughout the remainder of this dissertation.

1.2.1 Asymptotic safety

Asymptotic safety was first proposed in 1979 by Steven Weinberg as a way to define a quantum field theory of gravity that is predictive despite being nonrenormalizable [19], an important tool in trying to unite gravity with quantum field theory. Theories of asymptotically safe gravity provide a road toward describing gravity as a quantum field theory without the requirement of altering field theory or the standard model. In his seminal paper on the topic, Weinberg proposes a generalized notion of renormalizability in which degrees of freedom are given by the dimensionality of the UV critical surface (discussed

later in the section), thus making the theory finite and predictive if the surface is finite [19] (See also related work in Refs. [61,62]). As we will see in Chapters 2 and 3 of this dissertation, asymptotic safety is not only a useful constraint in searching for a theory of quantum gravity, it is also a great tool for constraining the parameter space of extensions of the standard model. This section will introduce the concept of asymptotic safety, a constraint on the UV behavior of a theory which affects low energy observables. We will first develop a foundation from which to understand asymptotically safe theories.

When we consider the asymptotic behavior of a theory, we are considering the flow of the theory's couplings, as determined by the renormalization group equations (RGEs). The RGEs tell us how a coupling constant g varies as a function of the energy scale μ,

$$\frac{\partial g}{\partial \ln\mu} = \beta(g) \ , \tag{1.2}$$

where the right-hand-side is a function of the couplings called the β function. Derivation of β functions can be automated using computational software such as PyR@TE 3 [27]. For example, the one loop β functions of the standard model gauge couplings are given by

$$\begin{aligned}
\beta(g_1) &= \frac{1}{16\pi^2}\,\frac{41}{10}\,g_1^3 \\
\beta(g_2) &= -\frac{1}{16\pi^2}\,\frac{19}{6}\,g_2^3 \\
\beta(g_3) &= -\frac{1}{16\pi^2}\,7\,g_3^3 \ .
\end{aligned} \tag{1.3}$$

RGEs are very useful in that they provide a means of looking at interactions at vastly different energy scales. By specifying an experimentally determined value of a coupling constant as an initial condition, we can look at the value of the coupling at any other energy scale, assuming the absence of new physics. Without further modification, these equations only reliably hold up to the Planck scale, where gravitational corrections become important.

In an asymptotically free theory, the RGEs can be used to show that all of the couplings

run to zero as the energy scale increases; coupling strengths weaken at smaller and smaller distance scales, until they eventually vanish. This effect is decidedly different from standard QED, where forces grow stronger at short distant scales and weaken with increasing separation. A notable example of an asymptotically free theory is QCD, as was discovered in 1973 by David Gross and Frank Wilczek [28], and concurrently by David Politzer [29]. The discovery was a big surprise, as it was contrary to the overarching expectations of the time [30]; many physicists did not believe it possible to construct an asymptotically free theory.

A considerable benefit of asymptotic freedom is the avoidance of Landau poles, where the coupling blows up to infinity. At no energy scale do the couplings become divergent, and so an asymptotically free theory is well behaved, even at the smallest of distance scales.

Any coupling that does not blow up to a Landau pole or run to zero must run to a nontrivial UV fixed point. In an asymptotically safe theory, at least one coupling runs to a non-zero fixed value called an interacting UV fixed point, while the rest are asymptotically free. The important feature is that there are no Landau poles, making theories consistent up to arbitrarily high energies. Asymptotic safety is defined by the condition,

$$\beta(g_{i\star}) = 0 \; , \tag{1.4}$$

where $g_{i\star}$ is the value of a coupling g_i at a UV fixed point as $\mu \to \infty$. The UV critical surface is made up of all of the low-energy coupling values that lead to the fixed point. The requirement that a theory be asymptotically safe can constrain the parameter space of the theory, since it is a nontrivial requirement to hit a desired UV fixed point. Living on the UV critical surface limits the number of free parameters in the theory, making even a nonrenormalizable theory predictive. For a review of asymptotic safety and a comprehensive list of references see, for example, Ref. [63].

If gravity is required to be asymptotically safe, then the other couplings in the theory must be either asymptotically free or safe as well, so that the entire theory will be valid up to

11

arbitrarily high energies. The standard model contains a Landau pole in the running of the U(1) hypercharge gauge coupling, but the standard model and standard model extensions can be made asymptotically safe by requiring that gravitational effects be modeled in the RGEs above the Planck scale [31–35]. Although there is no way to know the exact form trans-Planckian gravitational corrections may take, non-perturbative studies suggest a simple form that has appeared in the literarure, $\theta(\mu - M_{Pl}) f_g g_i$, where the Heaviside theta function turns the corrections on at the Planck scale and f_g is taken to be greater than zero [36–38]. In the β functions for the standard model gauge couplings given in Eq. (1.3), the gravitational corrections are modeled as

$$
\begin{aligned}
\beta(g_1) &= \frac{1}{16\pi^2} \frac{41}{10} g_1^3 - \theta(\mu - M_{Pl}) f_g\, g_1 \\
\beta(g_2) &= -\frac{1}{16\pi^2} \frac{19}{6} g_2^3 - \theta(\mu - M_{Pl}) f_g\, g_2 \\
\beta(g_3) &= -\frac{1}{16\pi^2} 7\, g_3^3 - \theta(\mu - M_{Pl}) f_g\, g_3 \ .
\end{aligned}
\tag{1.5}
$$

The correction f_g is identical for all of the gauge couplings. Other couplings, such as the Yukawa couplings, have corrections of a similar form; in the Yukawa sector the correction term has f_g replaced by f_y. In Chapters 2 and 3, we use gravitational corrections of this form to find UV fixed points that constrain the parameter space of two interesting extensions to the standard model.

1.2.2 Higher-derivative theories

The higher-derivative theories of interest to us are defined by the inclusion of an operator $F(\Box)$ in the quadratc terms, where $\Box \equiv \partial_\mu \partial^\mu$ is the usual d'Alembertian operator. Whether the function $F(\Box)$ takes a simple form such as $\Box^2$ or is described by a transcendental function such as $e^\Box$ determines the type of higher-derivative theory. In these theories, propagators grow more slowly as a function of Euclidean momentum, leading to quadratic divergences being regulated, a useful feature for the hierarchy problem, as will be discussed in this subsection. We introduce two types of higher-derivative theories, Lee-

Wick (LW) theories, in which $F(\Box)$ takes a simple finite polynomial form, and nonlocal theories, in which $F(\Box)$ takes the form of an entire transcendental function. We then discuss some of the characteristics of higher derivative theories.

LW theories are finite derivative, often containing as little as one Lagrangian term with higher order derivatives. They can also be built from polynomials in $\Box$, for example $F(\Box) = (\Box + m_1^2)(\Box + m_2^2)$. In this section we will focus on the simplest form, $F(\Box) = \Box^2$, as the discussion is much simpler, but the basic properties hold for more complex theories.

In the late 1960s, Lee and Wick were looking for a way to deal with the divergent ultraviolet behavior of QED. They looked to an existing regularization scheme, Pauli-Villars regularization. In this scheme, a term depending on a large energy scale is added to the photon propagator,

$$D_F(p) = \frac{i}{p^2 + i\epsilon} - \frac{i}{p^2 - \Lambda^2 + i\epsilon} \tag{1.6}$$

where Λ is a cut-off scale [39, 40]. Sufficiently below Λ, physics remains unchanged, yet near the scale of the cut-off and above, the new term becomes important. With the new term, a loop diagram that would otherwise be quadratic will now be regulated by Λ, giving a solution proportional to $\ln(\Lambda^2/m^2)$ where m is the mass of the electron. After the logarithmic divergence is cancelled by a counterterm, Λ can be taken to infinity and the usual photon propagator is recovered. Lee and Wick took the cut-off scale to instead be the mass of a heavy photon, M, with a propagator pole that has wrong-sign residue [41, 42]. They argued that the wrong-sign propagator does not present a problem for the theory because the heavy photon is not stable and will decay into ordinary particles. In other words, the heavy LW photon does not appear in asymptotic scattering states.

Grinstein, O'Connell, and Wise (GOW) expanded on this work in 2007 to the full standard model by noting that the LW poles can be produced by the addition of higher derivative terms in the standard model Lagrangian [43]. GOW also argue that the LW extension to the standard model provides a solution to the hierarchy problem, as will be

13

discussed below.

In the simplest example of a higher derivative theory, a $\Box^2$ term is added to the Lagrangian of a real scalar field,

$$\mathcal{L}_{\text{LW}} = -\frac{1}{2}\hat{\phi}\Box\hat{\phi} - \frac{1}{2M^2}\hat{\phi}\Box^2\hat{\phi} - \frac{1}{2}m_\phi^2\hat{\phi}^2 + \mathcal{L}_{\text{int}} . \tag{1.7}$$

We can easily identify a propagator of the form in Eq. (1.6) by following the approach of GOW in Ref. [43]. An auxiliary field, $\tilde{\phi}$ is introduced,

$$\mathcal{L} = -\frac{1}{2}\hat{\phi}\Box\hat{\phi} - \frac{1}{2}m_\phi^2\hat{\phi}^2 - \tilde{\phi}\Box\hat{\phi} + \frac{1}{2}M^2\tilde{\phi}^2 , \tag{1.8}$$

where we omit the interaction term because it does not affect our current analysis. By defining $\phi = \hat{\phi} + \tilde{\phi}$, the kinetic terms can be decoupled,

$$\mathcal{L} = -\frac{1}{2}\phi\Box\phi + \frac{1}{2}\tilde{\phi}\Box\tilde{\phi} - \frac{1}{2}m_\phi^2(\phi - \tilde{\phi})^2 + \frac{1}{2}M^2\tilde{\phi}^2 , \tag{1.9}$$

where ϕ can now be interpreted as an ordinary scalar, and $\tilde{\phi}$ a LW field. The mass mixing in the third term between ϕ and $\tilde{\phi}$ can be dealt with by performing a rotation with a matrix of the form,

$$\mathcal{R} = \begin{pmatrix} \cosh\theta & \sinh\theta \\ \sinh\theta & \cosh\theta \end{pmatrix} \tag{1.10}$$

with the angle θ defined by

$$\tanh 2\theta = \frac{-2m_\phi^2}{M^2 - 2m_\phi^2} . \tag{1.11}$$

This gives us the unmixed Lagrangian,

$$\mathcal{L} = -\frac{1}{2}\phi'\Box\phi' + \frac{1}{2}\tilde{\phi}'\Box\tilde{\phi}' - \frac{1}{2}m_\phi'^2\phi'^2 + \frac{1}{2}M'^2\tilde{\phi}'^2 , \tag{1.12}$$

where the primes denote the fields and mass eigenvalues after diagonalization. We then

easily find the propagators of the ordinary and LW fields,

$$D_F(p) = \frac{i}{p^2 - m_\phi'^2 + i\epsilon} \qquad \tilde{D}_F(p) = \frac{-i}{p^2 - M'^2 + i\epsilon} \, , \qquad (1.13)$$

noting the LW propagator has the wrong sign compared to the propagator of an ordinary field, and the propagators match the form of Eq. (1.6) for $m_\phi' = 0$ and $M' = \Lambda$.

Other recent work examining LW theories has included alternative formulations of LW theories such as a minimal LW standard model [44] and a higher-order LW standard model [45]. Results from the LW standard model and these other interpretations can be generalized to larger numbers of derivatives. This prospect will be explored further in Chapters 4 and 5.

Similar to the effects of supersymmetry discussed in Sec. 1.1.2, LW theories cancel quadratic divergences through the existence of partners for every SM particle, though this is the only similarity between the two. In the LW case, each particle has a partner with wrong-sign propagator, leading to cancellations of the quadratic corrections in Fig. 1.1. The remaining contributions are dominated by a term (in the notation above with the primes removed) $M^2 \ln(\Lambda^2/M^2)$. The addition of LW partners for every SM particle creates a new set of particles that can be searched for experimentally. The absence of any discovery of such particles in experiments to date threatens the viability of the LW idea. With the dependence on $M^2 \ln(\Lambda^2/M^2)$, if the mass of the LW particle becomes too high, problems with hierarchy are reintroduced. In general, any solution to the hierarchy problem requires new physics to be not much heavier than the TeV scale. This applies to Lee-Wick particles as well [46]. Current experiment probes the TeV scale for both supersymmetric theories and the theories with additional heavy particles. See, for example, Refs. [10, 49, 50].

Unitarity of the S-matrix is an important issue in the study of higher derivative theories. A unitary theory is one in which all of the probabilities of possible scattering in the theory sum to one. A non-unitary theory is therefore inconsistent because it is non-predictive and scattering in the theory cannot be well described.

The basic condition of unitarity of the S-matrix is given by $S^\dagger S = 1$. We define $S = 1 + iT$ so that the T-matrix gives the interaction part of the S-matrix,

$$-i(T - T^\dagger) = T^\dagger T \ . \tag{1.14}$$

This condition becomes the optical theorem,

$$\mathrm{Im}\, \mathrm{M}(k_1, k_2 \to k_1, k_2) = \sum_f \int d\Pi_f \, \mathcal{M}^*(k_1, k_2 \to f)\mathcal{M}(k_1, k_2 \to f) \tag{1.15}$$

where f runs over all possible final states.

The unitarity of LW theories has been addressed extensively in the literature. When Lee and Wick first proposed their theory in 1968, they provided a prescription for altering the path of contour integration to contain the LW poles, so that contours have the same relative orientation to poles as they would in the Feynman prescription [41]. In 1969, Cutkosky, Landshoff, Olive, and Polkinghorne developed a set of rules for dealing with LW poles [51], which have since been referred to as the CLOP prescription. This prescription provides a method for dealing with the situation where contours are pinched by poles in the LW prescription. The CLOP prescription introduces fictitious mass shifts to the pole positions, ensuring that the poles will not pinch for any momentum. Those shifts are taken to zero at the end of a loop calculation. GOW revisited the CLOP prescription in [52], clarifying several points and using an auxiliary field approach that simplifies calculation. Recent work by [53] has suggested an alternative to the CLOP prescription, noting that it does not work for all possible formulations of LW theories (See also [54, 55]).

In LW theories, as you add additional terms that are higher orders in derivatives, you add more poles to the theory, corresponding to more LW particles. In a nonlocal theory, the series of higher derivative terms never terminates. Nonlocal theories contain infinite derivative quadratic terms that involve an entire transcendental function of the derivative operator $\Box$. A key feature of nonlocal theories that we consider in this dissertation is

that they are ghost-free, meaning that they do not introduce new propagator poles. This means that the only parameter introduced by nonlocality is the nonlocal scale, Λ_{nl}, as will be discussed throughout this section.

Pais and Uhlenbeck presented an idea for a nonlocal field theory in 1950 [56]. With the discovery of a series of divergent theories describing particle physics (including QED), there was particular interest in theories that could lead to mitigation of divergences. They considered a nonlocal operator in the form of an exponential, $F(\Box) = e^{f(\Box)}$, for example,

$$\mathcal{L}_{\text{nl}} = -\frac{1}{2}\phi \,\Box\, F(\Box)\,\phi \;, \tag{1.16}$$

where in this case ϕ is taken to be massless.

Here we consider an example of the same form with $f(\Box) = \Box/\Lambda_{\text{nl}}^2$ in a theory with massive scalar ϕ,

$$\mathcal{L} = -\frac{1}{2}\phi\,(\Box + m_\phi^2)\,e^{\Box/\Lambda_{\text{nl}}^2}\,\phi + \mathcal{L}_{\text{int}} \;, \tag{1.17}$$

where $\mathcal{L}_{\text{int}}$ is the interaction Lagrangian, m_ϕ is the mass of the scalar field ϕ, and Λ_{nl} is the scale of nonlocality. Taking $F(\Box)$ to be this form leads to a decreasing exponential in the numerator of a propagator in the theory once it has been Wick rotated, which is a desirable feature for convergence.

A common application of nonlocality is in quantum gravity, where the exponential operator prevents singularities at the origin of spherically symmetric solutions like the Schwarzschild metric. Since the exponential never vanishes completely, its inverse does not contain any poles. This allows for singularity free gravity without adding any ghosts. (For a more complete discussion see Refs. [17, 57, 58] and additional references therein.)

Quadratic divergences are regulated in nonlocal field theories by the dampening exponential in the propagator. The propagator in the nonlocal theory discussed above is given by,

$$D_F(p) = \frac{ie^{p^2/\Lambda_{\text{nl}}^2}}{p^2 - m^2 + i\epsilon} \;. \tag{1.18}$$

Since the propagator falls off more quickly with Euclidean momentum after Wick rotation, i.e. $e^{p^2/\Lambda_{\rm nl}^2} = e^{-p_E^2/\Lambda_{\rm nl}^2}$, the loop amplitudes in the Higgs self-energy will fall off more quickly with momentum, eliminating the quadratic divergences. Similarly for other forms of nonlocal field theories, as long as the form of the function $F(\Box)$ causes the propagator to fall off more quickly, the same effect will be reproduced and the hierarchy problem will be resolved. The exponential in Eq. (1.18) regulates loops at the scale $\Lambda_{\rm nl}$ which suggests that effects of nonlocality should be detectable around the TeV-scale. A bound on the nonlocal scale based on collider phenomenology will be discussed in Chapter 5 of this dissertation.

Nonlocal theories have been shown to have problems with unitarity when they are formulated in Minkowski space. The historical solution has been to define the theory in Euclidean signature, in which case unitarity can be recovered. The external momenta in scattering amplitudes can be analytically continued to Minkowski space at the end of a calculation. Attempts to show unitarity when the theory is defined in the Minkowski signature lead to problems, originating from the fact that the exponential does not vanish for all directions in the complex p^0 plane as $|p^0| \to \infty$ [59, 60]. The imaginary part of the amplitude on the left-hand-side of Eq. (1.15) receives an additional contribution as a result, leading to disagreement with the right-hand-side. The optical theorem is therefore not satisfied.

In Chapters 4 and 5 we will discuss asymptotically nonlocal theories, a class of higher derivative theories that interpolates between infinite derivative nonlocal theories and finite derivative LW theories. These theories consist of a series of quadratic terms of finite order in the number of derivatives, yet they approach nonlocal theories as a limit. As in the case of LW and nonlocal theories, they can provide a solution to the hierarchy problem. We will expand on the topic later in the dissertation, but for now we will mention that asymptotically nonlocal theories create a new set of particles, much like LW theories; however in asymptotically nonlocal theories, these can be decoupled while leaving a much lighter, emergent regulator scale that avoids the hierarchy problem. Nonlocal theories avoid the problem of new particles altogether, but they have problems with unitarity,

whereas the unitarity of asymptotically nonlocal theories can be addressed through the same approach used for LW theories.

1.3 Summary

For the rest of this dissertation, we explore modifications to the high energy behavior of theories, motivated by the solutions to problems of quantum gravity and the hierarchy problem discussed in this introduction. In Chapters 2 and 3 we use the paradigm of asymptotic safety, with gravitational corrections above the Planck scale inspired by quantum gravity, to constrain model parameters. Chapter 2 examines a theory with gauged baryon number and shows how asymptotic safety restricts the kinetic mixing parameter in the theory. In Chapter 3, we build on the results of Chapter 2, adding to the earlier model a TeV-scale fermionic dark matter candidate, with the baryon number gauge boson acting as a portal between the visible and dark sectors. Chapters 4 and 5 explore asymptotic non-locality, a class of higher derivative theories that is finite in derivatives, yet approaches an infinite derivative nonlocal theory as a limit. These theories possess an emergent nonlocal scale that regulates quadratic divergences, potentially providing a solution to the hierarchy problem. In Chapter 4, we examine the center-of-mass energy dependence of scattering cross sections in asymptotically nonlocal theories. We show the behavior of cross sections reflects the emergent nonlocality at the scale where divergences are regulated, with the growth in cross sections truncated once the LW resonances are reached. In Chapter 5, we derive the Feynman rules for an asymptotically nonlocal generalization of QCD needed for investigations of strong interaction processes at hadron colliders. We then determine a bound on the nonlocal scale using data from the Large Hadron Collider (LHC). We offer concluding remarks in Chapter 6.

Chapter 2

Asymptotic safety and gauged baryon number[1]

In this chapter we consider a model with gauged baryon number that may be rendered asymptotically safe when gravitational effects above the Planck scale are taken into account. We study the ultraviolet fixed points in this theory and determine the restrictions on the parameter space of the model at the TeV scale following from the requirement that the asymptotic fixed points are reached. Assuming that the new gauge symmetry is broken at the TeV scale, we comment on the phenomenological implications of these restrictions.

2.1   Introduction

Extensions of the standard model typically involve a set of new couplings that are only partially constrained by low-energy experimental observables. A well-motivated restriction on the ultraviolet (UV) limit of such a theory is useful when it can remove some of this arbitrariness, leading to a more predictive low-energy theory. In this chapter, we consider a Z' model whose phenomenology is affected in a meaningful way by the requirement that the theory remain asymptotically safe when extrapolated to infinitely high energy scales.

---

[1]Work previously published in J. Boos, C. D. Carone, N. L. Donald and M. R. Musser, "Asymptotic safety and gauged baryon number," Phys. Rev. D **106**, no. 3, 035015 (2022).

We determine the UV restrictions on the model's parameter space at the TeV scale and comment briefly on the phenomenological consequences.

Just as asymptotic safety can reduce the otherwise infinite parameter space of a non-renormalizable theory, it can reduce the finite-dimensional parameter space of a renormalizable one. This fact has been used to constrain standard model extensions in several examples discussed in the recent literature [36–38, 64–68], focusing on issues including dark matter [36, 37], the current discrepancy between the standard model prediction and the measured value of the muon anomalous magnetic moment [37, 64], various aspects of neutrino and Higgs sector physics [65–67], flavor physics [69] and collider phenomenology [38, 68]. The present work considers another application, adding to this body of literature. The possibility that baryon number could be gauged has been discussed extensively in the past [70–77], both as a possible way of assuring proton stability and for its interesting TeV-scale phenomenology; the latter motivation is relevant for the present work. The phenomenology of the new U(1) gauge boson is largely determined by the gauge coupling g_B, the gauge boson mass m_B, and a parameter ϵ (defined later) that specifies the kinetic mixing between the U(1)$_B$ and hypercharge gauge groups. Notably, the U(1)$_B$ gauge boson would be entirely leptophobic if not for the kinetic mixing. Hence, decay channels that may be easier to discern in light of large QCD backgrounds (*i.e.*, decays to charged dileptons rather than dijets) are entirely controlled by the undetermined kinetic mixing parameter. The same parameter also controls mixing of the U(1)$_B$ and electroweak gauge bosons that is crucial in determining the constraints from precise electroweak measurements at the Z-boson scale. One way of fixing the kinetic mixing parameter, discussed in Ref. [71], is to require that it vanishes at some scale by embedding the two Abelian gauge group factors into a non-Abelian one. Here we explore a more economical alternative—and one motivated by the eventual inclusion of gravity—that asymptotic safety allows us to predict the kinetic mixing in terms of other model parameters based on the requirement that appropriate fixed points are reached in the UV. This reduces the space of possibilities for the properties of the Z' boson, and provides a guide for discerning the model at collider

21

experiments.[2]

This chapter is organized as follows. In Sec. 3.2 we define the model. In Sec. 3.3, we study the UV behavior of the theory, identifying a number of scenarios where the model can be extrapolated to infinite energy with some couplings reaching nontrivial fixed points, and where vacuum stability is maintained. We determine what these UV boundary conditions imply about the allowed parameter values at the TeV scale. In Sec. 3.4, we comment on the phenomenological implications of these results, presenting one example in which the branching fraction of the Z' boson into standard model particles is predicted. We summarize our conclusions in Sec. 4.5. Appendix A contains the complete list of one-loop renormalization group β-functions used in our analysis.

2.2   Model

We consider an extension of the standard model in which baryon number, $\mathrm{U}(1)_B$, is gauged. We normalize that gauge coupling so that that baryon number charge is $+1$ for a proton or neutron; the baryon number is 0 for any standard model lepton. A right-handed neutrino is included so that Dirac neutrino masses are possible. We do not address the problem of the flavor structure of the standard model, nor the smallness of neutrino masses, but remain content with the fact that the allowed couplings of the model are sufficient to accommodate all observed fermion masses and mixing angles. The charges for the particle content described thus far are shown in Table 2.1.

Additional fermions must be added to assure the cancellation of gauge and gravitational anomalies. We assume three generations of Dirac fermions ψ^ℓ, ψ^e and ψ^ν that are vector-like under the standard model gauge group, with quantum numbers identical to those of the lepton fields ℓ_L, e_R and ν_R, respectively; the new fields are chiral under $\mathrm{U}(1)_B$. We

---

[2]We note that Ref. [38] also considers asymptotic safety in a leptophobic model, but one in which only third-generation quarks are charged under a new U(1). This implies a different fixed point structure than the one predicted by the model proposed here. More significantly, the model in Ref. [38] has a serious problem: the stated charge assignments for the fermions that are vector-like under the standard model gauge group forbid the only possible Yukawa couplings that could generate their masses. This leads to massless, electrically charged fermions, ruling out the model.

	$SU(3)_C$	$SU(2)_W$	$U(1)_Y$	$U(1)_B$
q_L	3	2	$1/6$	$1/3$
u_R	3	1	$2/3$	$1/3$
d_R	3	1	$-1/3$	$1/3$
ℓ_L	1	2	$-1/2$	0
e_R	1	1	-1	0
ν_R	1	1	0	0

Table 2.1: Charge assignments for a single generation of standard model fields, including a right-handed neutrino.

temporarily denote the $U(1)_B$ charges of $\psi^\ell_{L,R}$, $\psi^e_{L,R}$ and $\psi^\nu_{L,R}$ as $x_{L,R}$, $y_{L,R}$, and $z_{L,R}$, respectively. For simplicity, we seek the cancellation of anomalies within each generation separately. The anomaly cancellation constraints are then summarized as follows:

- $U(1)_B\,SU(3)^2$: This anomaly is proportional to $2 \cdot \frac{1}{3} - \frac{1}{3} - \frac{1}{3} = 0$, and vanishes without help from the vector-like sector.

- $U(1)_B\,SU(2)^2$: This anomaly is proportional to $3 \cdot \frac{1}{3} + x_L - x_R$, which implies

$$x_L - x_R = -1 \ . \tag{2.1}$$

- $U(1)_B\,U(1)_Y^2$: This anomaly is proportional to $-\frac{1}{2} + \frac{1}{2}(x_L - x_R) + (y_L - y_R)$. With the constraint of Eq. (2.1), this implies

$$y_L - y_R = +1 \tag{2.2}$$

	$SU(3)_C$	$SU(2)_W$	$U(1)_Y$	$U(1)_B$
ψ^ℓ_L	1	2	$-1/2$	$x_L = 0$
ψ^ℓ_R	1	2	$-1/2$	$x_R = 1$
ψ^e_L	1	1	-1	$y_L = 1$
ψ^e_R	1	1	-1	$y_R = 0$
ψ^ν_L	1	1	0	$z_L = 1$
ψ^ν_R	1	1	0	$z_R = 0$

Table 2.2: Charge assignments for the vector-like fields, for a single generation. The last column shows the anomaly-free solution discussed in the text.

- $U(1)_B^2\, U(1)_Y$: The standard model particles do not contribute to this anomaly, but the new particles do, so that

$$-(x_L^2 - x_R^2) - (y_L^2 - y_R^2) = 0 \ .\tag{2.3}$$

- $U(1)_B^3$: Again, there is no contribution in total from the standard model particles, but the new particles contribute:

$$2\,(x_L^3 - x_R^3) + (y_L^3 - y_R^3) + (z_L^3 - z_R^3) = 0 \ .\tag{2.4}$$

- $gg\, U(1)_Y$: Here, g refers to a graviton. The hypercharge gravitational anomaly cancels in the standard model, and this is not affected by the new particles which are vector-like in their standard model charges.

- $gg\, U(1)_B$: In this case, the anomaly is proportional to $2\,(x_L - x_R) + (y_L - y_R) + (z_L - z_R)$. With the constraints of Eqs. (2.1) and (2.2), this implies

$$z_L - z_R = +1 \ .\tag{2.5}$$

All the constraints are satisfied with the choice $x_R = y_L = z_L = +1$ and $x_L = y_R = z_R = 0$, as indicated in Table 2.2.

We assume that the $U(1)_B$ symmetry is spontaneously broken by a complex scalar field ϕ which has baryon number $+1$ and is a singlet under the standard model gauge group. The charge assignment of ϕ is fixed by the requirement that it allows Yukawa couplings which generate masses for the ψ fields when ϕ develops a vacuum expectation value (vev). One finds that the desired Yukawa couplings are given by

$$\mathcal{L}_y = \overline{\psi_L^\ell}\, y_1\, \psi_R^\ell\, \phi^* + \overline{\psi_L^e}\, y_2\, \psi_R^e\, \phi + \overline{\psi_L^\nu}\, y_3\, \psi_R^\nu\, \phi + \text{ H.c. } ,\tag{2.6}$$

24

where the y_i are three-by-three matrices.[3] Since there are pairs of fields that have identical quantum numbers, namely (ψ_L^ℓ, ℓ_L), (ψ_R^e, e_R) and (ψ_R^ν, ν_R), we may choose a field basis in which there are no Yukawa couplings involving ϕ that mix a heavy and light field, such as $\overline{\ell_L}\psi_R^\ell\phi^*$. However, heavy-light couplings are possible involving the standard model Higgs field H:

$$\mathcal{L}_\kappa = \overline{\psi_L^\ell}\, H\, \kappa_1 e_R + \overline{\ell_L}\, H\, \kappa_2\, \psi_R^e + \overline{\ell_L}\, \widetilde{H}\, \kappa_3 \psi_R^\nu + \text{ H.c. },\tag{2.7}$$

where the κ_i are also three-by-three matrices. This set of Yukawa couplings serves a useful purpose phenomenologically, as it assures that the heavy fields can decay to light fields, thereby avoiding unwanted stable charged particles. (For the stringent bounds on heavy, stable charged particles, see *Other Particle Searches* in Ref. [78]).

It is worth noting that the spontaneous breaking of baryon number through the ϕ vev does not lead to any problems with proton decay. The Lagrangian has an anomalous global U(1) baryon number symmetry acting exclusively on the quark fields q, u and d, even in the presence of a ϕ vev. This implies that any gauge-invariant, dimension-six operator that contributes to proton decay, and violates this global symmetry, cannot be generated at any order in perturbation theory, where it might only be suppressed by a mass scales appearing in the Lagrangian. On the other hand, Planck-suppressed dimension-six operators, if present, would be sufficiently suppressed as the lower bound on the scale of dimension-six operators from proton decay is typically $\mathcal{O}(10^{16})$ GeV [78]. Interestingly, there is some evidence that asymptotically safe gravity may preserve global symmetries, in which case even these operators would not arise [79]; for additional discussion, see Ref. [37].

The rest of the theory consists of the scalar sector

$$V(\phi, H) = -m_H^2 H^\dagger H + \frac{\lambda}{2}(H^\dagger H)^2 - m_\phi^2 \phi^*\phi + \frac{\lambda_\phi}{2}(\phi^*\phi)^2 + \lambda_m \phi^*\phi H^\dagger H \ ,\tag{2.8}$$

which involves the new couplings λ_m and λ_ϕ, and the gauge kinetic mixing between U(1)$_B$

---

[3]For simplicity, we omit possible Majorana masses for ν_R and ψ_R^ν.

and hypercharge

$$\mathcal{L} \supset -\frac{1}{4} B^{\mu\nu} B_{\mu\nu} - \frac{1}{4} F_Y^{\mu\nu} F_{\mu\nu}^Y + \frac{\epsilon}{2} B^{\mu\nu} F_{\mu\nu}^Y \ , \qquad (2.9)$$

which involves the kinetic mixing parameter ϵ. Thus, in addition to the parameters of the standard model, the theory we have just defined has one new gauge coupling g_B, a gauge-kinetic mixing parameter ϵ, two new Higgs sector couplings λ_ϕ and λ_m, and the new Yukawa couplings in Eqs. (2.6) and (2.7). If one temporarily rescales the gauge fields so that the gauge couplings appear in the kinetic terms, Eq. (3.2) takes the form

$$\mathcal{L} = -\frac{1}{4} (G^{-2})_{AB} F_{\mu\nu}^A F^{B\,\mu\nu} \ , \qquad (2.10)$$

where the indices run over the two-dimensional space of Abelian gauge fields. In studying the renormalization group equations (RGEs) for models of this type, it is conventional [27] to redefine the gauge field basis so that the matrix G has the upper-triangular form

$$G = \begin{pmatrix} g_Y & \dfrac{\epsilon}{\sqrt{1-\epsilon^2}} g_Y \\ 0 & \dfrac{1}{\sqrt{1-\epsilon^2}} g_{B0} \end{pmatrix} \equiv \begin{pmatrix} g_Y & \tilde{g} \\ 0 & g_B \end{pmatrix} \ . \qquad (2.11)$$

Here g_{B0} is the baryon number gauge coupling in the original basis. The RGEs are then conveniently expressed in terms of $\tilde{g}$, g_Y and g_B. In the basis where the kinetic terms are canonical in form, the covariant derivative on a generic field χ may be expressed as

$$D_\mu \chi = [\partial_\mu - i\, g_B B_\mu Q_B - i\, (g_Y A_\mu^Y + \tilde{g}\, B_\mu) Q_Y]\, \chi \,, \qquad (2.12)$$

where Q_B and Q_Y are the baryon number and hypercharges of χ, respectively. This is a convenient form for studying some of the phenomenological consequences of the RGE output.

Finally, following the conventional approach [36–38,65–68], we adopt a simplified flavor structure of the theory for use in our numerical RGE analysis: we ignore standard model lepton Yukawa couplings and assume that the matrices y_i and κ_i, $i = 1 \ldots 3$, are each

proportional to the identity matrix; in other words, these couplings will be taken to represent six parameters rather than six arbitrary matrices. These assumptions are consistent with the renormalization group running of the couplings for the following reason: In the absence of standard model lepton Yukawa couplings, the Lagrangian has a $U(3)_\ell \times U(3)_e$ chiral symmetry. Writing the charge assignments via the representation pair $(\mathbf{r}_\ell, \mathbf{r}_e)$, this symmetry can be extended to the heavy leptons,

$$e_R \sim \psi_L^\ell \sim \psi_R^\ell \sim (\mathbf{1}, \mathbf{3})$$

$$\ell_L \sim \psi_L^e \sim \psi_R^e \sim \psi_L^\nu \sim \psi_R^\nu \sim (\mathbf{3}, \mathbf{1}) \ , \tag{2.13}$$

provided that the y_i and κ_i are proportional to three-by-three identity matrices. This global symmetry is not broken by any perturbative interaction, allowing us to conclude that the simple flavor structure *ansatz* we have assumed will not be altered by RGE running.

2.3 Fixed point analysis

With the model now fully developed, let us consider the structure of its renormalization group flow in detail. In particular, we will search for fixed points at one loop in perturbation theory, with gravitational effects parametrized, and consider in which parts of parameter space this model exhibits asymptotic safety. We extract the β-functions using PyR@TE 3 [27]; see also appendix A.

2.3.1 Generalities

Let us briefly recall some terminology. Consider some couplings g_i with their associated β-function denoted as β_i. To study the behavior of the RG flow around a fixed point $g_{i\star}$, consider the expansion

$$\beta_i = M_i{}^j \, \delta_j + P_i{}^{jk} \, \delta_j \, \delta_k + \mathcal{O}\left(\delta^3\right) \ , \tag{2.14}$$

where $\delta_j \equiv g_j - g_{j\star}$ and we defined the coefficients

$$M_i{}^j \equiv \left.\frac{\partial \beta_i}{\partial g_j}\right|_\star , \qquad P_i{}^{jk} \equiv \frac{1}{2}\left.\frac{\partial^2 \beta_i}{\partial g_j \partial g_k}\right|_\star . \qquad (2.15)$$

The matrix $M_i{}^j$ has eigenvectors $v_j{}^k$, where k labels the vectors such that $M_i{}^j v_j{}^k = \vartheta_k v_i{}^k$ (no summation over k). At linear order in δ_i, Eq. (2.14) is solved by

$$g_i(\mu) = g_{i\star} + \sum_k c_k v_i{}^k \left(\frac{\mu}{\Lambda}\right)^{\vartheta_k} , \qquad (2.16)$$

where Λ is an arbitrary reference energy scale defining the origin of "renormalization time" $t = \ln(\mu/\Lambda)$. The c_k are subject to the constraint $g_i(\mu \to \infty) = g_{i\star}$, which requires that $c_k \equiv 0$ for all k with $\vartheta_k \geq 0$. The eigendirections $v_i{}^k$ in coupling space are classified according to the sign of their respective eigenvalues: $\vartheta_k < 0$ ("relevant"), $\vartheta_k = 0$ ("marginal"), and $\vartheta_k > 0$ ("irrelevant"). Consequently, the UV critical surface is spanned by all the relevant eigendirections, as well as any marginal ones that lead to flow towards the fixed point. The latter behavior in the case of marginal directions, however, cannot be established by considering only the linear terms in Eq. (2.14), but requires study of the β-functions at higher order.

It is generally assumed that the influence of gravity can be safely neglected when considering particle physics well below the Planck scale. However, since the renormalization group flow extends to infinite energies in the scenarios of interest to us, gravitational corrections to the β-functions at and above the Planck scale need to be taken into account. (For a different approach towards realizing asymptotic safety see, for example, Ref. [80].) The precise form of these corrections depends on the exact matter content and gravitational theory under consideration, and they have been computed in several scenarios in the so-called Einstein–Hilbert truncation [31]; see also Refs. [32–35]. In a generic but simplified picture adopted in phenomenological literature [36–38], the gravitational corrections to the

β-functions are modeled by ($M_{\text{Pl}} = 1.2 \times 10^{16}$ TeV)

$$\beta(g_i) = \frac{1}{(4\pi)^2}\beta^{(1)}(g_i) - \theta\left(\mu - M_{\text{Pl}}\right) f_g\, g_i \,, \tag{2.17}$$

$$\beta(y_i) = \frac{1}{(4\pi)^2}\beta^{(1)}(y_i) - \theta\left(\mu - M_{\text{Pl}}\right) f_y\, y_i \,, \tag{2.18}$$

$$\beta(\lambda_i) = \frac{1}{(4\pi)^2}\beta^{(1)}(\lambda_i) - \theta\left(\mu - M_{\text{Pl}}\right) f_\lambda\, \lambda_i \,, \tag{2.19}$$

where θ denotes the Heaviside step function. Here, for compactness, g_i, y_i and λ_i represent the sets of couplings $\{g_1, g_2, g_3, g_B, \tilde{g}\}$, $\{y_t, y_b, y_1, y_2, y_3, \kappa_1, \kappa_2, \kappa_3\}$ and $\{\lambda, \lambda_\phi, \lambda_m\}$, respectively. Note that the universal coupling of gravity to matter implies that these corrections f_g, f_y, and f_λ are universal in the gauge, Yukawa, and quartic sectors of the model, respectively.[4] The form of the gravitational correction in Eq. (2.17) for the gauge couplings was shown first in Ref. [82] where it was found that f_g is renormalization scheme dependent and either positive or zero; the assumption that $f_g > 0$ that we adopt here is standard in the phenomenological literature, and corresponds to schemes that break certain classical gauge-gravity symmetries that would otherwise lead to a vanishing result [82]. For other discussion of f_g see Refs. [32–35]. On the other hand, the signs and magnitudes of the Yukawa and quartic gravitational corrections are typically less constrained. In what follows, we shall treat the triplet (f_g, f_y, f_λ) as an input parameter to our model, and explore the fixed point structure for a given triplet.

---

[4]Perhaps a more transparent way to understand the universality of the gravity correction term in the gauge coupling sector, when kinetic mixing is present, is to write the renormalization group equation in terms of the coupling matrix G^2_{AB}, defined in Eq. (2.10). Working in this basis, G^2_{AB} encodes all the dependence on the gauge couplings in any diagrammatic calculation. A universal gravitational correction term would be introduced through a term proportional to this coupling matrix,

$$\frac{\mathrm{d}G^2_{AB}}{\mathrm{d}t} = \frac{1}{2}\frac{1}{16\pi^2}\left[G^2_{AC}\beta^{(1)}_{CD}G^2_{DB} + (A \leftrightarrow B)\right] - 2\,G^2_{AB}\, f_g \,,$$

where the form of the non-gravitational part of the RGE can be found in Eq. (5.1) of Ref. [81]. This reduces to Eq. (2.17) when expressed in terms of the component couplings, and yields the desired form for the gravitational corrections in the case where kinetic mixing is vanishing.

2.3.2 Fixed points and critical surfaces

It is instructive to first consider the $U(1)_B \times U(1)_Y$ sector of our theory, including the kinetic mixing. Henceforth, we use the SU(5) normalization of hypercharge, $g_1 \equiv \sqrt{5/3}\, g_Y$; then the gravity-corrected β-functions are given by

$$\beta^{(1)}(g_1) = +\frac{77}{10}g_1^3 - \theta(\mu - M_{\text{Pl}})\,\hat{f}_g\, g_1 \,, \tag{2.20}$$

$$\beta^{(1)}(g_B) = +11g_B^3 + \frac{77}{6}g_B\tilde{g}^2 - \frac{16}{3}g_B^2\tilde{g} - \theta(\mu - M_{\text{Pl}})\,g_B\,\hat{f}_g \,, \tag{2.21}$$

$$\beta^{(1)}(\tilde{g}) = -\frac{16}{5}g_1^2 g_B - \frac{16}{3}g_B\tilde{g}^2 + \frac{77}{5}g_1^2\tilde{g} + 11g_B^2\tilde{g} + \frac{77}{6}\tilde{g}^3 - \theta(\mu - M_{\text{Pl}})\,\tilde{g}\,\hat{f}_g \,, \tag{2.22}$$

where we use the notation $\hat{f}_A \equiv (4\pi)^2 f_A$ with $A = g, y, \lambda$.

For energy scales $\mu < M_{\text{Pl}}$, Eq. (2.20) follows the usual logarithmic running

$$\alpha_1(\mu)^{-1} = \alpha_1(\mu_0)^{-1} - \frac{1}{2\pi}\frac{77}{10}\ln\left(\frac{\mu}{\mu_0}\right)\,, \quad \alpha_1(\mu) \equiv \frac{g_1^2(\mu)}{4\pi}\,, \tag{2.23}$$

or equivalently,

$$g_1(\mu) = \frac{g_1(\mu_0)}{\sqrt{1 - \frac{77}{10}\frac{2\,g_1^2(\mu_0)}{(4\pi)^2}\ln\left(\frac{\mu}{\mu_0}\right)}}\,, \tag{2.24}$$

and, if not for the gravity correction $\hat{f}_g$ taking over at $\mu > M_{\text{Pl}}$, the hypercharge gauge coupling would hit a Landau pole eventually. Note that the g_1 fixed point structure is independent of the couplings g_B and $\tilde{g}$ at one loop. In the trans-Planckian regime, the fixed point criterion for g_1 reads as follows:

$$\left(\frac{77}{10}g_{1\star}^2 - \hat{f}_g\right)g_{1\star} = 0\,. \tag{2.25}$$

This equation has a trivial solution, corresponding to a Gaussian fixed point, as well as a nontrivial solution, corresponding to an interacting fixed point. It is clear that these are the only two fixed point scenarios: if $\hat{f}_g$ is too small, then the cubic term in $\beta^{(1)}(g_1)$ will

dominate and drive g_1 to infinite values. If $\hat{f}_g$ is at a critical value $\hat{f}_g^{\text{crit}}$, however, g_1 will attain a fixed point exactly at the Planck scale. And if $\hat{f}_g$ is larger than this critical value, the linear term in $\beta^{(1)}(g_1)$ dominates and drives the coupling to zero at infinite energies:

$$
\begin{aligned}
\hat{f}_g < \hat{f}_g^{\text{crit}} & \qquad \text{no } g_1 \text{ fixed point} , \\
\hat{f}_g = \hat{f}_g^{\text{crit}} & \qquad \text{interacting } g_1 \text{ fixed point} , \\
\hat{f}_g > \hat{f}_g^{\text{crit}} & \qquad \text{Gaussian } g_1 \text{ fixed point} .
\end{aligned}
\tag{2.26}
$$

In what follows, we shall discuss the two fixed-point scenarios in more detail. We present numerical values to five significant figures since in some instances this is relevant for hitting unstable fixed point values when running up from the TeV scale. It is interesting to note that there is evidence that fixed points in the gauge sector do not destroy a nontrivial fixed point for the gravitational coupling [83], which makes the phenomenological approach described here sensible when considered in a broader context. For a review of the effects of matter couplings on asymptotic safety in the gravity sector, see Ref. [16].

2.3.2.1 Gaussian g_1 fixed point

The Gaussian fixed point, $g_{1\star} = 0$, is attainable if the gravity correction dominates at the Planck scale, amounting to the condition

$$
\hat{f}_g > \hat{f}_g^{\text{crit}} \equiv \frac{77}{10}\, g_1^2(M_{\text{Pl}}) = \frac{g_1^2(\mu_0)}{\frac{10}{77} - \frac{2\, g_1^2(\mu_0)}{(4\pi)^2} \ln\left(\frac{M_{\text{Pl}}}{\mu_0}\right)} \approx 7.9610 ,
\tag{2.27}
$$

where the numerical value follows from $\alpha^{-1}(\mu_0) = 57.527$ at $\mu_0 = 1$ TeV [68]. Assuming that the above bound is satisfied, the gravity correction will then drive g_1 to zero

asymptotically such that $g_{1\star} = 0$. Then, Eqs. (2.21) and (2.22) take the form

$$\beta^{(1)}(g_B)\Big|_{g_{1\star}=0} = g_B\, E(g_B, \tilde{g}, \hat{f}_g)\,, \tag{2.28}$$

$$\beta^{(1)}(\tilde{g})\Big|_{g_{1\star}=0} = \tilde{g}\, E(g_B, \tilde{g}, \hat{f}_g)\,, \tag{2.29}$$

$$E(g_B, \tilde{g}, \hat{f}_g) = \frac{77}{6}\,\tilde{g}^2 + 11\, g_B^2 - \frac{16}{3} g_B\, \tilde{g} - \hat{f}_g\,. \tag{2.30}$$

The fixed points are given by the Gaussian fixed point $(g_{B\star}, \tilde{g}_\star) = (0,0)$, as well as an ellipse $E(g_{B\star}, \tilde{g}_\star, \hat{f}_g) = 0$. This ellipse is rotated by an angle θ in $g_B\tilde{g}$-plane,

$$\tan\theta = \frac{32}{11 + \sqrt{1145}}\,, \qquad \theta \approx 36^\circ\,. \tag{2.31}$$

The new gauge coupling g_B and the mixing $\tilde{g}$ are bounded by

$$g_B \in \left[0, \sqrt{\frac{231\hat{f}_g}{2413}}\,\right]\,, \qquad \tilde{g} \in \left[-\sqrt{\frac{6\hat{f}_g}{77}}, \sqrt{\frac{198\hat{f}_g}{2413}}\,\right]\,. \tag{2.32}$$

Note that $\tilde{g}$ can be negative, given its relation to the Lagrangian parameter ϵ in Eq. (2.11). It is obvious from these expressions that in the limiting case of $\hat{f}_g \to 0$, that is, for vanishing gravity corrections, the ellipse shrinks to zero size and only the Gaussian fixed point survives. In other words, this non-trivial structure is generated by the gravitational corrections.

In order to understand the behavior in the $g_B\tilde{g}$-sector better, consider a graphical visualization of the two β-functions in Fig. 2.1. As it turns out, the ellipse corresponds to an unstable collection of fixed points, also referred to as "UV repulsive" in the asymptotic safety terminology, where all values inside the ellipse flow towards the Gaussian fixed point $(g_{B\star}, \tilde{g}_\star) = (0,0)$. All values outside the ellipse flow to infinite values. In other words, the ellipse corresponds to a projection of the UV critical surface into the subspace $g_1 = 0$. This implies that the values of g_B and $\tilde{g}$ are not independent if they are required to reach nontrivial fixed point values in the UV.

Given the UV critical surface, it is now pertinent to determine what range of coupling values at $\mu_0 = 1\,\text{TeV}$ flow to those fixed points, where we have selected a value for μ_0 that is representative of high-energy collider physics experiments. Since the UV ellipse of fixed points is unstable, it must be hit exactly when running up from lower energies, leading to greater predictivity than one would obtain in the case of fixed points that are attractive. There arises a technical complication: Since the Gaussian g_1 fixed point is an asymptotic one, attained at infinite energy, it is not possible to fully model this numerically. In order to keep the treatment tractable, we define a large energy scale

$$\ln\left(\frac{\mu_{\text{max}}}{M_{\text{Pl}}}\right) = 100 \ , \tag{2.33}$$

or equivalently, $t_{\text{max}} = \ln(\mu_{\text{max}}/\mu_0) \approx 137$. The scale μ_{max} is approximately 43 orders of magnitude higher than the Planck energy, high enough so that $g_1(\mu_{\text{max}}) \ll 1$ when $\hat{f}_g > \hat{f}_g^{\text{crit}}$. The choice $f_g = 0.1$, for example, gives $g_1(\mu_{\text{max}}) \approx 6.5 \times 10^{-5}$. A linearized analysis of the RG flow near the g_1 fixed point suggests that we may assume that the values of g_B and $\tilde{g}$ at the same scale are given approximately by their fixed point values on the ellipse $E(g_{B\star}, \tilde{g}_\star, \hat{f}_g) = 0$, completing our set of boundary conditions at the high energy scale μ_{max}. This provides us with a method of mapping the UV critical surface to a corresponding surface renormalized at $\mu_0 = 1\,\text{TeV}$. Once this surface is obtained, we may verify by running up from μ_0, to scales even higher than μ_{max}, that the couplings approach the desired fixed point, providing a numerical sanity check of our computations. In Fig. 2.2, we show (i) the exact UV critical surface, (ii) the resulting values at the Planck scale, and, finally, (iii) the resulting values at $\mu_0 = 1\,\text{TeV}$.

We conclude that asymptotically safe solutions with a Gaussian g_1 fixed point and nontrivial fixed points in the $g_B\tilde{g}$-plane lead to a correlation between the parameters g_B and $\tilde{g}$ at low energy scales.

2.3.2.2 Interacting g_1 fixed point

The remaining g_1 fixed point is non-trivial. In our one-loop approximation, the value $g_{1\star}$ obtained at infinite energy is also the value at the Planck scale, since the g_1 β-function vanishes for $\mu \geq M_{\text{Pl}}$ due to the choice of f_g,

$$g_{1\star} = g_1(M_{\text{Pl}}) = \sqrt{\frac{10}{77}\hat{f}_g} \,. \tag{2.34}$$

Since the value of g_1 at the Planck scale is fixed by the experimental value at μ_0, $\hat{f}_g$ is then determined

$$\hat{f}_g = \frac{77}{10}g_{1\star}^2 = \frac{77}{10}g_{\text{Planck}}^2 \equiv \hat{f}_g^{\text{crit}} \approx 7.9610 \,. \tag{2.35}$$

This corresponds to $f_g \approx 0.05$, consistent in magnitude with typical estimates of f_g appearing in the literature [36]. Inserting this critical value $\hat{f}_g^{\text{crit}}$, one finds the two UV fixed points

$$(g_B, \tilde{g}) = (0,0)\,, \quad (g_B, \tilde{g}) = \left(\sqrt{\frac{231\hat{f}_g^{\text{crit}}}{2413}}, \sqrt{\frac{768\hat{f}_g^{\text{crit}}}{185801}}\right)\,. \tag{2.36}$$

We again plot the β-functions in the $g_B\tilde{g}$-sector, albeit now for finite $g_{1\star}$, in Fig. 2.1. In this case, we see that the non-trivial $g_B\tilde{g}$ fixed point is connected to the Gaussian fixed point by a line. All values that fall onto this critical line (aside from the unstable fixed point at the right end) flow towards that Gaussian fixed point, whereas all values outside this interval are driven to infinite values. It is interesting to observe that the range of g_B coincides with the predicted range in the Gaussian g_1 fixed point scenario, whereas the maximum value of $\tilde{g}$ is much smaller. Similar to the previous case, the line represents the projection of the UV critical surface into the subspace $g_1 = g_{1\star}$ and again implies that the values of g_B and $\tilde{g}$ are not independent.

Since the fixed point values of the couplings in Eqs. (2.34)-(2.36) are reached at $\mu =$

M_{Pl}, it is straightforward to flow these back to our reference scale of $\mu_0 = 1\,\mathrm{TeV}$; see Fig. 2.2 for the fixed point coupling values renormalized at $\mu = \infty$, M_{Pl} and $1\,\mathrm{TeV}$. Again, we find a correlation between the parameters g_B and $\tilde{g}$ at low energy scales.
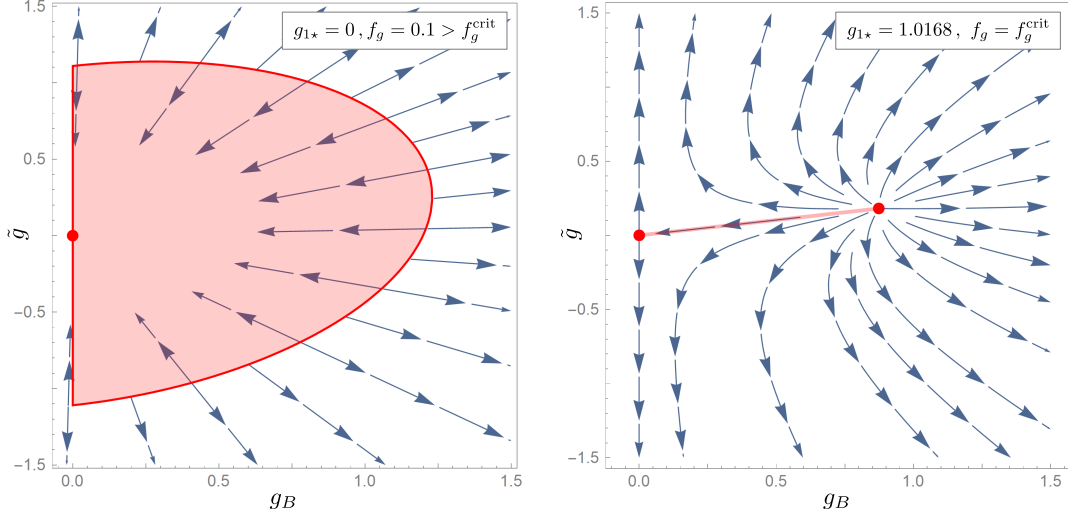
Figure 2.1: UV critical surfaces in the $g_B\tilde{g}$-plane. The interiors of the ellipse and the line are driven to Gaussian fixed points $(g_B, \tilde{g}) = (0, 0)$, whereas the ellipse's boundary and the line's right endpoint are non-trivial fixed points. Couplings outside the ellipse and outside the line interval are driven to infinite values.

2.3.3 Running couplings and stability of the Higgs sector

As is well known, the Higgs vacuum of the standard model is metastable. The model under consideration here has extended Higgs, gauge and fermion sectors, which affect the stability analysis and alter this conclusion. The Higgs potential in our model is given by Eq. (2.8), repeated here for convenience,

$$V = -m_H^2 H^\dagger H + \frac{\lambda}{2}(H^\dagger H)^2 - m_\phi^2 \phi^*\phi + \frac{\lambda_\phi}{2}(\phi^*\phi)^2 + \lambda_m \phi^*\phi H^\dagger H\,, \qquad (2.37)$$
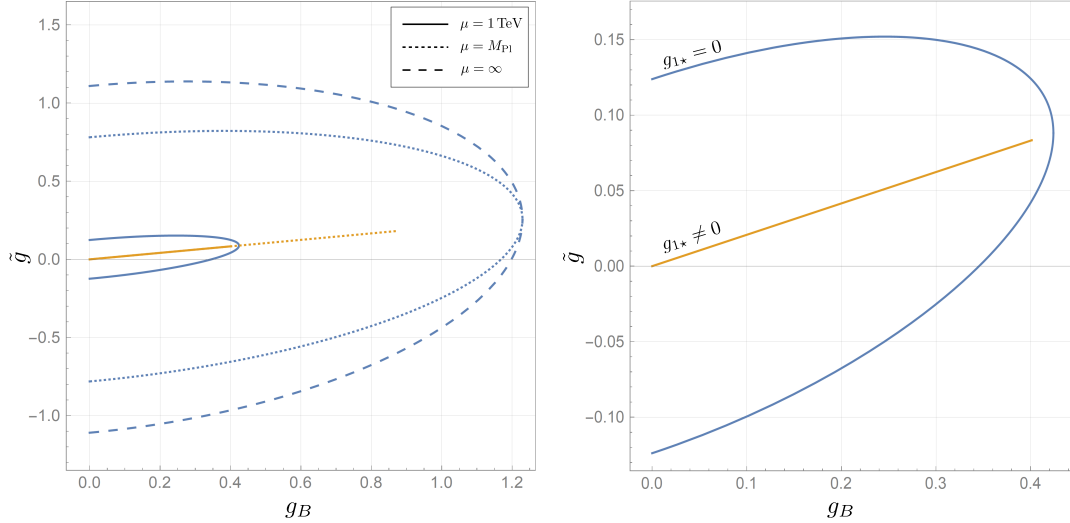
Figure 2.2: Left: UV critical surfaces (dashed line) mapped back to $\mu = M_{\mathrm{Pl}}$ (dotted line) and to $\mu_0 = 1\,\mathrm{TeV}$ (solid line). The Gaussian g_1 fixed point is described by the ellipses and the interacting g_1 fixed point by the line. The requirement that either the boundary of the ellipse or the line is reached leads to a unique relation between g_B and $\tilde{g}$, thereby reducing the degrees of freedom in parameter space of the model. Right: Infrared values in detail.

where λ_m couples the two scalars H and ϕ, and leads to mass mixing after these fields develop vevs. In unitary gauge,

$$H = \frac{1}{\sqrt{2}} \begin{pmatrix} 0 \\ v + h \end{pmatrix}, \quad \phi = \frac{v_\phi + \varphi}{\sqrt{2}}, \tag{2.38}$$

where we have denoted the vevs v and v_ϕ. Substituting into Eq. (2.37), one finds the following mass-squared matrix:

$$M^2 = \begin{pmatrix} \lambda\, v^2 & \lambda_m v\, v_\phi \\ \lambda_m v\, v_\phi & \lambda_\phi v_\phi^2 \end{pmatrix}. \tag{2.39}$$

The two eigenvalues are

$$m_\pm^2 = \frac{1}{2} \left[\lambda\, v^2 + \lambda_\phi v_\phi^2 \pm \sqrt{\lambda^2 v^4 + \lambda_\phi^2 v_\phi^4 - 2\, v^2 v_\phi^2 (\lambda \lambda_\phi - 2\lambda_m^2)} \right]. \tag{2.40}$$

As can be seen from the square root, if $\mathfrak{s} \equiv \lambda\lambda_\phi - \lambda_m^2 < 0$ the eigenvalue m_-^2 will become negative, indicating that we are no longer at a local minimum. This can also be verified via the determinant of the mass-squared matrix,

$$\det M^2 \equiv m_+^2 m_-^2 = v^2 v_\phi^2 (\lambda\lambda_\phi - \lambda_m^2) \equiv v^2 v_\phi^2 \mathfrak{s} \,. \tag{2.41}$$

Therefore, we require that $\mathfrak{s} > 0$ henceforth. This condition is also sufficient to guarantee stability of the potential at large field amplitudes, since Eq. (2.37) can be written as

$$V = -m_H^2 H^\dagger H - m_\phi^2 \phi^* \phi + \frac{\lambda}{2}\left[H^\dagger H + \frac{\lambda_m}{\lambda}\phi^* \phi \right]^2 + \frac{\mathfrak{s}}{2\,\lambda}[\phi^*\phi]^2 \,. \tag{2.42}$$

The last two terms are positive definite when

$$\mathfrak{s} > 0 \quad \text{and} \quad \lambda > 0 \,. \tag{2.43}$$

These inequalities reduce to $\lambda_\phi > 0$ and $\lambda > 0$ in the case where $\lambda_m = 0$, the expected constraints on the quartic terms in two decoupled scalar sectors; for a similar analysis, see Ref. [84]. In studying the RG evolution of the model, we may now track the sign of $\mathfrak{s}$ and λ to confirm that stability of the scalar potential is maintained. We will see in our subsequent examples that this is the case, and is also consistent with the existence of fixed points in the $(\lambda, \lambda_\phi, \lambda_m)$ parameter space that we will explicitly identify.

In the numerical examples that we present in the next two subsections, we adopt the following measured values of the standard model couplings, renormalized at $\mu_0 = 1$ TeV, also used by Hiller *et al.* [68]:

$$g_1(\mu_0) = 0.46738, \qquad g_2(\mu_0) = 0.63829, \qquad g_3(\mu_0) = 1.05737,$$

$$y_t(\mu_0) = 0.85322, \qquad y_b(\mu_0) = 0.01388 \,. \tag{2.44}$$

We take the scale of $U(1)_B$ breaking to be $v_\phi = 10$ TeV, and require that the lightest scalar

mass eigenstate correspond to the Higgs boson, with $m_h = 125$ GeV. To limit the scope of our following considerations somewhat, we choose

$$\lambda_\phi(\mu_0) = 0.2, \qquad \lambda_m(\mu_0) = -0.004 \,. \tag{2.45}$$

We note that the small negative value of $\lambda_m(\mu_0)$ seemed to lead more readily to solutions with the desired vacuum stability. With the Higgs doublet vev set at $v = 246$ GeV, the requirement that we obtain the correct Higgs boson mass then fixes $\lambda(\mu_0) = 0.25828$. The heavier scalar mass eigenstate will then have a mass of 4.472 TeV, heavy enough to not be of immediate phenomenological concern.[5] Finally we set the Yukawa couplings

$$\kappa_i(\mu_0) = y_i(\mu_0) = 0.1 \,, \quad i = 1 \ldots 3, \tag{2.46}$$

and the gravitational correction parameters

$$f_\lambda = f_y = 0.1 \,. \tag{2.47}$$

The value of the gravitational parameter f_g depends on whether we study the Gaussian g_1 fixed point $(f_g > f_g^{\mathrm{crit}})$, or the interacting one $(f_g = f_g^{\mathrm{crit}})$. The values of the remaining couplings and f_g in these two cases are summarized in Table 2.3. Note that the values of f_λ and f_y in Eq. (2.47), as well as the value of f_g assumed in the case of the Gaussian g_1 fixed point, are roughly comparable in magnitude to that of f_g in the interacting g_1 fixed point scenario where the gravitational parameter is determined by the measured value of g_1 at low energies.

---

[5]For example, given these choices, the mixing angle that diagonalizes Eq. (2.39) is $\mathcal{O}(10^{-4})$, compared to the experimental bound from Higgs signal strength measurements that is $\mathcal{O}(10^{-1})$ [69].

case	g_B	$\tilde{g}$	m_B	f_g
$g_{1\star} = 0$:	0.3	0.14988	$3\,\mathrm{TeV}$	$0.1\ (> f_g^{\mathrm{crit}})$
$g_{1\star} \neq 0$:	0.40128	0.08338	$4.01\,\mathrm{TeV}$	$0.05041\ (= f_g^{\mathrm{crit}})$

Table 2.3: Remaining model parameters and Z' masses for the two scenarios described in the text, renormalized at the reference scale $\mu_0 = 1\,\mathrm{TeV}$. The specific values of g_B and $\tilde{g}$ in these two examples were selected since they run to fixed point values $g_{B\star}$ and $\tilde{g}_\star$ that are both nonvanishing. The value of f_g in the $g_{1\star} \neq 0$ case is set by the requirement that the low-energy value of the hypercharge gauge coupling is reproduced.

2.3.3.1 Gaussian g_1 fixed point

In this example, we take $f_g = 0.1 > f_g^{\mathrm{crit}}$ so that we attain a Gaussian fixed point in g_1, and choose $g_B(\mu_0) = 0.3$ and $\tilde{g}(\mu_0) = 0.14988$, which assures that these couplings flow to a point on the UV ellipse of fixed points discussed earlier and displayed in Fig. 2.2. We plot the RG flow in the upper two panels of Fig. 2.3. The Higgs sector remains stable throughout, and by making use of the 1-loop β-functions we find the following fixed points for the quartic couplings:

$$\lambda_\star = 0.065871\,, \quad \lambda_{\phi\star} = 0.014456\,, \quad \lambda_{m\star} = 0.030760\,. \tag{2.48}$$

These values satisfy the stability conditions Eq. (2.43), and we have confirmed that they are approached in the numerical results presented in Fig. 2.3.

2.3.3.2 Interacting g_1 fixed point

Let us now consider $f_g = f_g^{\mathrm{crit}}$ such that we obtain an interacting g_1 fixed point, $g_{1\star} = g_1(M_{\mathrm{Pl}}) = 1.0168$. We further take $g_B(\mu_0) = 0.40128$ and $\tilde{g}(\mu_0) = 0.08338$ (the right endpoint of the solid, TeV line in the second panel of Fig. 2.2) to generate a non-zero fixed point for g_B and $\tilde{g}$ as well.

We plot the corresponding RG flow in the lower two panels of Fig. 2.3. The Higgs
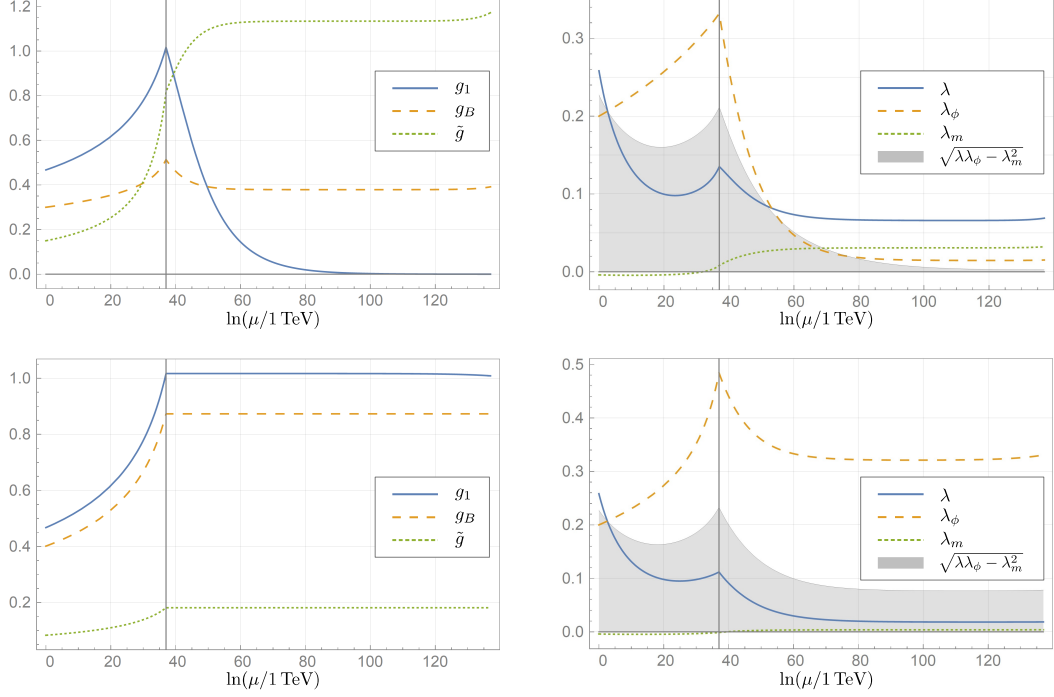
Figure 2.3: Renormalization group flow of the Abelian gauge couplings and the quartic couplings. Top: Gaussian g_1 fixed point, bottom: interacting g_1 fixed point. In the right plots, the shaded areas highlight the value of $\sqrt{\mathfrak{s}} \equiv \sqrt{\lambda\lambda_\phi - \lambda_m^2}$, where $\mathfrak{s}$, λ and λ_ϕ remain positive throughout the entire energy range considered here. The quartic couplings attain their numerically expected fixed point values within our numerical resolution, strongly suggesting stability of the Higgs sector up to arbitrarily high energies. The small deviations of the couplings away from their fixed point values visible at the right sides of the plots is an artifact caused by the finite resolution of our numerical approximation and the fact that the fixed points are unstable. By increasing the resolution of the initial conditions at 1 TeV, these deviations can be pushed out to arbitrarily high energies. At infinite initial resolution, the couplings would hit their fixed point values exactly.

sector again remains stable, and we extract the following fixed points:

$$\lambda_\star = 0.018256\,, \quad \lambda_{\phi\star} = 0.32076\,, \quad \lambda_{m\star} = 0.0037738\,. \tag{2.49}$$

These again are consistent with our stability criteria and agree with our numerical RG flow. In Fig. 2.4, we show the running of couplings in the present scenario compared to that of the standard model, up to the Planck scale. The curve for the quartic coupling in the standard model was computed at two loops and assumes the value of λ_{SM} extracted from the one-loop effective potential, $\lambda_{\mathrm{SM}}(\mu_0) = 0.19234$ [68]; this allows easy comparison

with what is typically displayed in the literature. The dashed line shows what we would find for the coupling λ in our model if we were to assume a boundary value identical to that of the standard model curve and also work at two loops. This illustrates that our model's ability to avoid the metastability of the standard model is a consequence of the new contributions to the β-functions rather than a different boundary condition at the TeV scale caused by the nonvanishing portal coupling λ_m. Analogous plots can be generated for the $g_{1\star} = 0$ scenario, but they are qualitatively indistinguishable from those shown in Fig. 2.4, and are not displayed.
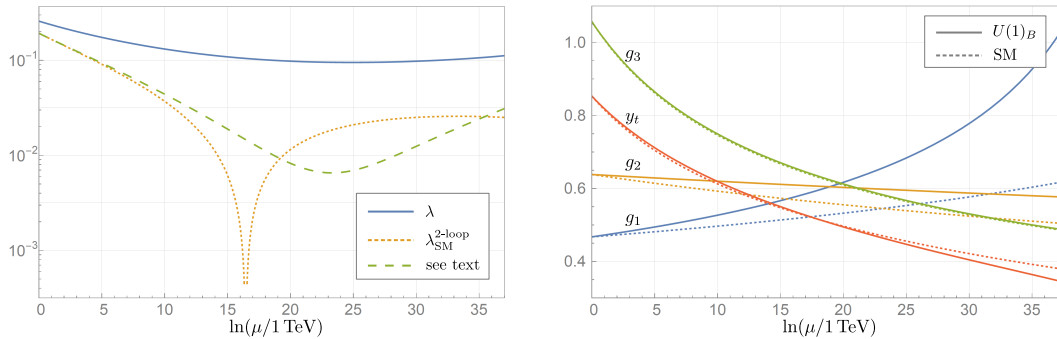
Figure 2.4: Comparison to the standard model. See the text for discussion.

Finally, we note that solutions like those presented in this section can be obtained for other values of the parameters in Eqs. (2.46) and (2.47). This is illustrated in Fig. 2.5, where we allow these parameters to vary and determine whether viable solutions are obtained. The solid circles represent solutions where all couplings reach perturbative ultraviolet fixed points and our conditions for vacuum stability are satisfied. Due to the large number of model parameters, there are many possible two-dimensional plots of this type that one could construct; however, Fig. 2.5 is sufficient to demonstrate that Eqs. (2.46) and (2.47) do not represent special choices.
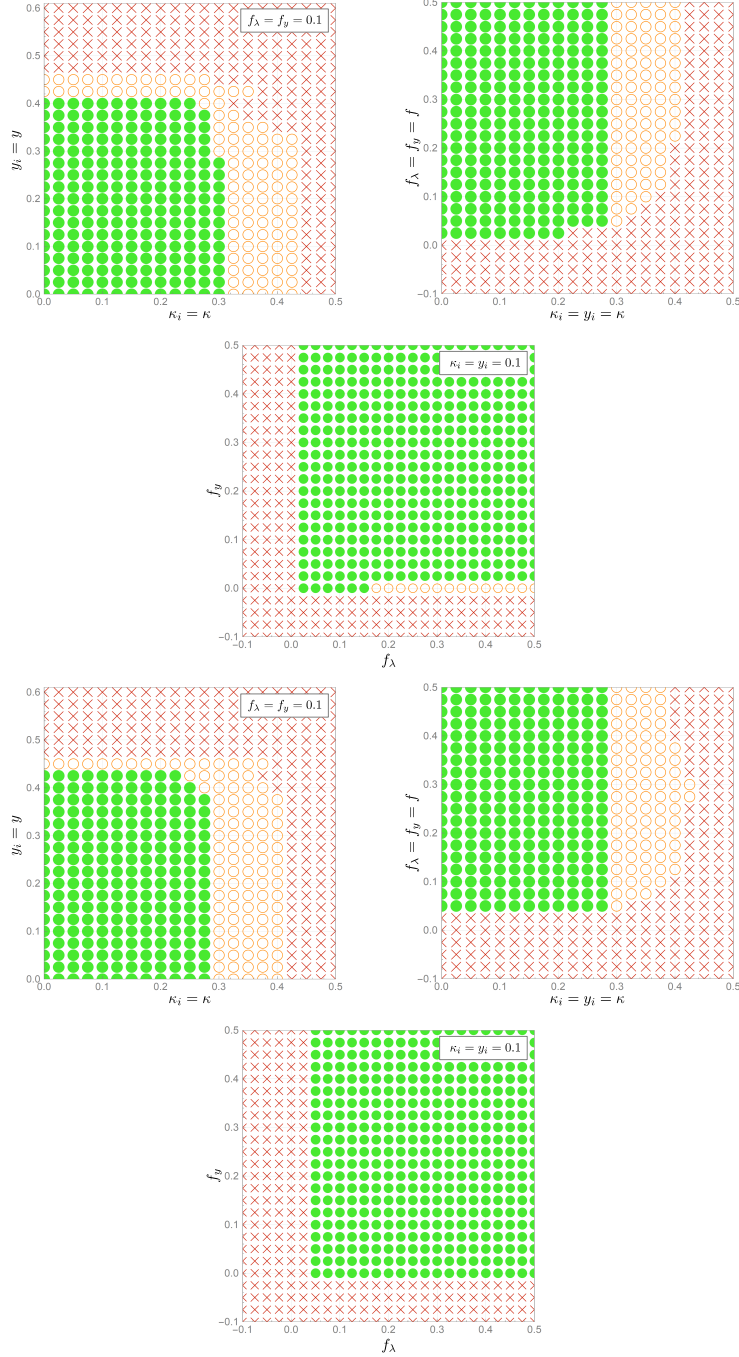
Figure 2.5: The effects of varying input parameter values. The first row corresponds to the Gaussian g_1 fixed point, while the second corresponds to the interacting one. The solid circles indicate viable solutions with perturbative fixed points that satisfy Eq. (2.43) everywhere, while the crosses represent excluded points. The open circles indicate models with vacuum metastability.

2.4 Branching fractions

While it is not the purpose of the present work to engage in an exhaustive phenomenological study of this model (studies of gauged baryon number in a more general context exist in the literature [70–72,85]), we would like to illustrate in this section how the UV restrictions placed on the parameter space at the TeV scale can lead to meaningful predictions of the Z' boson properties. To do so, we focus on the case of the interacting g_1 fixed point, discussion in Secs 2.3.2.2 and 2.3.3.2. In the previous section, we found that the ultraviolet critical surface corresponded to a line segment in the $g_B\tilde{g}$-plane which, when run down to the TeV scale, is given by

$$\tilde{g} = \frac{16}{77}g_B \quad \text{for} \quad 0 \leq g_B \lesssim 0.4013 \ . \tag{2.50}$$

Let us consider the implications of this result for branching fractions of the Z' boson. For a Z' in the multi-TeV mass range, it is a reasonable approximation to neglect the masses of all the standard model particles (we comment on the effect of including them later). In this case, the partial decay widths take relatively simple form. For decays to fermions with N_c colors one has

$$\Gamma(f\bar{f}) = \frac{N_c}{48\pi}\left(C_V^2 + C_A^2\right)m_B g_B^2 \ , \tag{2.51}$$

where the C_V and C_A can be derived from the form of the covariant derivative, Eq. (3.3), and we use Eq. (2.50) to eliminate any dependence on $\tilde{g}$. Numerically, we find that $|C_V|$ is given by 0.8008, 0.6398, 0.2414, and 0.0805 for the up-type quarks, down-type quarks, charged leptons, and neutrinos, respectively; the $|C_A|$ are each 0.0805. This is sufficient to determine the partial width to dijets (including all quarks except the top), and to charged dileptons. We also take into account that there are decays to W^+W^-: this is easiest to compute in the original basis where the coupling ϵ is present in the gauge boson kinetic terms and is treated here as a perturbative interaction. In this case, at lowest order in ϵ, we find (with help from Feyn Calc [86])

$$\Gamma(W^+W^-) = \frac{\alpha \cos\theta_w^2 \epsilon^2}{12}m_B\frac{y^4}{(1-y^2)^2}\sqrt{1-\frac{1}{x^2}}\left(4x^4 + 16x^2 - \frac{3}{x^2} - 17\right) \ , \tag{2.52}$$

where $x = \frac{m_B}{2m_W}$, $y = m_Z/m_B$ and θ_w is the weak mixing angle. Using $m_W = m_Z \cos\theta_w$ and assuming $m_B \gg m_Z$, one may show that this result approaches

$$\Gamma(W^+W^-) \approx \frac{4}{29645\pi} m_B g_B^2 \ , \tag{2.53}$$

provided the kinetic mixing is small. The consequence of Eq. (2.50) is that Eqs. (2.51) and (2.53) are proportional to $m_B g_B^2$, which implies that the Z' branching fractions are approximately fixed provided that the Z' boson is sufficiently heavy and that we live within the range $0 \leq g_B \lesssim 0.4013$. We find that

$$
\begin{aligned}
\mathrm{BF}(Z' \to \mathrm{jets}) &= 77.8\,\% \\
\mathrm{BF}(Z' \to t\bar{t}) &= 19.8\,\% \\
\mathrm{BF}(Z' \to \ell^+\ell^-) &= 2.0\,\% \\
\mathrm{BF}(Z' \to W^+W^-) &= 0.1\,\%
\end{aligned}
\tag{2.54}
$$

with the remainder going to invisible decays (*i.e.*, neutrinos). For example, $m_B = 3$ TeV and $g_B = 0.3$ is a choice that satisfies our assumptions and is consistent with current experimental bounds. For this point in model parameter space, we have checked that the effect of including final state particle masses, including that of the top quark, affects the branching fractions shown above only at the next decimal place. LHC searches for new resonances decaying to dijets allow the Z' of the present model for $m_B = 3$ TeV and $g_B = 0.3$ (see Fig. 3 in Ref. [85], where the value of the coupling to quarks would be 0.6 in their conventions, well within their allowed region.). Moreover, Eq. (2.50) implies the value $\tilde{g} = 0.0623$, corresponding to the kinetic mixing parameter $\epsilon = 0.1321$, consistent with the kinetic mixing bounds in Ref. [87] for a 3 TeV Z'. One might expect the model to provide similar predictivity for heavier Z' bosons which will be less constrained by current experimental bounds.

2.5 Conclusions

We have considered a model with gauged baryon number that is asymptotically safe due to gravitational corrections introduced above the Planck scale. Three generations of vector-like fermions, which are chiral under the baryon gauge symmetry, cancel the gauge and gravitational anomalies in the theory. The baryon number gauge symmetry is spontaneously broken after a new complex scalar field obtains a non-zero vacuum expectation value. By requiring that the couplings flow to asymptotic fixed points, we restrict the parameter space of the model, in some cases relating the kinetic mixing to the baryon gauge coupling. This allows us to predict measurable quantities, such as branching fractions, of the Z' boson at future collider experiments.

The ultraviolet behavior of the model depends on the size of the gravitational corrections. For sufficiently large gravitational correction terms in the RGEs, there exists either a Gaussian fixed point or an interacting fixed point for the GUT-normalized hypercharge coupling, g_1. For each of these cases, we examined the parameter space of the baryon gauge coupling and the kinetic mixing, $(g_B, \tilde{g})$, to find the subspace that flows to ultraviolet fixed points, thereby defining the UV critical surface. In the Gaussian case, there is a stable trivial fixed point for $(g_{B\star}, \tilde{g}_\star) = (0, 0)$ and an unstable ellipse of fixed points whose size is determined by the magnitude of the gravitational correction terms in the RGEs. In the interacting case, one finds a trivial fixed point as well as an unstable non-trivial fixed point. Any value on the line connecting these fixed points flows to the trivial fixed point. Any values off of this line or outside of the ellipse flow to infinite values and correspond to unphysical theories.

In the Higgs sector of our model, we stated the conditions on the quartic couplings for vacuum stability and confirmed that they are satisfied under the RG flow. After fixing values for the couplings at the TeV scale and running them up to fixed points, we included gravitational effects on the trans-Planckian RG flow. Within our stated approximations, we obtained numerical evidence suggesting that the Higgs sector retains its vacuum stability

to arbitrarily high energies, with all of its couplings approaching nontrivial fixed points.

We briefly examine the phenomenology of the model by determining the restrictions on the parameter space at the TeV scale imposed by asymptotic safety. Considering the case where the g_1 fixed point is nonzero, we were able to predict values for the branching fractions of the Z' boson into jets, $t\bar{t}$, charged dileptons, and W^+W^-, from the relationship between the kinetic mixing and baryon gauge coupling. To good approximation, the partial decay widths are proportional to $m_B g_B^2$, when $m_B \gg m_Z$, which implies that the branching fractions are all fixed if the Z' boson is sufficiently massive.

In future work, we look forward to exploring other aspects of the phenomenology of this asymptotically safe gauged baryon number model, including how the heavy vector-like leptons affect the muon $g - 2$ and how a viable dark matter candidate may be included.

Chapter 3

Asymptotically safe dark matter with gauged baryon number[1]

In this chapter we consider the inclusion of TeV-scale, fermionic dark matter in an asymptotically safe model of gauged baryon number of Chapter 2. The new gauge boson serves as a portal between the dark and the visible sectors. The range of the baryon number gauge coupling and the kinetic mixing between baryon number and hypercharge are constrained by the requirement that nontrivial ultraviolet fixed points are reached. We show that this asymptotically safe dark matter model can achieve the correct dark matter relic density while remaining consistent with direct detection bounds.

3.1   Introduction

Asymptotic safety has been used as a principle to restrict the parameter space of a number of beyond-the-standard-model scenarios [36–38, 64–69, 88–96], including models of dark matter [36,37,89], of new contributions to the muon anomalous magnetic moment [37,64], of modified Higgs, neutrino [65,66,90] and gauge sectors [38,67], of B-meson anomalies [69, 91, 92] and of new TeV-scale physics with collider physics implications [68, 93]. In this

---

chapter, we follow up on the model of asymptotically safe gauged baryon number proposed in Chapter 2 (Ref. [88]). There is an extensive literature on the possibility of gauged baryon number; for discussion of the motivations and phenomenology, see, for example, Refs. [70–76]. The most important parameters for determining the properties of the new U(1) gauge boson are the gauge coupling g_B, the gauge boson mass m_B, and a coupling $\tilde{g}$ that determines the kinetic mixing between hypercharge and the U(1)$_B$ gauge group. In the absence of this mixing, the tree-level couplings of the new gauge boson to standard model matter fields are entirely leptophobic; the degree to which the model deviates from leptophobia is determined by the kinetic mixing parameter, making its value of critical importance in determining the phenomenology of the model. One of the benefits of an asymptotically safe version of the gauged baryon number scenario is that the kinetic mixing is fixed in terms of g_B at the TeV scale due to the constraints on the couplings in the deep UV. This leads to greater predictivity. Reference [88] mapped out the ultraviolet fixed points in a simple model of gauged baryon number and discussed the phenomenological consequences, assuming that the scale of new physics (including new fermions to cancel anomalies) was around 1 TeV.

The model of Ref. [88] did not include a dark matter candidate, an omission that we will remedy here. In addition to the TeV-scale particle content included to cancel anomalies, we add a fermion, χ, that is vector-like under U(1)$_B$ and carries no other gauge quantum numbers:

$$\chi_L \sim \chi_R \sim (1, 1, 0, 1/6) \ . \tag{3.1}$$

Here, the first two numbers shown are the dimensionalities of the SU(3)$_C$ and SU(2)$_W$ representations, while the last two are the U(1)$_1$ and U(1)$_B$ charges. We work with the grand unified theory (GUT) normalization of hypercharge, $i.e.$, $g_Y = \sqrt{3/5}\, g_1$ where g_Y is the hypercharge coupling of the standard model; g_B is normalized so that the baryon number of a nucleon is $+1$. The baryon number charge assignment in Eq. (3.1) renders the χ field stable, as we explain in the next section, and allows the U(1)$_B$ gauge field to

serve as a portal between the dark and the visible sectors. Other work on such "baryonic" dark matter candidates appears in Refs. [74–76]. Aside from differences in the particle content and charge assignments that we assume, our approach differs in that we work in the framework of asymptotic safety where both the allowed range of g_B and the value of the kinetic mixing parameter $\tilde{g}$ are constrained by the ultraviolet boundary conditions on the theory. With $\tilde{g}$ predicted in terms of g_B, we include leptonic channels in the new gauge boson decay width and the dark matter annihilation cross section, without introducing dependence on an additional free parameter. In addition, our calculation of the relic density incorporates a relativistic treatment of the thermally averaged dark matter annihilation cross section times relative velocity, which is expected to be more accurate for the near-resonant annihilation [97] that we encounter in the present study.

The purpose of the present work is to establish three important conceptual results that may motivate more detailed phenomenological studies in future work, namely: (1) that our model provides a natural symmetry mechanism for establishing dark matter stability, (2) that the introduction of dark matter does not qualitatively alter the asymptotic fixed point structure found in our earlier model of gauged baryon number, and (3) that viable dark matter solutions exist for a number of qualitatively different fixed point scenarios. Discussion of these points is organized as follows. In Sec. 3.2 we consider the choice in Eq. (3.1), how dark matter stability is assured, and how the fixed-point structure of the model of Ref. [88] is affected by the additional particle content. In Sec. 3.3, we study the dark matter relic density, and in Sec. 3.4 we consider the direct detection bounds for points in model parameter space where the correct relic density is obtained. We summarize our conclusions in Sec. 4.5.

3.2   Gauged baryon number model

The model of Ref. [88] includes the U(1)$_B$ gauge boson B_μ, a scalar field ϕ with baryon number $+1$, and a number of new fermions that are introduced to cancel gauge and grav-

itational anomalies. The new gauge boson and fermions become massive when ϕ acquires a vacuum expectation value (vev); we assume their mass spectrum lies at or above 1 TeV. The charge assignments of the fields can be found in Ref. [88]; what is important here is that the magnitudes of the baryon number charges $|Q_B|$ are either 0, 1/3 or 1. Under a $U(1)_B$ phase rotation $\exp(i\,Q_B\,\alpha)$, all of these fields are left invariant in the case where $\alpha = 6\pi$. On the other hand, the field χ in Eq. (3.1) changes sign under that action of the same group element. This establishes that there is a Z_2 symmetry which is a subgroup of $U(1)_B$ and that remains unbroken after spontaneous symmetry breaking. Since the χ field is the only field that is odd under this symmetry, its stability is guaranteed, making it a potential dark matter candidate. The fact that the stabilizing symmetry is a subgroup of a gauge symmetry renders it safe from violation by any possible quantum gravitational effects.

The hypercharge and $U(1)_B$ gauge fields can mix through their kinetic terms,

$$\mathcal{L} \supset -\frac{1}{4}F_Y^{\mu\nu}F_{\mu\nu}^Y - \frac{1}{4}B^{\mu\nu}B_{\mu\nu} + \frac{\epsilon}{2}B^{\mu\nu}F_{\mu\nu}^Y \ . \tag{3.2}$$

We follow a standard approach of working in a basis where the kinetic terms are diagonal and canonically normalized, but where the gauge-covariant derivative for a generic field Ψ takes the form [36, 38, 88]

$$D_\mu\Psi = [\partial_\mu - i\,g_B B_\mu Q_B - i\,(g_1 A_\mu^Y + \tilde{g}\,B_\mu)Q_1]\,\Psi\,. \tag{3.3}$$

Here, Q_B and $Q_1 = \sqrt{3/5}\,Q_Y$ denote the baryon number and hypercharges of Ψ, respectively, and $\tilde{g} = \epsilon\,g_1/\sqrt{1-\epsilon^2}$.

The one-loop β functions for g_1, g_B and $\tilde{g}$ (computed using PyR@TE 3 [27]) are

$$\beta^{(1)}(g_1) = \frac{77}{10}g_1^3 - \hat{f}_g g_1\,\theta(\mu - M_{\text{Pl}})\,,$$

$$\beta^{(1)}(g_B) = \frac{298}{27}g_B^3 - \frac{16}{3}g_B^2\tilde{g} + \frac{77}{6}g_B\tilde{g}^2 - \hat{f}_g g_B\,\theta(\mu - M_{\text{Pl}})\,, \tag{3.4}$$

$$\beta^{(1)}(\tilde{g}) = \frac{77}{6}\tilde{g}^3 - \frac{16}{3}\tilde{g}^2 g_B + \frac{298}{27}\tilde{g}g_B^2 + \frac{77}{5}\tilde{g}g_1^2 - \frac{16}{5}g_1^2 g_B - \hat{f}_g\tilde{g}\,\theta(\mu - M_{\text{Pl}})\,.$$

We use the notation $\beta(g) = \beta^{(1)}(g)/(4\pi)^2$ and $\hat{f}_g \equiv (4\pi)^2 f_g$, for convenience. The inclusion of gravitational correction terms to the gauge coupling β functions, with a universal parameter $\hat{f}_g$, is motivated by functional renormalization group (RG) calculations [36–38]. (For an alternative approach towards realizing asymptotic safety, see Ref. [80, 98–100]; for work that casts doubt on this approach, see Ref. [101].) The general one-loop gravitational contributions to the gauge β functions were first computed in Ref. [82] and found to be independent of gauge coupling, but renormalization scheme dependent, with $f_g \geq 0$. We make an assumption that is standard in the phenomenological literature that $f_g > 0$, which is obtained in schemes that break specific gauge-gravity symmetries, defined by Eq. (26) in Ref. [82]. Since the RG running of g_1 decouples from that of g_B and $\tilde{g}$, we will distinguish between two different fixed point scenarios, corresponding to the solution of

$$\left(\frac{77}{10}g_{1\star}^2 - \hat{f}_g\right)g_{1\star} = 0\,. \tag{3.5}$$

A non-trivial, interacting fixed point is obtained provided that $\hat{f}_g$ has a critical value $\hat{f}_g^{\text{crit}} = \frac{77}{10}g_{1\star}^2$; in this case, g_1 remains constant and nonvanishing above the Planck scale, with $\hat{f}_g^{\text{crit}} \approx 7.9610$ to match the experimental value of g_1 at the electroweak scale [88]. For $\hat{f}_g$ larger than the critical value, the gravitational term drives g_1 to a trivial, Gaussian fixed point. In either case, the requirement that g_1 reaches a fixed point constrains the evolution of the remaining couplings g_B and $\tilde{g}$. Their flow as one evolves to higher renormalization scales is shown graphically in Fig. 3.1.

When g_1 flows to its Gaussian fixed point, the locus of fixed points in the $g_B\tilde{g}$-plane is
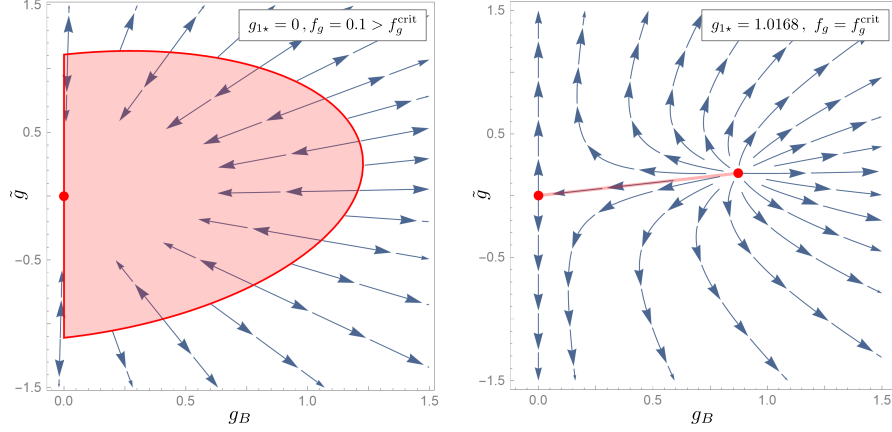
Figure 3.1: Visualization of the RG flow in the $g_B\tilde{g}$-plane. The inside of the ellipse and the interior of the line segment are driven to the Gaussian fixed point $(g_B, \tilde{g}) = (0,0)$; the ellipse's boundary and the line's right endpoint are non-trivial fixed points. In the conventions adopted here, the arrows on the flow lines point towards the UV.

constrained to the ellipse $E(g_{B\star}, \tilde{g}_\star, \hat{f}_g) = 0$, where

$$E(g_B, \tilde{g}, \hat{f}_g) = \frac{77}{6}\tilde{g}^2 + \frac{298}{27}g_B^2 - \frac{16}{3}g_B\tilde{g} - \hat{f}_g \,. \tag{3.6}$$

Points inside this ellipse flow toward $(g_{B\star}, \tilde{g}_\star) = (0,0)$, while points outside flow to infinite radius. Loosely speaking, the gravitational correction factor f_g sets the size of this ellipse. On the other hand, when g_1 flows to its interacting fixed point, there are two $g_B\tilde{g}$ fixed points connected by a line segment in the $g_B\tilde{g}$-plane,

$$\tilde{g} = \frac{16}{77}\, g_B \,. \tag{3.7}$$

The end point $(g_{B\star}, \tilde{g}_\star) = (0.87145, 0.18108)$ is an unstable fixed point, while points on the interior of the line segment flow to a trivial fixed point at $(g_{B\star}, \tilde{g}_\star) = (0,0)$. While the largest fixed point coupling values shown in Fig. 3.1 are of order unity, the relevant expansion parameter is $\alpha_i/(4\pi) \equiv g_i^2/(16\pi^2)$, where g_i represents either g_B or $\tilde{g}$. Hence, we expect the higher-loop contributions to the β functions to be small compared to the one-loop results included here.

52

The inclusion of the dark matter particle χ changes the β functions from those given in Ref. [88]. However, the numerical effects are small and the pattern of fixed points and flow lines remains qualitatively unchanged. Given the multitude of choices for ultraviolet fixed points, we will limit our consideration to what are plausibly three representative cases:

(ia) Interacting g_1 fixed point: One end of the line segment shown in Fig. 3.1 is an unstable fixed point with $(g_{1\star}, g_{B\star}, \tilde{g}_\star) = (1.0168, 0.87145, 0.18108)$ and $\hat{f}_g^{\rm crit} \approx 7.9610$. The requirement of reaching an unstable fixed point leads to the greatest predictivity in the low-energy theory. At 1 TeV, the couplings are $(g_1, g_B, \tilde{g}) = (0.46738, 0.40049, 0.083219)$. Note that $\tilde{g} = 16/77\, g_B$ is preserved by the RG flow.

(ib) Interacting g_1 fixed point: Choosing a point on the interior of the line segment with $\tilde{g} = 16/77\, g_B$ at 1 TeV and $\hat{f}_g^{\rm crit} \approx 7.9610$ again yields an interacting fixed point for g_1, but g_B and $\tilde{g}$ now flow to Gaussian fixed points. For this example, we take $g_B = 0.2$, *i.e.*, $(g_1, g_B, \tilde{g}) = (0.46738, 0.20000, 0.041558)$ at 1 TeV; this flows to $(g_{1\star}, g_{B\star}, \tilde{g}_\star) = (1.0168, 0, 0)$.

(ii) Gaussian g_1 fixed point: We choose $f_g = 0.1$, below the critical value, so that g_1 flows to a Gaussian fixed point. Choosing a point on the ellipse provides nontrivial fixed points for g_B and $\tilde{g}$. For easy comparison to case (ib), we choose a solution for which $g_B = 0.2$ at 1 TeV: we assume $(g_{1\star}, g_{B\star}, \tilde{g}_\star) = (0, 0.209651, 1.13654)$ which leads to the 1 TeV values $(g_1, g_B, \tilde{g}) = (0.46738, 0.20000, 0.15067)$.

In each of these cases, at least one coupling flows to a non-trivial fixed point, corresponding to an asymptotically safe scenario. It is worth stressing that f_g is treated as a phenomenological parameter, which allows us to reproduce the desired value of g_1 at the electroweak scale in cases (ia) and (ib), and to freely choose a representative value of f_g in case (ii). In this sense, we follow a bottom-up approach, like that of Ref. [37]. Alternatively, in specific quantum gravitational scenarios and specific truncations, one may relate f_g to the gravitational constant and the cosmological constant (for discussion, see Ref. [36]); while

motivated by functional renormalization group studies, the effective phenomenological approach remains somewhat agnostic to the details of the gravitational physics.

In what follows, we will evaluate the constraints on the model parameter space from the dark matter relic density and direct detection bounds.

3.3   Relic density

To good approximation, the dark matter χ remains in thermal equilibrium as long as the annihilation rate to standard model particles exceeds the expansion rate of the universe. Dark matter annihilation to standard model fermions via exchange of the $U(1)_B$ gauge boson provides the dominant contribution to the annihilation cross section. We will see later that the kinetic mixing produces roughly a 15% correction to the annihilation cross section, by allowing dark matter annihilation to dileptons. The nonvanishing kinetic mixing also allows gauge-gauge and gauge-Higgs final states, but we find that they contribute less than $\sim 0.3\%$ to the total annihilation cross section. Effects due to mixing in the ϕ-Higgs sector, which were studied in Ref. [88], are much smaller, at least for parameter choices where asymptotic safety has been demonstrated in the model. In particular, the mixing angle between the ϕ and Higgs boson was found in Ref. [88] to be $\mathcal{O}(10^{-4})$, so that annihilation to ϕ-Higgs and Higgs-Higgs final states are negligible compared to the leading contributions.

Given our assumption that the new fermions in the model have TeV-scale masses, we neglect the mass of standard model fermions, aside from that of the top quark. The cross section for annihilation into a standard model fermion f is given by

$$\sigma\left(\chi\bar{\chi} \to f\bar{f}\right) = \frac{N_c\, g_B^4}{1728\,\pi} \frac{1}{s} \sqrt{\frac{s - 4\,m_f^2}{s - 4\,m_\chi^2}}\left(s + 2\,m_\chi^2\right) \left[\frac{C_V^2(s + 2\,m_f^2) + C_A^2(s - 4\,m_f^2)}{(s - m_B^2)^2 + \Gamma^2\,m_B^2}\right]. \quad (3.8)$$

Here, N_c is the number of colors, m_f, m_χ, and m_B are the masses of the standard model fermion, the dark matter particle, and the $U(1)_B$ gauge boson, respectively, and Γ is the

gauge boson decay width. The partial decay width to an $f\bar{f}$ final state is given by

$$\Delta\Gamma\left(B \to f\bar{f}\right) = \frac{N_c\,g_B^2\,m_B}{48\,\pi}\sqrt{1 - \frac{4m_f^2}{m_B^2}}\left[C_V^2\left(1 + \frac{2m_f^2}{m_B^2}\right) + C_A^2\left(1 - \frac{4m_f^2}{m_B^2}\right)\right]. \quad (3.9)$$

The coefficients C_V and C_A are vector and axial-vector couplings in units of g_B. One finds numerically that $|C_V|$ is given by 0.8008, 0.6398, 0.2414, and 0.0805 for up-type quarks, down-type quarks, charged leptons, and neutrinos, respectively, whereas the $|C_A|$ are all 0.0805.

Dark matter falls out of thermal equilibrium at the freeze-out temperature T_f, which we determine by the condition

$$\frac{\Gamma}{H(T_f)} \equiv \frac{n_\chi^{EQ}\langle\sigma v\rangle}{H(T_f)} \approx 1. \quad (3.10)$$

Here, n_χ^{EQ} is the equilibrium number density and $H(T) = 1.66\sqrt{g_*}\,T^2/M_{\mathrm{Pl}}$ is the Hubble parameter for a radiation dominated universe written in terms of the number of relativistic degrees of freedom, g_*, and the Planck mass $M_{\mathrm{Pl}} = 1.22 \times 10^{19}$ GeV. For a radiation dominated universe, it is appropriate to assume the non-relativistic equilibrium number density

$$n_\chi^{\mathrm{EQ}} = 2\left(\frac{m_\chi T}{2\pi}\right)^{3/2} e^{-m_\chi/T}. \quad (3.11)$$

A relativistic treatment of the thermally averaged annihilation cross section times relative velocity is given by [97]

$$\langle\sigma v\rangle = \frac{1}{8m_\chi^4 T K_2^2\left(\frac{m_\chi}{T}\right)} \int_{4m_\chi^2}^\infty \mathrm{d}s\,\sigma_{tot} \times (s - 4m_\chi^2)\sqrt{s}K_1\left(\frac{\sqrt{s}}{T}\right), \quad (3.12)$$

where the K_i are modified Bessel functions of order i. For the sufficiently large freeze-out temperatures considered in this analysis, the ratio of the equilibrium number density to

55

the entropy density at freeze-out, Y_f, is given by

$$Y_f = 0.145 \frac{g}{g_*} x_f^{3/2} e^{-x_f} , \qquad (3.13)$$

where $x_f \equiv m_\chi / T_f$ and $g = 4$ is the number of internal degrees of freedom of the dark matter particles plus antiparticles. This ratio at freeze-out can then be propagated to the ratio Y_0 at the present temperature of the universe,

$$\frac{1}{Y_0} = \frac{1}{Y_f} + \sqrt{\frac{\pi}{45}} M_{\text{Pl}} m_\chi \int_{x_f}^{x_0} \mathrm{d}x \frac{\sqrt{g_*}}{x^2} \frac{\langle \sigma v \rangle}{2} , \qquad (3.14)$$

where the factor of $1/2$ takes into account that annihilation only occurs between a dark matter particle and its antiparticle, while the Y_i in this expression include both [97].

The dark matter relic density is then given by

$$\Omega_{\text{D}} h^2 \approx \frac{2.8 \times 10^8}{\text{GeV}} Y_0\, m_\chi . \qquad (3.15)$$

We now compute the relic density in each of the previously described cases (ia), (ib), and (ii). This analysis relies on numerical integration which can be performed to high accuracy. Since the couplings are fixed by the asymptotic safety criterion, the only free parameters entering this analysis are the dark matter mass m_χ as well as the $U(1)_B$ gauge boson mass m_B. The latter is assumed to be in the TeV-range, comparable to the masses of the other heavy fermions; see Ref. [88] for details.

To analyze how the choice of these mass parameters affects the predicted relic density, we scan over the gauge boson mass m_B and determine the relic density as a function of m_χ; Fig. 3.2 shows results for three choices of m_B. A resonance effect is apparent when $m_B \approx 2\, m_\chi$. At this resonance, the total cross section assumes a maximum value related to the gauge boson decay width, resulting in a minimum relic density. The value of the minimum relic density increases as the mass of the the $U(1)_B$ gauge boson increases, because the gauge boson width scales with m_B. The observed dark matter relic density
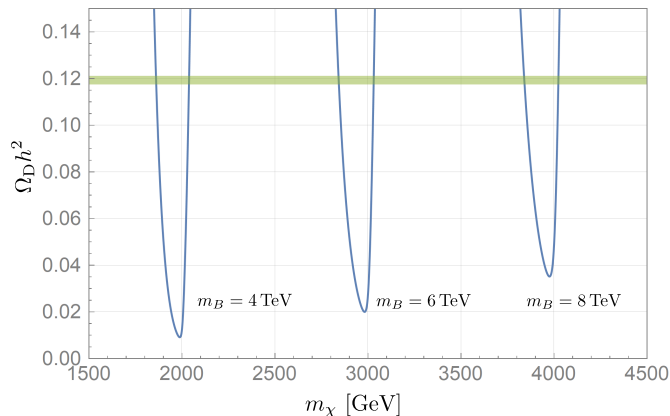
Figure 3.2: Relic density curves for several choices of m_B. The horizontal band represents the observed value $\Omega_{\rm D} h^2 = 0.1193 \pm 0.0009$ [102].

is [102]

$$\Omega_{\rm D} h^2 = 0.1193 \pm 0.0009 \,. \tag{3.16}$$

In Fig. 3.2 we superpose this band; for a given m_B, there are two disconnected mass ranges for m_χ in which a relic density consistent with observation is obtained. The allowed ranges of m_χ can be extracted as a function of m_B for each asymptotically safe scenario defined in Sec. 3.2; these will be used in the study of the dark matter-nucleon elastic scattering cross section in the next section.

3.4   Direct detection

For each point in model parameter space that leads to the correct relic density, we must check that the experimental bounds from the direct detection of dark matter-nucleon elastic scattering are satisfied. We consider only the most stringent bounds that follow from the spin-independent scattering cross section. For TeV-scale dark matter, the momentum transfer in the relevant t-channel Feynman diagrams can be neglected, $q^2 \approx 0$. The effective dimension-six operators, which are suppressed by $1/m_B^2$, have vector-vector, vector-axial

vector, and axial vector-axial vector parts. Only the vector-vector part, *i.e.* the $\bar{\chi}\gamma^\mu\chi\bar{q}\gamma_\mu q$ operator, contributes to the spin-independent cross section [103–105]. Nucleon matrix elements of a quark vector current have form factors that simply count the number of quarks, so there is no hadronic uncertainty in going from quark to nucleon matrix elements. For example, elastic scattering off a nucleon $N = p$ or n in our model is given by

$$\sigma_N = \frac{g_B^4}{36\,\pi}\frac{\mu_{\chi N}^2}{m_B^4}\left(1 + \sqrt{\frac{3}{5}}c_N\frac{\tilde{g}}{g_B}\right)^2 \, , \tag{3.17}$$

where $c_N = 1/4$ or $3/4$ for a neutron or proton, respectively, and $\mu_{\chi N} = m_\chi m_N/(m_\chi + m_N)$ is the dark matter-nucleon reduced mass. To compare to experimental bounds, we take into account that the dark matter scatters coherently off of the entire nucleus so we must sum over protons and neutrons in the amplitude. To obtain an effective dark matter-nucleon cross section we then divide the cross section by the square of the atomic mass number. For a Xenon target, with atomic number 54 and atomic mass 131.293, we find

$$\sigma_{\text{SI}} = \frac{g_B^4}{36\,\pi}\frac{\mu_{\chi N}^2}{m_B^4}\left(1 + 0.35\,\frac{\tilde{g}}{g_B}\right)^2 \, , \tag{3.18}$$

where numerically we use an average mass for the nucleon, $m_N \approx 939$ MeV. We note that in the limit $\tilde{g} = 0$, our result agrees with the cross section given in Ref. [74]; for sample points (ia) and (ib), $\tilde{g} = \frac{16}{77}g_B$ and the kinetic mixing term represents a 15% correction. In Fig. 3.3, for each of the asymptotically safe scenarios defined in Sec. 3.2, we display σ_{SI} for parameter choices corresponding to relic densities within two standard deviations of the central value as per Eq. (3.16). We compare to the bounds from the PandaX–II experiment [106], which uses a Xenon detector and constrains TeV-scale dark matter masses. All three scenarios considered here are allowed by current experimental bounds for dark matter masses $m_\chi \gtrsim 1.5$ TeV.

Finally, we note that the DARWIN experiment [107] may probe the mass range shown in Fig. 3.3. For example, for a dark matter mass of 1 TeV, the projected cross section reach
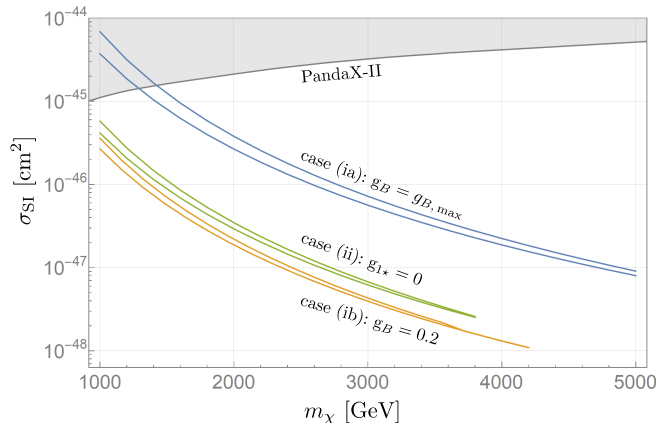
Figure 3.3: Spin-independent dark matter-nucleon elastic scattering cross sections σ_{SI}, for parameter choices (m_χ, m_B) that yield the correct dark matter relic density.

of DARWIN, assuming 200 ton-years of exposure, is $\sim 2 \times 10^{-48}$ cm^2 [107], compared to the current Xenon1T bound of $\sim 9 \times 10^{-46}$ cm^2 [108]. However, we know of no published projections of DARWIN's sensitivity to dark matter in the 1 to 5 TeV mass range considered here. The model might also be probed at the LHC though a variety of final states with observable particles and large missing transverse momentum, or through indirect studies of the contribution of dark matter annihilation to the hadronic component of the cosmic ray spectrum, but establishing specific bounds would require separate dedicated analyses.

3.5   Conclusions

In this chapter, we have modified the gauged baryon number model proposed in Chapter 2 to include a TeV-scale, fermionic dark matter candidate. The stability of the dark matter is guaranteed by a discrete subgroup of the additional gauge symmetry, and the new gauge boson serves as the portal between the dark and visible sectors. The new ingredient in our study is the assumption of asymptotic safety, which reduces the space of free model parameters due to the constraint that (at least some) couplings reach nontrivial ultraviolet fixed points. The effect of this organizing principle is that the range of the baryon number gauge coupling at the TeV scale is constrained, and the kinetic mixing parameter at the

same scale becomes a function of the baryon number gauge coupling. This fixes the degree of gauge boson leptophobia once the gauge coupling of the theory is specified. Taking into account these constraints, and including the leptonic dark matter annihilation channels that are induced by the kinetic mixing, the correct dark matter relic density can be obtained in a number of asymptotically safe scenarios with different patterns of ultraviolet fixed points. For these solutions, the predicted dark matter-nucleon elastic scattering cross section is consistent with the bounds from the PandaX–II experiment [106] which probes the dark matter masses above 1 TeV. Measurements of new gauge boson properties at colliders and of the dark matter-nucleon elastic scattering cross section at direct-detection experiments may someday provide nontrivial tests of the relationships between couplings expected in this and other asymptotically safe gauge extensions of the standard model.

Chapter 4

Note on scattering in asymptotically nonlocal theories[1]

It is possible to formulate theories with many Lee-Wick particles such that a limit exists where the low-energy theory approaches the form of a ghost-free nonlocal theory. Such asymptotically nonlocal quantum field theories have a derived regulator scale that is hierarchically smaller than the lightest Lee-Wick resonance; this has been studied previously in the case of asymptotically nonlocal scalar theories, Abelian and non-Abelian gauge theories, and linearized gravity. In this chapter we consider the dependence on center-of-mass energy of scattering cross sections in these theories. While Lee-Wick resonances can be decoupled from the low-energy theory, scattering amplitudes nonetheless reflect the emergent nonlocality at the scale where the quadratic divergences are regulated. This implies observable consequences in theories designed to address the hierarchy problem, even when the Lee-Wick resonances are not directly accessible.

---

[1]Work previously published in C. D. Carone and M. R. Musser, "Note on scattering in asymptotically nonlocal theories," Phys. Rev. D **108**, no. 9, 095015 (2023).

4.1 Introduction

As discussed in Chapter 4, it is possible to formulate a class of theories that interpolates between Lee-Wick theories and ghost-free nonlocal theories: these are the asymptotically nonlocal theories described in Refs. [113–116]. An asymptotically nonlocal theory is one of a sequence of finite-derivative theories that approaches a ghost-free nonlocal theory as a limit point. We review the construction of asymptotically nonlocal theories in Sec. 4.2. In an ordinary Lee-Wick theory, the scale at which quadratic divergences are cancelled is set by the mass of the lightest Lee-Wick resonance. For example, if one were to decouple the Lee-Wick partners in the Lee-Wick Standard Model, fine-tuning in the Higgs boson squared mass would be reintroduced. In asymptotically nonlocal theories, the Lee-Wick partners may be heavy, while the light scalar mass is regulated by an emergent nonlocal scale $M_{\rm nl}$, that is hierarchically smaller than the lightest Lee-Wick resonance mass, m_1,

$$M_{\rm nl}^2 \sim \mathcal{O}\left(\frac{m_1^2}{N}\right) . \tag{4.1}$$

Here, N is the number of propagator poles in a given theory, which provides a source of parametric suppression [113–116]. Note that approaches to achieving a parametric suppression of the regulator scale have appeared in other contexts in the literature [117, 118].

Asymptotically nonlocal theories have been explored previously in scalar theories [113], Abelian [114] and non-Abelian gauge theories [115], and in linearized gravity [116]. These papers discussed the higher-derivative and auxiliary field formulation of these theories (that is, equivalent theories in which higher-derivative terms are eliminated in favor of additional fields). These papers also demonstrated the emergence of the nonlocal regulator scale in a variety of loop amplitudes, and in resolving gravitational singularities. However, what was not considered was the implications for scattering cross sections. For example, if asymptotically nonlocal theories interpolate between Lee-Wick and ghost-free nonlocal

theories, how is this transition reflected in the dependence of scattering cross sections on center-of-mass energy? If propagators fall off exponentially with Euclidean momentum in asymptotically nonlocal theories, does one expect scattering amplitudes to grow without bound above the emergent nonlocal scale, given that the momentum transfers are not Euclidean? (We will see later that the answer is no.) In general, one expects that the physics associated with the emergent nonlocal regulator scale should also be apparent in scattering amplitudes as the Lee-Wick resonances are decoupled. We explore this expectation in the present note by considering the momentum-dependence of an s-channel scattering cross section in an asymptotically nonlocal toy model that captures the qualitative features one expects to find in more realistic theories. This fills a gap in the discussion that appeared in the previous literature [113–116].

This chapter is organized as follows. In Sec. 4.2, we review the construction of asymptotically nonlocal theories, including our assumptions about how the limiting nonlocal theory is reached. We define the model that we study later and discuss the form of the self-energy corrections to the propagator in the higher-derivative formulation of the theory. Loop corrections encode the resonance widths, which truncate the growth in the scattering amplitudes that is associated with the emergent nonlocality. In Sec. 4.3, we show in a simple example that the same results are obtained whether one works in the higher-derivative or (with more effort) in the auxiliary-field formulation of the theory. In Sec. 4.4, we describe how we implement mass and wave function renormalization in the higher-derivative theory and we present numerical results for the momentum dependence of the amplitudes that are of interest to us. In Sec. 4.5, we summarize our conclusions.

4.2 Framework and a toy model

Our framework can be illustrated in a theory of a real scalar field ϕ: We seek a sequence of theories that approaches the nonlocal form

$$\mathcal{L}_\infty = -\frac{1}{2}\phi\left(\Box + m_\phi^2\right)e^{\ell^2\Box}\phi - V(\phi) \tag{4.2}$$

as a limit point. The exponential of the box operator shown in Eq. (4.2) is familiar from the literature on ghost-free nonlocal theories [17, 57, 109–112], and regulates loop integrals at the scale $1/\ell$. A theory that approaches Eq. (4.2) when $N \to \infty$ is given by

$$\mathcal{L} = -\frac{1}{2}\phi\left(\Box + m_\phi^2\right)\left(1 + \frac{\ell^2\Box}{N-1}\right)^{N-1}\phi - V(\phi)\,, \tag{4.3}$$

However, the propagator in this theory contains an $(N-1)^{\text{th}}$ order pole, which has no immediate particle interpretation. We can remedy this by taking the ℓ_j to be nondegenerate,

$$\mathcal{L}_N = -\frac{1}{2}\phi\left(\Box + m_\phi^2\right)\left[\prod_{j=1}^{N-1}\left(1 + \frac{\ell_j^2\Box}{N-1}\right)\right]\phi - V(\phi)\,, \tag{4.4}$$

which approaches the same limiting theory, Eq. (4.2), provided that ℓ_j approach a common value ℓ as N becomes large. For finite N, the propagator is given by

$$D_F(p^2) = \frac{i}{p^2 - m_\phi^2}\prod_{j=1}^{N-1}\left(1 - \frac{\ell_j^2 p^2}{N-1}\right)^{-1}\,. \tag{4.5}$$

This has N first-order poles; the massive states associated with the higher-derivative quadratic terms have masses $m_j^2 \equiv (N-1)/\ell_j^2$. The results of Refs. [113–116] were not sensitive to how the $N \to \infty$, $\ell_j \to \ell$ limit was reached. A convenient parameterization was given by

$$m_j^2 = \frac{N}{\ell^2}\frac{1}{1 - \frac{j}{2N^P}}\,, \qquad \text{for } j = 1 \ldots N-1\,, \tag{4.6}$$

for $P > 1$. Away from the limit point, the propagator in Eq. (5.4) can be decomposed using partial fractions as a sum over simple poles with residues of alternating signs (a familiar outcome in higher-derivative theories [56]). These correspond to an alternating tower of ordinary particles and ghosts. We refer the reader to Ref. [113] for the construction of an auxiliary field formulation that holds for arbitrary N. We will discuss an auxiliary field formulation that is useful in the case where $N = 2$ in Sec. 4.3.

Writing the tree-level propagator in terms of the resonance masses m_j, one has

$$D_F(p^2) = \frac{i}{(p^2 - m_\phi^2) \prod_{j=1}^{N-1} (1 - p^2/m_j^2)} \ , \tag{4.7}$$

The product in the denominator approaches a growing exponential for Euclidean momentum, which accounts for the better convergence properties of loop amplitudes discussed in Refs. [113–116]. To study the consequences of this form in scattering, we couple the ϕ field to complex scalar fields χ_a, for $a = 1, 2$:

$$\mathcal{L}_{toy} = \mathcal{L}_N^{(2)} - \chi^{a*} \left(\Box + m_\chi^2 \right) \chi^a - g \, \phi \, \chi^{a*} \chi^a \ . \tag{4.8}$$

Here the summation on a is implied, and $\mathcal{L}_N^{(2)}$ represents the quadratic terms

$$\mathcal{L}_N^{(2)} = -\frac{1}{2} \phi \left(\Box + m_\phi^2 \right) \left[\prod_{j=1}^{N-1} \left(1 + \frac{\ell_j^2 \Box}{N-1} \right) \right] \phi \ . \tag{4.9}$$

Motivated by simplicity, we have assumed that the $\phi \, \chi^{a*} \chi^a$ coupling is the only scalar interaction term, and we consider the s-channel scattering process $\chi_1 \chi_1 \rightarrow \chi_2 \chi_2$ in the center-of-mass frame. We focus on s-channel processes as they are often associated with large momentum transfers in realistic theories at colliders, and they provide a relatively direct way to study the energy-dependence implied by the distinctive form of the propagators found in asymptotically nonlocal theories. We expect that the example we study will provide a qualitative understanding of s-channel processes in these theories, independent

Figure 4.1: Full ϕ propagator

of the precise choice of fields appearing on the external lines or the spin of the exchanged particle. The study of a completely general scalar potential may be interesting but goes beyond the scope of the present work. The product in the denominator of Eq. (5.6) approaches an exponential that rapidly decreases as a function of the squared center-of-mass energy s, above the emergent nonlocal scale $M_{\mathrm{nl}} \equiv 1/\ell$. What prevents arbitrary growth of the propagator is the widths of the resonances (just as it would be had we chosen, for example, $s = m_\phi^2$). To capture that physics, we define the one-particle irreducible self-energy function $-iM^2(p^2)$ and compute the full propagator shown in Fig. 4.1. The diagrammatic resumation gives

$$D_F^{\mathrm{full}} = \frac{i}{(p^2 - m_\phi^2)\prod_{j=1}^{N-1}(1 - p^2/m_j^2) - M^2(p^2)} \, , \tag{4.10}$$

which reduces to the familiar expression [39] when $N = 1$, where the product is replaced by the identity. We will see in Sec. 4.4 that the imaginary part of $M^2(p^2)$ limits the maximum value of the scattering amplitude.

4.3 Equivalent approaches

Before considering the implications of the momentum dependence of Eq. (4.10), we briefly digress to consider the general form of this expression. In an auxiliary field formulation of the higher-derivative theory, the higher-derivative terms are eliminated in favor of additional fields (each corresponding to a propagator pole). In that theory, there are a number of possible one-particle irreducible self energy diagrams, depending on the choice of external lines. Here we look at the scattering process $\chi_1\chi_1 \to \chi_2\chi_2$ in the auxiliary theory in the simplest case of $N = 2$ and show how the loop corrections conspire to exactly reproduce the

corrected form of the higher-derivative propagator in Eq. (4.10). We expect this to hold for arbitrary N on general grounds; however, this example illustrates how computations that are easy in the higher-derivative form of the theory can become prohibitively complicated in its auxiliary form. Hence, in Sec. 4.4, we return to working with the higher-derivative theory.

In the case where $N = 2$, the Lagrangian is given by

$$\mathcal{L} = -\frac{1}{2}\hat{\phi}\,(\Box + m_\phi^2)(1 + \ell^2 \Box)\,\hat{\phi} + \mathcal{L}_{\text{int}} \ , \tag{4.11}$$

where the Lee-Wick partner to the particle with mass m_ϕ has mass $M \equiv 1/\ell$, and $\mathcal{L}_{\text{int}}$ contains the coupling to the χ fields. We assume $M > m_\phi$. We place a hat on the field that appears in the higher-derivative form of the theory for later notational convenience. An equivalent theory can be identified using an auxiliary field $\widetilde{\phi}$:

$$\mathcal{L} = -\frac{1}{2}\left(1 + \frac{m_\phi^2}{M^2}\right)\hat{\phi}\,\Box\,\hat{\phi} - \widetilde{\phi}\,\Box\,\hat{\phi} + \frac{1}{2}M^2\widetilde{\phi}^2 - \frac{1}{2}m_\phi^2\,\hat{\phi}^2 + \mathcal{L}_{\text{int}} \ . \tag{4.12}$$

The $\widetilde{\phi}$ is non-dynamical and can be eliminated from the generating functional for the theory by performing the corresponding Gaussian functional integral. Operationally, the resulting Lagrangian is what one obtains from Eq. (4.12) by replacing $\widetilde{\phi}$ using its equation of motion,

$$\widetilde{\phi} = \frac{1}{M^2}\Box\hat{\phi} \ . \tag{4.13}$$

With this substitution, one recovers Eq. (4.11). It is convenient to rescale $\hat{\phi} = \xi^{-1}\hat{\phi}_1$ and $\widetilde{\phi} = \xi\widetilde{\phi}_1$, with

$$\xi \equiv \left(1 + \frac{m_\phi^2}{M^2}\right)^{1/2} \ , \tag{4.14}$$

so that

$$\mathcal{L} = -\frac{1}{2}\hat{\phi}_1\,\Box\,\hat{\phi}_1 - \widetilde{\phi}_1\,\Box\,\hat{\phi}_1 + \frac{1}{2}M^2\xi^2\widetilde{\phi}_1^2 - \frac{1}{2}\xi^{-2}m_\phi^2\,\hat{\phi}_1^2 + \mathcal{L}_{\text{int}} \ . \tag{4.15}$$

Shifting $\hat{\phi}_1 = \phi_1 - \widetilde{\phi}_1$ leads to the following form:

$$\mathcal{L} = -\frac{1}{2}\Phi^T \Box \mathcal{K}\Phi - \frac{1}{2}\Phi^T \mathcal{M}\Phi + \mathcal{L}_{\text{int}} \tag{4.16}$$

where

$$\Phi \equiv \begin{pmatrix} \phi_1 \\ \widetilde{\phi}_1 \end{pmatrix} , \quad \mathcal{K} = \begin{pmatrix} 1 & 0 \\ 0 & -1 \end{pmatrix} \quad \text{and} \quad \mathcal{M} = \xi^{-2}m_\phi^2 \begin{pmatrix} 1 & -1 \\ -1 & 1 - \xi^4 \frac{M^2}{m_\phi^2} \end{pmatrix} . \tag{4.17}$$

The kinetic matrix $\mathcal{K}$ has the form one expects in a Lee-Wick theory, with one field having a canonically normalized, but wrong-sign kinetic term. The mass squared matrix $\mathcal{M}$ is off-diagonal. A transformation of the form $\Phi = R\Phi_0$ with

$$R = \begin{pmatrix} \cosh\theta & \sinh\theta \\ \sinh\theta & \cosh\theta \end{pmatrix} \tag{4.18}$$

will leave $\mathcal{K}$ unchanged but can be used to diagonalize $\mathcal{M}$. We find that this is the case for

$$\theta = \frac{1}{2}\ln\left(\frac{M^2 - m_\phi^2}{M^2 + m_\phi^2}\right) , \tag{4.19}$$

which leads to the simple form

$$R = \frac{1}{\sqrt{M^4 - m_\phi^4}}\begin{pmatrix} M^2 & -m_\phi^2 \\ -m_\phi^2 & M^2 \end{pmatrix} . \tag{4.20}$$

. In terms of the mass eigenstate fields Φ_0, the Lagrangian becomes

$$\mathcal{L} = -\frac{1}{2}\Phi_0^T \left(\Box \mathcal{K}_0 + \mathcal{M}_0\right)\Phi_0 + \mathcal{L}_{\text{int}} , \tag{4.21}$$

where

$$\Phi_0 \equiv \begin{pmatrix} \phi_0 \\ \widetilde{\phi}_0 \end{pmatrix} , \quad \mathcal{K}_0 = \begin{pmatrix} 1 & 0 \\ 0 & -1 \end{pmatrix} \quad \text{and} \quad \mathcal{M}_0 = \begin{pmatrix} m_\phi^2 & 0 \\ 0 & -M^2 \end{pmatrix} . \tag{4.22}$$

This result reproduces the same propagator poles expected in the higher-derivative theory, Eq. (4.11).

The field redefinitions that led to Eq. (4.22) allow us to rewrite $\hat{\phi}$ in terms of the mass eigenstate fields

$$\hat{\phi} = \frac{M}{\sqrt{M^2 - m_\phi^2}} [\phi_0 - \widetilde{\phi}_0] \ . \tag{4.23}$$

The interaction assumed in our toy model, shown in Eq. (4.8), then becomes

$$\mathcal{L}_{\text{int}} = -g \frac{M}{\sqrt{M^2 - m_\phi^2}} v_0^T \Phi_0 \chi^* \chi \ , \tag{4.24}$$

where we define $v_0^T \equiv (1, -1)$. In the Φ_0 field basis, the self-energy function can be written as a two-by-two matrix, $-iM^2(p^2)_{\alpha\beta}$, where the indices represent either ϕ_0 or $\widetilde{\phi}_0$. The full matrix propagator takes the form

$$D_F^{\text{full}}(p^2) = i \left[p^2 \mathcal{K}_0 - \mathcal{M}_0 - M^2(p^2) \right]^{-1} \ . \tag{4.25}$$

However, the self-energy matrix in Eq. (4.25) can be expressed in terms of the self-energy function that appears in the higher-derivative theory:

$$M^2(p^2)_{\alpha\beta} = [v_0 v_0^T]_{\alpha\beta} \frac{M^2}{M^2 - m_\phi^2} \hat{M}^2(p^2) \ . \tag{4.26}$$

One can understand Eq. (4.26) as follows: the one-χ-loop amplitude following from Eq. (4.24) is the same as in the higher-derivative theory, up to the prefactors appearing in Eq. (4.26). Higher-loop contributions may involve additional internal χ loops, as well as ϕ_0 and $\widetilde{\phi}_0$ internal lines, where the latter will always appear together and re-sum to give the higher-derivative propagator for $\hat{\phi}$. Hence, the function $\hat{M}^2(p^2)$ is diagrammatically the same as the one appearing in the higher-derivative theory. Using the vertex in Eq. (4.24) the

69

Feynman amplitude for the s-channel process $\chi_1\chi_1 \to \chi_2\chi_2$ is given by

$$i\mathcal{A}(\chi_1\chi_1 \to \chi_2\chi_2) = \frac{-i\,g^2 M^2}{M^2 - m_\phi^2}\, v_0^T \left[p^2 \mathcal{K}_0 - \mathcal{M}_0 - [v_0 v_0^T]\frac{M^2}{M^2 - m_\phi^2}\,\hat{M}^2(p^2)\right]^{-1} v_0 \ . \quad (4.27)$$

With the matrix structure of Eq. (4.27) completely specified, one may evaluate the inverse and simplify. One finds

$$i\mathcal{A}(\chi_1\chi_1 \to \chi_2\chi_2) = -g^2 \frac{i}{(p^2 - m_\phi^2)(1 - p^2/M^2) - \hat{M}^2(p^2)} \ , \quad (4.28)$$

which precisely reproduces the form expected in the higher-derivative formulation, following from Eq. (4.10), when $N = 2$. For larger N, it is clearly preferable to work directly with the higher-derivative form of the loop-corrected propagator, avoiding the field redefinitions and other avoidable algebra that was illustrated by this example. We use the higher-derivative approach in the section that follows.

4.4 Energy dependence of amplitudes

To evaluate a scattering amplitude that contains the full propagator in Eq. (4.10), we must adopt an explicit form for the self-energy function $M^2(p^2)$. In the theory presented in Eq. (4.8), one finds at one-loop using dimensional regularization[2] that

$$M^2(p^2) = -\frac{n_\chi g^2}{16\pi^2}\int_0^1 dx\left[\frac{2}{\epsilon} - \gamma + \ln 4\pi - \ln\frac{\Delta}{\mu^2}\right]$$
$$= -\frac{n_\chi g^2}{16\pi^2}\left[\int_0^1 dx\left[\frac{2}{\epsilon} - \gamma + \ln 4\pi - \ln\frac{|\Delta|}{\mu^2}\right] + i\pi\sqrt{1 - \frac{4m_\chi^2}{p^2}}\,\Theta(p^2 - 4\,m_\chi^2)\right] \ , \quad (4.29)$$

where $n_\chi = 2$ is the number of χ fields, $\Delta \equiv m_\chi^2 - x(1-x)\,p^2$ and Θ is the Heaviside step function. For $p^2 > 4\,m_\chi^2$, the self-energy has an imaginary part, which approaches a constant value when $p^2 \gg m_\chi^2$. The logarithmic divergence in Eq. (4.29) is absent in

---

[2]Alternatively, one could use a cut off regulator with the on-shell renormalization scheme discussed later, with no effect on the results.

physical quantities after mass and wave function renormalization.[3] Since the quadratic
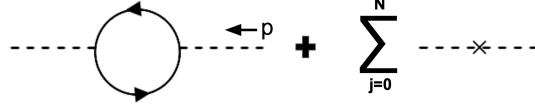
Figure 4.2: One-loop diagram corresponding to the ϕ self-energy with counterterms proportional to $a_k\,p^{2k}$.

operator in our theory takes the form of a polynomial in $\Box$, as can be seen in Eq. (5.3), we can define our renormalized theory as

$$\mathcal{L}_N = -\frac{1}{2}\phi\,(\Box + m_\phi^2)\left[\prod_{j=1}^{N-1}\left(1 + \frac{\Box}{m_j^2}\right) - \sum_{k=0}^{N}\delta_k\,\Box^k\right]\phi - V(\phi)\;, \qquad (4.30)$$

where m_ϕ and the $N-1$ masses m_j are physical masses and the δ_k correspond to counterterms that will be determined by renormalization conditions. It follows from Eq. (4.30) that the renormalized propagator is

$$D_F^{\text{full}} = \frac{i}{(p^2 - m_\phi^2)\prod_{j=1}^{N-1}(1 - p^2/m_j^2) - M_r^2(p^2)}\;, \qquad (4.31)$$

where

$$M_r^2(p^2) = M^2(p^2) - \sum_{k=0}^{N}a_k\,p^{2k}\;, \qquad (4.32)$$

with $a_k \equiv -\delta_k(-1)^k$. The coefficients a_k need to be fixed by $N+1$ renormalization conditions. Taking into account that Lee-Wick particles are unstable, we require that the location of the propagator poles on the real axis correspond to the physical masses m_j, giving us N conditions

$$\text{Re}\,M_r^2(m_j^2) = 0\;, \qquad j = 0\ldots N-1, \qquad (4.33)$$

[3]One could alternatively consider the possibility that the χ-sector is asymptotically nonlocal, which would lead to a much more cumbersome, but finite, one-loop self-energy function. Such a complication is unnecessary for the present study.

where $m_0 \equiv m_\phi$. Fixing the wave function renormalization of the ϕ field in the higher-derivative theory gives us the remaining condition. As ϕ is only relevant for internal lines in the diagrams of interest to us, there are no problems introduced by leaving the wave function renormalization at any pole non-canonical, as no compensating factors need to be introduced in the scattering amplitudes of interest. Hence, we make a convenient choice for the remaining condition

$$\mathrm{Re}\, M_r^2(0) = 0 \ . \tag{4.34}$$

Note that this is equivalent to identifying g as the physical coupling defined at the reference point $p^2 = 0$. Eq. (4.34) determines the coefficient a_0 which absorbs the divergent part of Eq. (4.29):

$$a_0 = -\frac{n_\chi g^2}{16\pi^2} \left[\frac{2}{\epsilon} - \gamma + \ln 4\pi - \ln \frac{m_\chi^2}{\mu^2} \right] \ . \tag{4.35}$$

With this choice, the remaining conditions, Eq. (4.33), may be written

$$\mathrm{Re}\, M_r^2(m_j^2) = \frac{n_\chi g^2}{16\pi^2} \int_0^1 dx \, \ln \left(\frac{|m_\chi^2 - x(1-x)m_j^2|}{m_\chi^2} \right) - \sum_{k=1}^N a_k \, m_j^{2k} = 0 \ , \tag{4.36}$$

for $j = 0 \ldots N - 1$. These N equations allow one to solve for the remaining coefficients and therefore the full loop-corrected propagator. Defining $\mathrm{Re}\, M_r^2(m_j^2) = \tilde{M}^2(m_j^2) - \sum_{k=1}^N a_k \, m_j^{2k} = 0$, we may write Eq. (4.36) in matrix form

$$
\begin{pmatrix}
\tilde{M}^2(m_0^2) \\
\tilde{M}^2(m_1^2) \\
\vdots \\
\tilde{M}^2(m_{N-1}^2)
\end{pmatrix}
=
\begin{pmatrix}
m_0^2 & m_0^4 & \cdots & m_0^{2N} \\
m_1^2 & m_1^4 & \cdots & m_1^{2N} \\
 & & \vdots & \\
m_{N-1}^2 & m_{N-1}^4 & \cdots & m_{N-1}^{2N}
\end{pmatrix}
\begin{pmatrix}
a_1 \\
a_2 \\
\vdots \\
a_N
\end{pmatrix}
, \tag{4.37}
$$

or more compactly, $\tilde{M}_i = m_{ij}\, a_j$. Hence, the desired coefficients may be computed numerically by evaluating

$$a_k = [m^{-1}]_{kj}\, \tilde{M}_j \ . \tag{4.38}$$

Note that the a_k for $k = 1 \ldots N$ are independent of $1/\epsilon$ and represent finite radiative corrections that vanish when $g \to 0$.
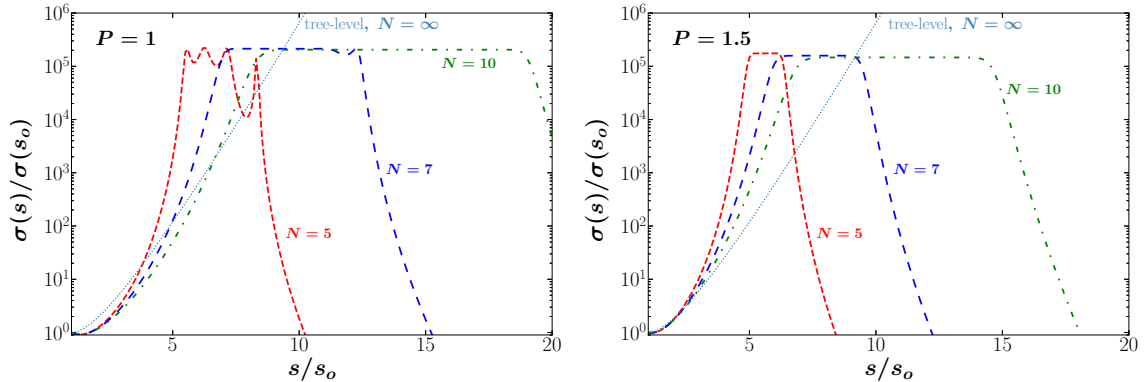
Figure 4.3: Dependence of the scattering cross section for $\chi_1\chi_1 \to \chi_2\chi_2$ with the squared center of mass energy s, normalized to the cross section at $s_0 = M_{\mathrm{nl}}^2$ for the values of N and P shown. In units where $M_{\mathrm{nl}} = 1$, this example corresponds to the choices $g = 1$, $m_\phi = 0.01$ and $m_\chi = m_\phi/4$.

As discussed earlier, we focus on the s-channel scattering process $\chi_1\chi_1 \to \chi_2\chi_2$. The choice of different χ fields in the initial and final state eliminates t- and u-channel diagrams, which do not affect our qualitative conclusions but would complicate the discussion. We plot the s-dependence of the scattering amplitudes for both $P = 1$ and $P = 1.5$, where P is the parameter appearing in Eq. (5.5). Note that for $P > 1$, Eq. (5.5) implies that all the m_j approach a common value as $N \to \infty$. This is not the case for $P = 1$ when j is of order N. However, it was found in Ref. [113] that even in this case loop amplitudes approach the asymptotically nonlocal form, with Euclidean loop momenta exponentially suppressed above an emergent nonlocal scale. Hence, we present this case here as well.

Results for the scattering cross section, for a number of choices for N (the total number of poles), and for $P = 1$ and $P = 1.5$ are shown in Fig. 4.3. The cross section results are normalized to their values when $\sqrt{s}$ is set equal to the nonlocal scale, $i.e.$, $s = M_{\mathrm{nl}}^2$. We see that the results for $P = 1$ and $P = 1.5$ are qualitatively similar. The cross section plots have a region in s immediately above the nonlocal scale where the cross section grows, with the growth gradually approaching the exponential form expected in the nonlocal limiting theory as N becomes large. The cross section levels off in the resonance region above the mass of the first Lee-Wick particle, with hints of resonants peaks visible at the smaller values of N and P, due to the smaller overlap between adjacent resonances. We

do not expect the product in Eq. (4.31) to approximate an exponential as the resonance region is approached for two reasons: (1) mathematically, the product deviates from its exponential limiting form as s increases at finite N, and (2) this rapidly decreasing term is eventually surpassed by the contribution from the self-energy term as s increases. Above the resonance region, the result falls off as the square of the highest power of momentum in the polynomial that appears in the propagator denominator. Our numerical results in Fig. 4.3 are consistent with these expectations. We also note that the normalization factor $\sigma(s_0)$ asymptotes to a constant as N becomes large, so the results shown do not hide any uncontrolled growth or suppression.[4]

Previous work on asymptotic nonlocality focused on loop amplitudes where momentum is Euclidean after Wick rotation. At higher-loop order, the full propagator may appear within other loops, which motivates us to check the behavior of Eq. (4.31) for Euclidean momentum. In Fig. 4.4, we plot the magnitude of the propagator for Euclidean values of the s-channel momentum (normalized to the same quantity evaluated at $s = -M_{\mathrm{nl}}^2$), as a point of comparison. We see that the results monotonically decrease with increasing $|s|$ and approach the exponential form of the limiting theory with increasing N. This is qualitatively consistent with the behavior encountered in the study of loop amplitudes in Refs. [113–115].

Finally, it is interesting to note that in the cross section examples we present in Fig. 4.3, the range in $\sqrt{s}$ that we consider is relatively small, a factor of at most ~ 4.5 between the smallest and largest values. Yet within this range, one can see an energy dependence for the scattering cross section that differs from what one might expect to find in either a simple Lee-Wick theory or a ghost-free nonlocal theory. This may make these class of theories phenomenologically distinguishable from the other two in realistic theories, at least in the case where it is possible experimentally to probe the relevant range of center-of-mass energies.

---

[4]For example, in units where $M_{\mathrm{nl}} = 1$ and $s_0 = M_{\mathrm{nl}}^2$, we find numerically that $\sigma(s_0) = a_0 + b_0/N + c_0/N^2 + \mathcal{O}(1/N^3)$, with $a_0 = 17.187$, $b_0 = 7.826$ and $c_0 = 5.526$, in the case where $P = 1$, assuming the other parameter choices given in the caption of Fig. 4.3.
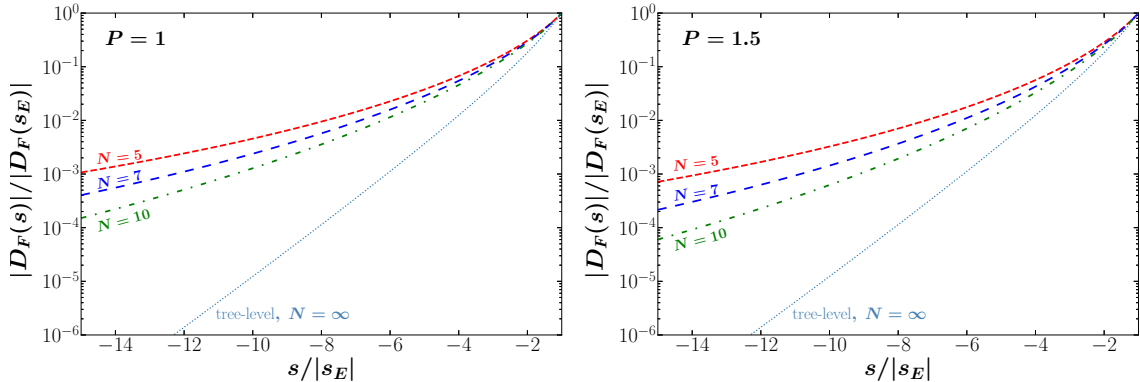
Figure 4.4: Dependence of the magnitude of the full propagator, at one loop, for Euclidean s, normalized to the same quantity evaluated at $s_E = -M_{\mathrm{nl}}^2$ for the values of N and P shown. In units where $M_{\mathrm{nl}} = 1$, this example corresponds to the choices $g = 1$, $m_\phi = 0.01$ and $m_\chi = m_\phi/4$.

4.5   Conclusions

Asymptotically nonlocal theories are a sequence of Lee-Wick theories that approach a ghost-free nonlocal theory in their low-energy limit [113–116]. The nonlocal modification of the quadratic terms that is obtained in the limiting theory suggests that a derived nonlocal regulator scale will emerge in theories with a finite number of Lee-Wick particles, as the appropriate limit is approached. This regulator scale is hierarchically smaller than the mass of the lightest Lee-Wick resonance, and its emergence has been explored in past work on scalar field theories [113], gauge theories [114,115] and in linearized gravity [116]. The regulator appears because the nonlocal form factor in the limiting theory provides a suppression factor for Euclidean momentum, and hence a faster fall-off in the Wick-rotated propagators that appear in loop diagrams. For simple scattering processes, where momentum transfers are not Euclidean, one may worry that the effect of the form factor is to cause all scattering amplitudes to diverge. This is not the case, for the same reason that propagators are not infinite when the center-of-mass energy sits exactly at a resonance value: the growth is limited by the resonance width. In the present case, we take the resonance widths into account by including the self-energy in the propagator, working in the higher-derivative form of the theory for arbitrary N. We showed in the simple case

where $N = 2$ that the same results are obtained whether one formulates the problem in the higher-derivative or Lee-Wick forms of the theory, where the latter exchanges higher-derivative terms for additional fields; however, the higher-derivative form is easier to work with as the number of propagator poles N becomes large.

With the self-energy included in the propagator in an s-channel scattering process in a simple toy model, we identified mass and wave function renormalization conditions and explored how the propagator behaves as moved towards the asymptotically nonlocal limit; we considered the case where the squared momentum transfer s flowing through the propagator is positive (relevant for scattering) or negative (relevant for loop amplitudes due to Wick rotation). For $s > 0$ we found that cross sections will grow above the nonlocal scale, will plateau in the region of Lee-Wick resonances, and then fall off at s larger than the heaviest resonance. The region of growth gradually approaches an exponential form as N increases and the maximum is determined by the imaginary part of the self-energy in the higher-derivative theory. On the other hand, for $s < 0$, one finds monotonic suppression as $|s|$ becomes large, with the magnitude of the propagator approaching a dying exponential in the same way.[5] This is consistent with the behavior that leads to an emergent regulator scale in loop amplitudes discussed in our earlier work [113–116].

The growth of cross sections with center-of-mass energy followed by a broad resonant plateau and then subsequent fall off is neither the qualitative behavior of a simple Lee-Wick theory nor a ghost-free nonlocal theory; this is not surprising since the model we study interpolates between the two. Qualitatively, the first signs of growth in the cross section due to emergent nonlocality might not look very different at a collider experiment (assuming a realistic theory) from what one might expect from the tail of a heavy resonance whose mass is just outside an experiment's kinematic reach. Since such heavy resonances are not observed, the bounds on the emergent nonlocality scale are likely in the multi-TeV range. An exact bound would require a dedicated collider analysis in a realistic theory,

---

[5]In fact, one can show that the deviation of the finite-N result from the exponential limiting form is what one would expect for an exponential that is approximated by a product, as in Eq. (5.3).

which may be of interest for future work.

Chapter 5

Dijet spectrum in nonlocal and asymptotically nonlocal theories[1]

Asymptotically nonlocal field theories approximate ghost-free nonlocal theories at low energies, yet are theories of finite order in the number of derivatives. These theories have an emergent nonlocal scale that regulates loop diagrams and can provide a solution to the hierarchy problem. Asymptotic nonlocality has been studied previously in scalar theories, Abelian and non-Abelian gauge theories with complex scalars, and linearized gravity. In this chapter we extend that work by considering an asymptotically nonlocal generalization of QCD, which can be used for realistic phenomenological investigations. In particular, we derive Feynman rules relevant for the study of the production of dijets at hadron colliders and compute the parton-level cross sections at leading order. We use these to determine a bound on the scale of new physics from Large Hadron Collider data, both for a typical choice of model parameters, and in the nonlocal limit.

5.1 Introduction and Framework

As discussed in Chapter 1, the Lee-Wick Standard Model (LWSM), like the minimal super-symmetric extension of the Standard Model, predicts heavy particles that have not been observed. While new particle masses can always be pushed just above current experimental bounds, doing so gradually reintroduces the unwanted fine-tuning needed to keep the Higgs boson mass close to the weak scale. While the precise amount of fine-tuning that is tolerable may be debated, the reintroduction of fine tuning motivates consideration of higher-derivative theories that do not predict unobserved heavy particles at the TeV scale.

Nonlocal theories present such a possibility (see, for example, Refs. [17, 57, 109, 111, 119–121]). In these theories, the mass and kinetic terms in the Lagrangian are typically modified by a nonlocal form factor, an infinite-derivative operator that is an entire function of $\Box/\Lambda_{\mathrm{nl}}^2$, where $\Box \equiv \partial_\mu \partial^\mu$ and Λ_{nl} is the nonlocal scale. Such a choice modifies the ultraviolet behavior of propagators without introducing additional poles. The simplest constructions have employed the exponential of the $\Box$ operator, as in this generalization of the theory of a real scalar field:

$$\mathcal{L}_\infty = -\frac{1}{2}\phi \left(\Box + m_\phi^2\right) e^{\ell^2 \Box} \phi - V(\phi) \ . \tag{5.1}$$

Here $\ell \equiv 1/\Lambda_{\mathrm{nl}}$. The ϕ propagator involves a factor of $e^{\ell^2 p^2}$ which becomes $e^{-\ell^2 p_E^2}$ in loop amplitudes after Wick rotation, where p_E is the Euclidean momentum. This leads to improved convergence, with Λ_{nl} serving as a regulator scale.

Asymptotically nonlocal theories represent another possibility, one that interpolates between Lee-Wick theories and ghost-free nonlocal theories [113–116, 122]. These theories allow the decoupling of the Lee-Wick particles without reintroducing the fine-tuning problem due to the emergence of a derived regulator scale (*i.e.*, one that does not appear as a fundamental parameter in the Lagrangian) that is hierarchically smaller than the lightest Lee-Wick resonance mass. Asymptotically nonlocal theories have been explored in the

recent literature in the context of scalar theories [113], Abelian gauge theories [114], non-Abelian gauge theories [115] and linearized gravity [116]. To review the basic construction, we note that Eq. (5.1) is recovered from

$$\mathcal{L} = -\frac{1}{2}\phi\left(\Box + m_\phi^2\right)\left(1 + \frac{\ell^2\Box}{N-1}\right)^{N-1}\phi - V(\phi) , \qquad (5.2)$$

in the limit that N is taken to infinity. At finite N, this theory is not quite what we want, since the ϕ propagator has an $(N-1)^{\text{th}}$ order pole, which does not have a simple particle interpretation. However, we can obtain the same limiting form by working instead with

$$\mathcal{L}_N = -\frac{1}{2}\phi\left(\Box + m_\phi^2\right)\left[\prod_{j=1}^{N-1}\left(1 + \frac{\ell_j^2\Box}{N-1}\right)\right]\phi - V(\phi) , \qquad (5.3)$$

where the ℓ_j are nondegenerate but approach a common value, ℓ, as N becomes large. In this case, the propagator is given by

$$D_F(p^2) = \frac{i}{p^2 - m_\phi^2}\prod_{j=1}^{N-1}\left(1 - \frac{\ell_j^2 p^2}{N-1}\right)^{-1} , \qquad (5.4)$$

which has N first-order poles, representing a spectrum of particles with masses m_ϕ and $m_j \equiv \sqrt{N-1}/\ell_j$, for $j = 1 \ldots N-1$. In the past literature [113–116, 122], a convenient parameterization was chosen for how the m_j are decoupled as N becomes large, while the regulator scale ℓ is held fixed, namely

$$m_j^2 = \frac{N}{\ell^2}\frac{1}{1 - \frac{j}{2N^P}} , \qquad j = 1 \ldots N-1 \;\; , \;\; P > 1 . \qquad (5.5)$$

The results discussed in Refs. [113–116, 122] did not depend strongly on how the nonlocal limiting theory was approached. For any finite N, the propagator, Eq. (5.4), may be expressed via a partial fraction decomposition as a sum over simple poles with residues of alternating signs (a behavior that is expected in higher-derivative theories [56]). The poles with wrong-sign residues are Lee-Wick particles. Lee-Wick theories involving higher-

derivative terms that are of higher-order than those found in the LWSM have been considered before [45], including the identification of equivalent auxiliary field formulations (that is, with Lagrangians expressed in terms of additional fields but without higher-derivative terms). Auxiliary field formulations were also considered in the context of asymptotically nonlocal theories in Refs. [113–116, 122]; here, we work exclusively in the higher-derivative formulation of these theories.

The propagator in Eq. (5.4) can be expressed in terms of the masses m_j,

$$D_F(p^2) = \frac{i}{(p^2 - m_\phi^2) \prod_{j=1}^{N-1} (1 - p^2/m_j^2)} \ .$$

(5.6)

For Euclidean momentum, the product in the denominator of Eq. (5.6) approaches a growing exponential in the large N limit of Eq. (5.5). This regulates loop diagrams at the scale $\Lambda_{\rm nl}$, where $\Lambda_{\rm nl}^2$ is roughly a factor of N smaller than the square of the lightest Lee-Wick resonance mass m_1^2.

Asymptotically nonlocal theories represent a class of higher-derivative theories that are different from the simplest Lee-Wick theories and ghost-free nonlocal theories, which makes study of their properties and phenomenology well motivated. These theories may provide a different approach to considering unitarity in nonlocal theories [59, 60, 123–125], namely by applying approaches that are known to work in Lee-Wick theories of finite order [41, 51, 53, 54] and then taking the limit as N becomes large. Of greater relevance to the present work is that asymptotically nonlocal theories can be considered the ultraviolet completions of theories that appear nonlocal at low energies. Tree-level scattering processes at the Large Hadron Collider (LHC) exist in Minkowski space, where the exponential factor in Eq. (5.1) may produce unbounded growth in cross sections with center-of-mass energy. In asymptotically nonlocal theories, however, such growth is truncated due to the change in the theory at the scale of the first Lee-Wick resonance, m_1 [122]. In other words, if one were to integrate out all the heavy particles in an effective field theory approach, then the effective theory below the cutoff m_1 would look (approximately) like a ghost-free nonlocal

81

theory; the asymptotically nonlocal theory provides an ultraviolet completion.

From a phenomenological perspective, it is natural to seek a bound on the nonlocal scale Λ_{nl} [126]. While asymptotically nonlocal theories delay the appearance of new particles, the momentum dependence of scattering amplitudes is nonetheless affected by the same physics that accounts for the regulation of loop diagrams which, based on naturalness arguments, one would expect to be associated with the TeV scale. Since the LHC is currently the highest-energy collider available to probe new physics, it is natural to investigate how the relevant physics might be probed there, in one of the most common processes: the production of dijets. Hence, we will focus on computing the parton-level cross sections in an asymptotically nonlocal generalization of QCD that determine the proton-proton cross section for dijet production, in particular, the differential cross section with respect to the dijet invariant mass. The dijet invariant mass spectrum has been used in other contexts to bound new physics, for example, to determine a lower bound on the mass of colorons in Ref. [127]. The Feynman rules for asymptotically nonlocal QCD have not appeared in the literature (only scalar QCD was considered in Ref. [115]), so we first determine the rules relevant to two-into-two scattering in the next section. We then give our expressions for the parton-level cross sections $\hat{\sigma}$, which are significantly more complicated than what one obtains in QCD, and explain how gauge-fixing and the identification of asymptotic states works in our higher-derivative construction. The expressions for the various $\hat{\sigma}$ also have not appeared before in the literature and can be incorporated in detailed collider physics studies. While an exhaustive collider physics study is not the focus of the present work, we nevertheless use our theoretical results and data from the LHC to obtain a bound on the nonlocal scale from the dijet invariant mass spectrum. In the final section, we summarize our conclusions.

5.2 Asymptotically nonlocal QCD

An asymptotically nonlocal SU(N) gauge theory with complex scalar matter was presented in Ref. [115], where loop corrections to the scalar two-point function were studied given their relevance to the hierarchy problem. Here we are interested in a realistic SU(3) gauge theory with spin-1/2 fermions, namely QCD with color-triplet quarks, for phenomenological applications. Following the notation of Ref. [115], we define a covariant box operator $\Box \equiv D_\mu D^\mu$, with SU(3) covariant derivative $D_\mu = \partial_\mu - i g T^a A_\mu^a$ and

$$f(\Box) \equiv \prod_{j=1}^{N-1} \left(1 + a_j^2 \Box\right) \ , \tag{5.7}$$

where we define $a_j^2 \equiv \ell_j^2/(N-1)$. Eq. (5.7) is a gauge-covariant version of the higher-derivative product that appears in Eq. (5.3). We then define the asymptotically nonlocal extension of QCD by inserting $f(\Box)$ in the kinetic and mass terms, in analogy to Eq. (5.3),

$$\mathcal{L} = -\frac{1}{2}\text{Tr } F_{\mu\nu} f(\Box) F^{\mu\nu} + \frac{1}{2}\bar{q}\{(i\slashed{D} - m_q), f(\Box)\}q + \mathcal{L}_{\text{g.f.}} \ , \tag{5.8}$$

where $\mathcal{L}_{\text{g.f.}}$ represents gauge-fixing terms. Here, $F^{\mu\nu} \equiv F^{\mu\nu a}T^a$, and the flavor indices on the quark field have been suppressed. The braces in the first term represent an anti-commutator, defined by $\{X, Y\} \equiv XY + YX$, which is included to preserve the hermiticity of the Lagrangian. In the local limit, $f(\Box) \to 1$, one obtains the usual QCD Lagrangian. We assume a familiar form for the gauge-fixing term,

$$\mathcal{L}_{\text{g.f.}} = -\frac{1}{2\xi}(\partial^\mu A_\mu^a)^2 \ . \tag{5.9}$$

A nonlocal modification to the gauge-fixing term is unnecessary, as nothing physical depends on this choice; the form in Eq. (5.9) is convenient for implementing the usual Fadeev-Popov gauge fixing ansatz.

5.2.1 Feynman rules

The quark and gluon propagators follow from the purely quadratic terms in Eqs. (5.8) and (5.9). For the quark fields we find
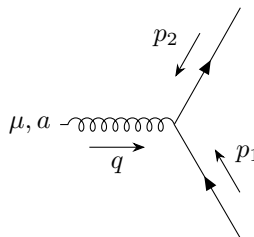
$$D(p) = \frac{i \left(\not{p} + m_q \right)}{(p^2 - m_q^2) f(-p^2)} \, ,$$

(5.10)

while for the gluons

$$D_{\mu\nu}^{ab}(p) = -\frac{i}{p^2 f(-p^2)} \left[\eta_{\mu\nu} - \frac{p_\mu p_\nu}{p^2} \left(1 - \xi f(-p^2) \right) \right] \delta^{ab} \, ,$$

(5.11)

where a and b are color indices. In the calculations that we present in Sec. 5.2.2, we will work in the nonlocal equivalent of Landau gauge, where $\xi = 0$, as this simplifies intermediate algebraic steps. We note that the factor of $f(-p^2)$ in the denominator of Eq. (5.11) becomes a growing exponential as a function of Euclidean momentum in the nonlocal limit, which accounts for the elimination of quadratic divergences in the theory of complex scalars discussed in Ref. [115].

To evaluate the two-into-two scattering processes of interest to us, we need the interaction vertices involving at least one gluon and no more than 4 lines of any type. It is straightforward, though somewhat tedious, to extract the interactions involving a specified number of gluon fields from the Lagrangian that involves the product of an arbitrary number of covariant box operators defined in Eq. (5.7). For vertices involving a quark line, one can have either one or two gluon lines. We find the Feynman rules
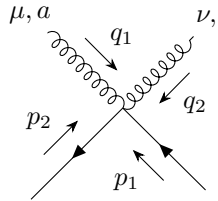

$$= i\, g\, T^a\, V_{1g}^\mu(p_1, p_2) \, ,$$

(5.12)

where

$$V_{1g}^{\mu}(p_1, p_2) \equiv \frac{1}{2}\left[f_1(p_1^2) + f_1(p_2^2)\right]\gamma^{\mu} - (p_1 - p_2)^{\mu}\left(\frac{\not{p}_1 - \not{p}_2}{2} - m_q\right)f_2(p_1^2, p_2^2) \ , \qquad (5.13)$$

and
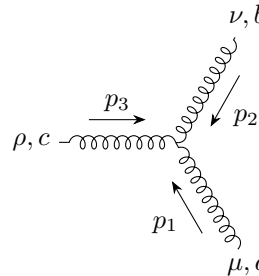
$$= -i\,g^2\,T^a T^b\,V_{2g}^{\mu\nu}(p_1, p_2, q_1, q_2) + \left[\{q_1, \mu, a\} \leftrightarrow \{q_2, \nu, b\}\right], \qquad (5.14)$$

where

$$V_{2g}^{\mu\nu}(p_1, p_2, q_1, q_2) \equiv \eta^{\mu\nu}\left(\frac{\not{p}_1 - \not{p}_2}{2} - m_q\right)f_2(p_2^2, p_1^2) + (q_1 + 2\,p_2)^{\mu}(q_2 + 2\,p_1)^{\nu}$$
$$\times \left(\frac{\not{p}_1 - \not{p}_2}{2} - m_q\right)f_3(p_2^2, (q_2 + p_1)^2, p_1^2) + \frac{1}{2}\gamma^{\mu}(q_2 + 2\,p_1)^{\nu}f_2((q_2 + p_1)^2, p_1^2)$$
$$- \frac{1}{2}(q_1 + 2\,p_2)^{\mu}\gamma^{\nu}f_2(p_2^2, (q_2 + p_1)^2) \ . \qquad (5.15)$$

The three- and four-gluon self-interactions are the same as those found in Ref. [115].
We provide these Feynman rules here for completeness:

$$= -g\,f^{abc}\,V_{3g}^{\mu\nu\rho}(p_1, p_2, p_3) + \text{ all permutations}, \qquad (5.16)$$

where

$$V_{3g}^{\mu\nu\rho}(p_1, p_2, p_3) \equiv \eta^{\mu\rho}p_1^{\nu}f_1(p_1^2) + \frac{1}{2}(p_1 - p_3)^{\nu}(p_1 \cdot p_3\,\eta^{\mu\rho} - p_1^{\rho}p_3^{\mu})\,f_2(p_1^2, p_3^2) \ . \qquad (5.17)$$

Here "all permutations" refers to the 3! ways we may permute the elements of the set $\{(p_1, \mu, a), (p_2, \nu, b), (p_3, \rho, c)\}$, which label the lines of the vertex. Finally,

$$= -ig^2 f^{abe} f^{cde} V_{4g}^{\mu\nu\rho\sigma}(p_1, p_2, p_3, p_4) + \text{ all permutations,} \qquad (5.18)$$

where

$$
\begin{aligned}
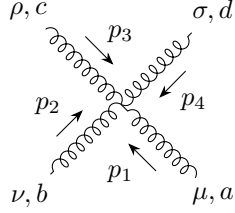V_{4g}^{\mu\nu\rho\sigma}(p_1, p_2, p_3, p_4) = {} & \frac{1}{4} \eta^{\mu\rho} \eta^{\nu\sigma} f_1\big((p_3 + p_4)^2\big) \quad - \quad \eta^{\nu\sigma} p_4^\mu (p_3 + 2\,p_4)^\rho f_2\big((p_1 + p_2)^2, p_4^2\big) \\
& - \frac{1}{2} \eta^{\nu\rho} (p_1 \cdot p_4\, \eta^{\mu\sigma} - p_1^\sigma p_4^\mu)\, f_2(p_1^2, p_4^2) \quad - \quad \frac{1}{2}(2\,p_1 + p_2)^\nu (p_3 + 2\,p_4)^\rho \\
& \times (p_1 \cdot p_4\, \eta^{\mu\sigma} - p_1^\sigma p_4^\mu) \quad f_3\big(p_1^2, (p_1 + p_2)^2, p_4^2\big) \quad .
\end{aligned}
\qquad (5.19)
$$

In these Feynman rules, we define the functions f_1, f_2 and f_3 as follows:

$$
f_1(p^2) \equiv \prod_{j=1}^{N-1} (1 - a_j^2 p^2) \,, \qquad (5.20)
$$

$$
f_2(p_1^2, p_2^2) \equiv \sum_{k=1}^{N-1} a_k^2 \left[\prod_{j=1}^{k-1} (1 - a_j^2 p_1^2) \right] \left[\prod_{j=k+1}^{N-1} (1 - a_j^2 p_2^2) \right] \,, \qquad (5.21)
$$

$$
f_3(p_1^2, p_2^2, p_3^2) \equiv \sum_{n=1}^{N-1} \sum_{k=n+1}^{N-1} a_n^2 a_k^2 \left[\prod_{j=1}^{n-1} (1 - a_j^2 p_1^2) \right] \left[\prod_{j=n+1}^{k-1} (1 - a_j^2 p_2^2) \right] \left[\prod_{j=k+1}^{N-1} (1 - a_j^2 p_3^2) \right] \,.
$$
$$\qquad (5.22)$$

As one might surmise, the functions f_2 and f_3 arise by extracting the one- and two-gluon parts of the product in Eq. (5.7), respectively. As noted in Ref. [115], these functions are totally symmetric under interchange of their arguments and approach the following

exponential forms in the large N limit:

$$\lim_{N\to\infty} f_1(p^2) = e^{-\ell^2 p^2} \, , \tag{5.23}$$

$$\lim_{N\to\infty} f_2(p_1^2, p_2^2) = \frac{e^{-\ell^2 p_1^2} - e^{-\ell^2 p_2^2}}{p_2^2 - p_1^2} \, , \tag{5.24}$$

$$\lim_{N\to\infty} f_3(p_1^2, p_2^2, p_3^2) = \frac{e^{-\ell^2 p_1^2}}{(p_2^2 - p_1^2)(p_3^2 - p_1^2)} + \frac{e^{-\ell^2 p_2^2}}{(p_1^2 - p_2^2)(p_3^2 - p_2^2)} + \frac{e^{-\ell^2 p_3^2}}{(p_1^2 - p_3^2)(p_2^2 - p_3^2)} \, . \tag{5.25}$$

In the limit that $\Lambda_{nl} \to \infty$, the $a_k \to 0$, so that $f_1(p^2) \to 1$, $f_2(p_1^2, p_2^2) \to 0$ and $f_3(p_1^2, p_2^2, p_3^2) \to 0$, independent of the arguments of these functions and the value of N. One thereby recovers the QCD Lagrangian in this limit.

5.2.2   Two-into-two parton-level cross sections

Following the notation of Ref. [128], the cross-section for a two-jet final state can be expressed as

$$\frac{d\sigma}{dy_1 dy_2 dp_\perp} = \frac{2\pi}{s} p_\perp \sum_{ij} \left[f_i^{(a)}(x_a, Q^2) f_j^{(b)}(x_b, Q^2) \, \hat{\sigma}_{ij}(\hat{s}, \hat{t}, \hat{u}) \right.$$
$$\left. + f_j^{(a)}(x_a, Q^2) f_i^{(b)}(x_b, Q^2) \, \hat{\sigma}_{ij}(\hat{s}, \hat{u}, \hat{t}) \right] / (1 + \delta_{ij}) \, , \tag{5.26}$$

where y_1 and y_2 are the jet rapidities, $p_\perp$ is the jet transverse momentum, the f_i are parton distribution functions, and s, t, and u are the Mandelstam variables with a hat indicating those of the parton-level process. We comment further on the kinematical variables that are relevant to our later analysis and on the arguments of the parton distribution functions in Sec. 5.3. Here, we simply note that Eq. (5.26) defines the parton-level cross sections $\hat{\sigma}_{ij}$, which have been known for some time in QCD but are modified in the asymptotically nonlocal theories we consider here. In this section and in an Appendix, we summarize the results we obtain for the $\hat{\sigma}$, which were computed using the Feynman rules of Sec. 5.2.1 via the FeynCalc package [86] in Mathematica.

Before proceeding to these results, we make a few technical comments. First, we note that a field in the higher-derivative theory is associated with a number of distinct particle states, while we are interested in diagrams where the external lines correspond to the lightest of these states. As described in Refs [113–116, 122], a higher-derivative field can be decomposed into a sum of quantum fields in an auxiliary field description where each exclusively creates or annihilates one type of particle. The coefficient of the component field that annihilates or creates the lightest state is determined by the wave function renormalization factor that one finds at the corresponding pole in the higher-derivative theory. For massless partons, the form of our Lagrangian assures that this factor is unity [since $f(0) = f_1(0) = 1$], so that the field in the higher-derivative theory creates or annihilates the lightest particle component without any numerical correction factor compared to a canonically normalized quantum field in a theory that has conventional mass and kinetic terms. Secondly, we mentioned earlier that we work in the higher-derivative generalization of Landau gauge, which implies that we must include ghosts if we sum over all possible polarization states of the external gluon lines. Alternately, we may omit the ghosts if we also omit the unphysical polarization states that the ghosts would cancel in the polarization sums. This can be accomplished using standard techniques involving an auxiliary vector (see, for example, Sec. 3 of Ref. [129]). This is the approach we follow and we have verified as a consistency check that our cross sections correctly reproduce all the expected QCD results in the limit that the scale of new physics is taken to be infinitely large.

For the case of quark-antiquark annihilation through s-channel gluon exchange, the cross section is given by

$$\hat{\sigma}_{q_i \bar{q}_i \to q_j \bar{q}_j} = \frac{4\,\alpha_s^2}{9\,\hat{s}} \frac{\hat{t}^2 + \hat{u}^2}{\hat{s}^2 f_1(\hat{s})^2} \;, \quad i \neq j, \tag{5.27}$$

where i and j are quark flavor indices. Here, and henceforth, we assume all partons are massless, and the final state jets include five light flavors, with the top quark excluded.

88

For t-channel scattering of different flavors of quark or antiquark, the cross section is

$$\hat{\sigma}_{q_i q_j \to q_i q_j} = \frac{4\,\alpha_s^2}{9\,\hat{s}} \frac{\hat{s}^2 + \hat{u}^2}{\hat{t}^2 f_1(\hat{t})^2} \,, \quad i \neq j. \tag{5.28}$$

For the special case of quark-antiquark scattering into quark-antiquark of the same flavor, there are both s- and t-channel contributions

$$\hat{\sigma}_{q_i \bar{q}_i \to q_i \bar{q}_i} = \frac{4\,\alpha_s^2}{9\,\hat{s}} \left(\frac{\hat{t}^2 + \hat{u}^2}{\hat{s}^2 f_1(\hat{s})^2} + \frac{\hat{s}^2 + \hat{u}^2}{\hat{t}^2 f_1(\hat{t})^2} - \frac{2\hat{u}^2}{3\hat{s}\hat{t} f_1(\hat{s}) f_1(\hat{t})} \right) \,, \tag{5.29}$$

and for the similar case of quark-quark scattering of a single flavor, there are t- and u-channel diagrams, leading to

$$\hat{\sigma}_{q_i q_i \to q_i q_i} = \frac{4\,\alpha_s^2}{9\,\hat{s}} \left(\frac{\hat{s}^2 + \hat{u}^2}{\hat{t}^2 f_1(\hat{t})^2} + \frac{\hat{s}^2 + \hat{t}^2}{\hat{u}^2 f_1(\hat{u})^2} - \frac{2\hat{s}^2}{3\hat{t}\hat{u} f_1(\hat{t}) f_1(\hat{u})} \right) \,. \tag{5.30}$$

While the modified form of the $\hat{\sigma}$ for processes exclusively involving quarks and/or antiquarks might be easy to intuit, those involving gluon external lines are much more complicated due to the modification of the Feynman rules in Eqs. (5.16)-(5.19). The cross section for a quark-antiquark pair scattering into two gluons may be expressed in the form

$$\hat{\sigma}_{q\bar{q} \to gg} = \frac{\alpha_s^2}{9\,\hat{s}} \sum_{i,j,k=0}^{4} f_2(0,0)^i f_2(\hat{t},0)^j f_2(\hat{u},0)^k F_{ijk}(\hat{s},\hat{t},\hat{u}) \,, \tag{5.31}$$

where the coefficients $F_{ijk}(\hat{s},\hat{t},\hat{u})$ are given in Appendix B.1. The function f_2 vanishes in the $\Lambda_{\mathrm{nl}} \to \infty$ limit, which implies that the QCD result lives entirely in the F_{000} part of Eq. (5.31) in the same limit. The parton-level cross sections $\hat{\sigma}_{gg \to q\bar{q}}$ and $\hat{\sigma}_{qg \to qg}$ can be obtained from Eq. (5.31) by means of crossing symmetry. This involves specific interchanges of Mandelstam variables, as well as adjustments in overall signs and spin/color factors, as discussed in standard textbooks [39]. We find

$$\hat{\sigma}_{gg \to q\bar{q}} = \frac{9}{64} \hat{\sigma}_{q\bar{q} \to gg}(\hat{t} \leftrightarrow \hat{u}) \,. \tag{5.32}$$

89

and

$$\hat{\sigma}_{qg \to qg} = \hat{\sigma}_{\bar{q}g \to \bar{q}g} = -\frac{3}{8}\,\hat{\sigma}_{q\bar{q} \to gg}(\hat{s} \leftrightarrow \hat{t}) \ , \tag{5.33}$$

Finally, the cross section for gluon-gluon scattering to two gluons may be written in the form

$$\hat{\sigma}_{gg \to gg} = \frac{\alpha_s^2}{\hat{s}} \sum_{i,j,k,\ell,m=0}^{4} f_2(0,0)^i f_2(\hat{t},0)^j f_2(\hat{u},0)^k f_3(0,\hat{t},0)^\ell f_3(0,\hat{u},0)^m F_{ijk\ell m}(\hat{s},\hat{t},\hat{u}) \ , \tag{5.34}$$

where the coefficients $F_{ijk\ell m}(\hat{s},\hat{t},\hat{u})$ are provided in Appendix B.2. Again, the QCD limit lives entirely in the term involving $F_{00000}(\hat{s},\hat{t},\hat{u})$.[2]

5.3   A bound from the dijet invariant mass spectrum

With the parton-level cross sections $\hat{\sigma}$ defined in the previous section, we may compute the cross section for $p\,p \to$ jet jet with the goal of determining a bound on the nonlocal scale $\Lambda_{\rm nl}$ using LHC data. We focus on the dijet invariant mass spectrum which is related to the $\hat{\sigma}$ via

$$\begin{aligned}
\frac{d\sigma}{d\mathcal{M}} =& \frac{\pi\,\mathcal{M}}{2\,s} \int_{-Y}^{Y} dy_1 \int_{y_{\rm min}}^{y_{\rm max}} dy_2 \ {\rm sech}^2 y_* \sum_{ij} \Big[f_i^{(a)}(x_a, Q^2) f_j^{(b)}(x_b, Q^2)\, \hat{\sigma}_{ij}(\hat{s},\hat{t},\hat{u}) \\
&+ f_j^{(a)}(x_a, Q^2) f_i^{(b)}(x_b, Q^2)\, \hat{\sigma}_{ij}(\hat{s},\hat{u},\hat{t}) \Big] \Big/ (1 + \delta_{ij}) \ .
\end{aligned} \tag{5.35}$$

Here $\mathcal{M}$ is the dijet invariant mass, the y_i are the jet rapidities in the proton-proton center of mass frame, with the boost-invariant quantity $y_* \equiv (y_1 - y_2)/2$. Since we treat the partons as massless, there is no distinction between rapidty and pseudorapidity, so we use these terms interchangeably. The parton distribution function for the $i^{\rm th}$ parton within hadron a, $f_i^{(a)}(x_a, Q^2)$, is a function of the parton momentum fraction x_a and the renormalization scale Q. The Mandelstam variables $\hat{s}$, $\hat{t}$ and $\hat{u}$, and the momentum

---

[2]A Mathematica file with all the $\hat{\sigma}$ used in our analysis is available upon request.

fractions x_a and x_b, are related to $\mathcal{M}$ and the integration variables by

$$\hat{s} = \mathcal{M}^2 \ , \tag{5.36}$$

$$\hat{t} = -\frac{1}{2}\mathcal{M}^2\left(1 - \tanh y_*\right) \ , \tag{5.37}$$

$$\hat{u} = -\frac{1}{2}\mathcal{M}^2\left(1 + \tanh y_*\right) \ , \tag{5.38}$$

$$x_a = \frac{\mathcal{M}}{\sqrt{s}}\,e^{\,y_{\mathrm{boost}}} \ , \tag{5.39}$$

$$x_b = \frac{\mathcal{M}}{\sqrt{s}}\,e^{-y_{\mathrm{boost}}} \ , \tag{5.40}$$

where $y_{\mathrm{boost}} \equiv (y_1 + y_2)/2$ and $\sqrt{s}$ is the proton-proton center-of-mass energy. The proton-proton cross section in Eq. (5.35) assumes a cut $Y > 0$ is placed on the jet rapidity, such that $|y_i| < Y$; this leads to the integration region shown with

$$y_{\mathrm{min}} = \max\left(-Y, \ln\tau - y_1\right) \ , \tag{5.41}$$

$$y_{\mathrm{max}} = \max\left(Y, -\ln\tau - y_1\right) \ , \tag{5.42}$$

where $\tau = \mathcal{M}^2/s$. Eqs. (5.41) and (5.42) follow from the allowed range of the momenta fractions x_a and x_b which must fall between 0 and 1. Note that Eqs. (5.35)-(5.42) are well established and can be found in the literature on hadron collider physics, for example, in Ref. [128].

We wish to compare the predictions of our scenario with data on the dijet invariant mass spectrum from the LHC. The dijet spectrum has been considered in searches for new, heavy resonances (see, for example, Refs [2,47,48]) providing us with experimental results that we can utilize to determine a bound in the present scenario. For definiteness, we use the results from the CMS experiment that are displayed in Fig. 5 of Ref. [47]. To match this data, we assume a rapidity cut of $Y = 2.5$; Ref. [47] places an additional cut on the difference between the pseudorapidities, translating to $|y_1 - y_2| < 1.1$, which we impose by including an appropriate Heaviside theta-function in the integrand of Eq. (5.35) that vanishes when
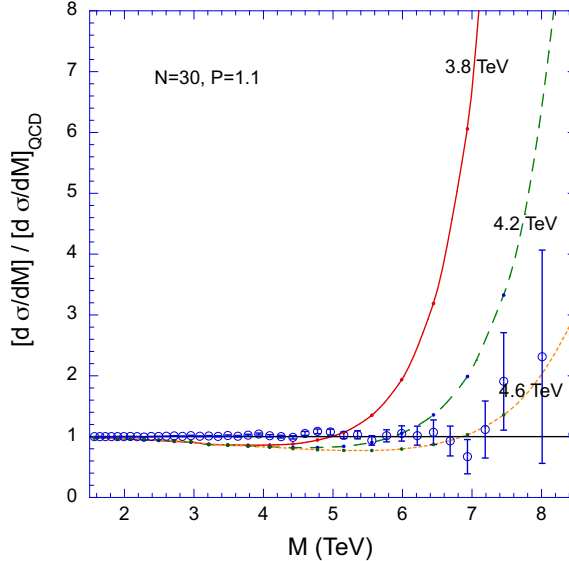
Figure 5.1: Ratio of the predicted dijet invariant mass spectrum to the Standard Model expectation, for $N = 30$, $P = 1.1$ and $\Lambda_{\mathrm{nl}} = 3.8$, 4.2 and 4.6 TeV. The open circles represent LHC data from Ref. [47], normalized by their prediction for the QCD background.

this constraint is not satisfied. To compare to this data set, we set the proton-proton center of mass energy $\sqrt{s} = 13$ TeV, and evaluate the dijet spectrum over the range 1.5 TeV$\leq$ $\mathcal{M} \leq 8.5$ TeV, with the renormalization scale Q set equal to the dijet invariant mass $\mathcal{M}$. Eq. (5.35) is evaluated numerically on Mathematica using the ManeParse package [130] which provides convenient access to parton distribution functions (pdfs) [131]. We used the nCTEQ15 pdfs for free protons in this computation. We normalize our theoretical prediction for a given nonlocal scale Λ_{nl} to the result that is obtained when the nonlocal scale is taken to infinity, *i.e.*, setting $f_1 = 1$ and $f_2 = f_3 = 0$, which gives the leading order QCD prediction. We compare this to the same ratio of data to QCD prediction given in Ref. [47]. The data and the prediction for the QCD backround are both shown in Fig. 5 of Ref. [47] and we take the ratio of those values for the points shown in Fig. 5.1 and 5.2.

As an example of typical results, we show in Fig. 5.1 the case where there are $N = 30$ poles, with $P = 1.1$ in the parameterization given by Eq. (5.5), for $\Lambda_{\mathrm{nl}} = 3.8$, 4.2 and 4.6 TeV. The theoretical predictions shown in the figures are computed at leading order, as no computation of next-to-leading-order (NLO) effects exists for the nonlocal theory.

We assume these effects are captured by 20% theoretical errors independent from point-to-point, which are comparable in size to NLO effects that have been studied in QCD (see, for example, Ref. [132]). To determine a bound, we compute a χ^2 that captures the agreement between the theoretical prediction and the data points, with total error for each data point in the χ^2 function determined by adding the experimental and the assumed theoretical errors in quadrature. We find for the case shown in Fig. 5.1 that

$$\Lambda_{\rm nl}^{30} > 4.2 \text{ TeV} \quad (95\% \text{ C.L.}), \tag{5.43}$$

where the superscript on $\Lambda_{\rm nl}$ denotes the number of poles N. Note that our bound is consistent with the discrepancy between the predicted and experimental results in the 3-7 TeV region when one takes into account our assumed theoretical uncertainties. We do not find that the bound differs appreciably as we vary N, since this parameter does not have to be very large before f_1, f_2 and f_3 approach their $N \to \infty$ limiting forms. We can compute the results in the nonlocal limit using those limiting forms, given in Eq. (5.23), which lead to Fig. 5.2. In this case, the same procedure for determining a bound on the nonlocal scale gives

$$\Lambda_{\rm nl}^{\infty} > 4.7 \text{ TeV} \quad (95\% \text{ C.L.}). \tag{5.44}$$

As a consistency check, we computed the same bound using the CTEQ 6.1 pdfs and found a qualitatively similar result, $\Lambda_{\rm nl}^{\infty} > 4.9$ TeV (95% C.L.). We note that the choices of $\Lambda_{\rm nl}$ for the curves displayed in Figs. 5.1 and 5.2 were selected to be near the bounds in Eqs. (5.43) and (5.44), respectively. We also note that the bound does not change dramatically when one increases $N = 30$ to $N = \infty$. Hence, we do not plot the dependence of the bound on N explicitly.

We view the results of this section at finite N as illustrative and similar in spirit to the analysis of the bounds on coloron models presented in Ref. [127]. Our results assume a particular parameterization of resonance masses, namely Eq. (5.5), but the value of the theoretical results presented in our earlier sections is that they can be applied to any
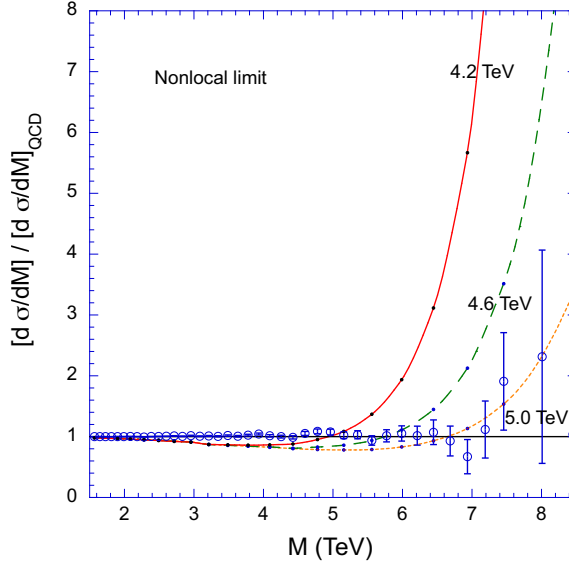
Figure 5.2: Ratio of the predicted dijet invariant mass spectrum to the Standard Model expectation, for the nonlocal limit $N \rightarrow \infty$, for $\Lambda_{nl} = 4.2$, 4.6 and 5.0 TeV. The open circles represent LHC data from Ref. [47].

desried parameterization leading to different forms for the functions f_1, f_2 and f_3; all should approach the same $N \rightarrow \infty$ limit. These general results can also be used in more detailed collider physics investigations, including realistic modeling of jets (for example, jet cone algorithms), detector acceptances and efficiencies, and studies of jet angular distributions. Those topics go beyond the scope of the present work, and may be better motivated after a calculation of NLO effects in the nonlocal theory are at hand.

5.4   Conclusions

In this chapter, we have built upon earlier work on asymptotically nonlocal field theories. These theories appear nonlocal at low energies but have sensible ultraviolet completions in terms of Lee-Wick theories that are finite order in derivatives. We focused on the strongly interacting sector [115], whose modification affects the physics of jets at the highest energy hadron colliders; our goal was to obtain preliminary bounds on the scale of new physics, Λ_{nl}, and provide the necessary tools for future collider analyses. We began by determining

the relevant Feynman rules for an asymptotically nonlocal SU(3) theory of fermions, since the past literature only considered a theory with complex scalar matter [115]. While the gluon self-interactions and the procedure for gauge-fixing to obtain the gluon propagator are the same as those given in Ref. [115], the one- and two-gluon vertices involving fermions were not previously available in the literature. With the complete set of Feynman rules in hand, we considered the most basic jet process, dijet production from two-into-two parton scattering. We found that the relevant parton-level cross sections are in some cases considerably more complicated than those in ordinary QCD (See, for example, Appendix B). Nevertheless, we checked that in the limit $\Lambda_{nl} \to \infty$, we precisely recover the QCD results we expect in the absence of new physics. We then computed the dijet invariant mass spectrum in proton-proton collisions at $\sqrt{s} = 13$ TeV, to compare the deviation from the QCD expectation at high dijet invariant mass with experimental data from the LHC. We found that in the exactly nonlocal limit (where the number of resonances N in the asymptotically nonlocal theory is taken to infinity), the scale of new physics was bounded by $\Lambda_{nl} > 4.7$ TeV at the 95% confidence level. For finite N, we obtain bounds that are similar in magnitude, but that depend in detail on the parameterization of the Lee-Wick mass spectrum. We presented one example with $N = 30$ where we found $\Lambda_{nl} > 4.2$ TeV (95% C.L.). These bounds are similar in magnitude to other collider bounds on nonlocal theories that have been discussed in the literature [126].

Our approach to obtaining a bound at leading order on the scale of new physics from the dijet invariant mass spectrum is similar in spirit to the bound on the coloron mass in Ref. [127]. More detailed leading-order studies might include modeling of jet hadronization, detector acceptances and efficiencies, and the effect of new physics on the angular dependence of jet cross sections. The theoretical results presented here make such studies feasible, but they go beyond the scope of the present work. A more accurate assessment of the bounds on the nonlocal scale would require the computation of next-to-leading-order (NLO) effects that are not known in the asymptotically nonlocal or nonlocal theories; these have been taken into account in our assumed theoretical error bars. A full NLO calcula-

tion in the present framework would no doubt be complicated, both diagramatically and algebraically; it may be sensible to defer such a task until some indication of a deviation from the QCD expectations is observed at high dijet invariant masses.

Chapter 6

Conclusions

In this dissertation, we have examined how the requirement that we have specific UV behavior can impact physics at collider energies (*i.e.* the TeV scale). In the case of asymptotic safety, requiring couplings to run to a UV fixed point constrains the parameter space at collider energies to live on the UV critical surface. In Chapter 2, we demonstrated the value of this constraint in a theory with gauged baryon number by including gravitational corrections above the Planck scale and finding when the UV fixed points of the theory are reached. By doing so, we were able to determine a relationship between the baryon number gauge coupling and a coupling related to the kinetic mixing between baryon number and hypercharge, which effectively removed one of the degrees of freedom. In Chapter 3, we considered an extension of the model in Chapter 2 with the baryon number gauge boson acting as a portal between dark and visible sectors. The dark sector includes a TeV-scale, fermionic dark matter candidate, and we used the constraints imposed on the gauge couplings by asymptotic safety to determine the dark matter relic density for various fixed point scenarios. We found our predictions for the relic density produced reproduced experimental observation for a range of dark matter masses (within $1-5$ TeV) in each of the fixed point scenarios.

In the case of asymptotic nonlocality, the desire to avoid large radiative corrections to the Higgs mass leads to a theory that regulates divergences at an emergent nonlocal scale.

The requirement that the nonlocal scale not be so large that it reintroduces fine-tuning tells us that observable effects are likely not far out of the reach of TeV-scale colliders. In Chapter 4, we studied the center-of-mass energy dependence of the propagator for Minkowski-space momentum, corresponding to scattering, and Euclidean momentum, corresponding to loops. In the case of the loops, we found the propagator fell off, approaching a decreasing exponential as the magnitude of the Euclidean momentum increased. This behavior is as expected if the theory is to offer a solution to the hierarchy problem. In the case of scattering, the cross section approached a growing exponential as the center-of-mass energy increased at low energies, but the growth was truncated once the LW resonances were reached and the cross section eventually fell off. In Chapter 5, we provided the tools necessary for a study of the collider phenomenology of an asymptotically nonlocal generalization of QCD. We determined the Feynman rules relevant for dijet production and calculated the parton-level cross sections for two-into-two scattering of quarks and gluons. We then determined an upper bound on the nonlocal scale from LHC data. We found that the nonlocal scale should be larger than ~ 5 TeV, comparable to existing bounds on new particles decaying to dijets [47].

Appendix A

Renormalization group equations at one loop

This appendix gives the one-loop β functions for the gauged baryon number model defined in Chapter 2.

Definition:

$$\beta(c) = \sum_{\ell=1}^{\infty} \frac{1}{(4\pi)^{2\ell}} \beta^{(\ell)}(c) \tag{A.1}$$

Gauge couplings:

$$\beta^{(1)}(g_1) = +\frac{77}{10} g_1^3 \,, \tag{A.2}$$

$$\beta^{(1)}(g_B) = +11 g_B^3 + \frac{77}{6} g_B \tilde{g}^2 - \frac{16}{3} g_B^2 \tilde{g} \,, \tag{A.3}$$

$$\beta^{(1)}(\tilde{g}) = -\frac{16}{5} g_1^2 g_B - \frac{16}{3} g_B \tilde{g}^2 + \frac{77}{5} g_1^2 \tilde{g} + 11 g_B^2 \tilde{g} + \frac{77}{6} \tilde{g}^3 \,, \tag{A.4}$$

$$\beta^{(1)}(g_2) = -\frac{7}{6} g_2^3 \,, \tag{A.5}$$

$$\beta^{(1)}(g_3) = -7 g_3^3 \,. \tag{A.6}$$

Yukawas ($\kappa^2 \equiv \kappa_1^2 + \kappa_2^2 + \kappa_3^2$, $y^2 \equiv 2y_1^2 + y_2^2 + y_3^2$):

$$\beta^{(1)}(y_t) = \left(\frac{9}{2}y_t^2 + \frac{3}{2}y_b^2 + 3\kappa^2 - \frac{17}{20}g_1^2 - \frac{9}{4}g_2^2 - 8g_3^2 - \frac{2}{3}g_B^2 - \frac{5}{3}g_B\tilde{g} - \frac{17}{12}\tilde{g}^2 \right) y_t \,, \quad \text{(A.7)}$$

$$\beta^{(1)}(y_b) = \left(\frac{3}{2}y_t^2 + \frac{9}{2}y_b^2 + 3\kappa^2 - \frac{1}{4}g_1^2 - \frac{9}{4}g_2^2 - 8g_3^2 - \frac{2}{3}g_B^2 + \frac{1}{3}g_B\tilde{g} - \frac{5}{12}\tilde{g}^2 \right) y_b \,, \quad \text{(A.8)}$$

$$\beta^{(1)}(y_1) = \left(3y^2 + y_1^2 + \frac{1}{2}\kappa_1^2 - \frac{9}{10}g_1^2 - \frac{9}{2}g_2^2 - 3g_B^2 + 3g_B\tilde{g} - \frac{3}{2}\tilde{g}^2 \right) y_1 \,, \quad \text{(A.9)}$$

$$\beta^{(1)}(y_2) = \left(3y^2 + y_2^2 + \kappa_2^2 - \frac{18}{5}g_1^2 - 3g_B^2 + 6g_B\tilde{g} - 6\tilde{g}^2 \right) y_2 \,, \quad \text{(A.10)}$$

$$\beta^{(1)}(y_3) = \left(3y^2 + y_3^2 + \kappa_3^2 - 3g_B^2 \right) y_3 \,, \quad \text{(A.11)}$$

$$\beta^{(1)}(\kappa_1) = \left(3y_t^2 + 3y_b^2 + \frac{1}{2}y_1^2 + \frac{9}{2}\kappa_1^2 + 3\kappa_2^2 + 3\kappa_3^2 - \frac{9}{4}g_1^2 - \frac{9}{4}g_2^2 - \frac{15}{4}\tilde{g}^2 \right) \kappa_1 \,, \quad \text{(A.12)}$$

$$\beta^{(1)}(\kappa_2) = \left(3y_t^2 + 3y_b^2 + \frac{1}{2}y_2^2 + 3\kappa_1^2 + \frac{9}{2}\kappa_2^2 + \frac{3}{2}\kappa_3^2 - \frac{9}{4}g_1^2 - \frac{9}{4}g_2^2 - \frac{15}{4}\tilde{g}^2 \right) \kappa_2 \,, \quad \text{(A.13)}$$

$$\beta^{(1)}(\kappa_3) = \left(3y_t^2 + 3y_b^2 + \frac{1}{2}y_3^2 + 3\kappa_1^2 + \frac{3}{2}\kappa_2^2 + \frac{9}{2}\kappa_3^2 - \frac{9}{20}g_1^2 - \frac{9}{4}g_2^2 - \frac{3}{4}\tilde{g}^2 \right) \kappa_3 \,. \quad \text{(A.14)}$$

Quartic couplings ($\kappa^2 \equiv \kappa_1^2 + \kappa_2^2 + \kappa_3^2$, $K^4 \equiv \kappa_1^4 + \kappa_2^4 + \kappa_3^4$, $y^2 \equiv 2y_1^2 + y_2^2 + y_3^2$, $Y^4 \equiv 2y_1^4 + y_2^4 + y_3^4$):

$$\begin{aligned}
\beta^{(1)}(\lambda) = \; & +12\lambda^2 + 2\lambda_m^2 - \frac{9}{5}g_1^2\lambda - 9g_2^2\lambda - 3\tilde{g}^2\lambda \\
& + \frac{27}{100}g_1^4 + \frac{9}{10}g_1^2 g_2^2 + \frac{9}{10}g_1^2\tilde{g}^2 + \frac{9}{4}g_2^4 + \frac{3}{2}g_2^2\tilde{g}^2 + \frac{3}{4}\tilde{g}^4 \\
& + 12\lambda \left(y_t^2 + y_b^2 + \kappa^2 \right) - 12 \left(y_t^4 + y_b^4 + K^4 \right) \,, \quad \text{(A.15)}
\end{aligned}$$

$$\beta^{(1)}(\lambda_\phi) = +10\lambda_\phi^2 + 4\lambda_m^2 - 12g_B^2\lambda_\phi + 12g_B^4 + 12\lambda_\phi y^2 - 12\,Y^4 \,, \quad \text{(A.16)}$$

$$\begin{aligned}
\beta^{(1)}(\lambda_m) = \; & \left[6\lambda + 4\lambda_\phi + 4\lambda_m - \frac{9}{10}g_1^2 - \frac{9}{2}g_2^2 - 6g_B^2 - \frac{3}{2}\tilde{g}^2 + 6(y_t^2 + y_b^2 + y^2 + \kappa^2) \right]\lambda_m \\
& + 3g_B^2\tilde{g}^2 - 12(\kappa_1^2 y_1^2 + \kappa_2^2 y_2^2 + \kappa_3^2 y_3^2) \,. \quad \text{(A.17)}
\end{aligned}$$

Appendix B

Cross section coefficient expressions

This appendix gives the two-into-two parton-level cross sections for scattering involving gluons on external lines in the model presented in Chapter 5.

B.1 $q\bar{q} \to gg$ scattering amplitude

The parton-level cross section $\hat{\sigma}_{q\bar{q} \to gg}$ was written in Sec. 5.2.2 in the form

$$\hat{\sigma}_{q\bar{q} \to gg} = \frac{\alpha_s^2}{9\,\hat{s}} \sum_{i,j,k=0}^{4} f_2(0,0)^i f_2(\hat{t},0)^j f_2(\hat{u},0)^k F_{ijk}(\hat{s},\hat{t},\hat{u}) \ . \tag{B.1}$$

The cross section $\hat{\sigma}_{gg \to q\bar{q}}$ and $\hat{\sigma}_{qg \to qg} = \hat{\sigma}_{\bar{q}g \to \bar{q}g}$ were then related to this result by crossing symmetry, in Eqs. (5.32) and (5.33), respectively. In this appendix, we present the functions $F_{ijk}(\hat{s},\hat{t},\hat{u})$. For each F_{ijk} that we display, there is another non-vanishing one, F_{ikj}, found by swapping the $\hat{t}$ and $\hat{u}$ variables:

$$F_{ikj}(\hat{s},\hat{t},\hat{u}) = F_{ijk}(\hat{s},\hat{u},\hat{t}) \ . \tag{B.2}$$

Any coefficients not listed below, or obtained from those shown by Eq. (B.2), are zero. We find:

$$F_{200}(\hat{s}, \hat{t}, \hat{u}) = \frac{12\hat{t}\hat{u}}{f_1(\hat{s})^2} \quad , \tag{B.3}$$

$$F_{022}(\hat{s}, \hat{t}, \hat{u}) = \frac{2\hat{t}^3\hat{u}^3}{3\hat{s}^2 f_1(\hat{t}) f_1(\hat{u})} \quad , \tag{B.4}$$

$$F_{040}(\hat{s}, \hat{t}, \hat{u}) = \frac{8\hat{t}^3\hat{u}^3}{3\hat{s}^2 f_1(\hat{t})^2} \quad , \tag{B.5}$$

$$F_{030}(\hat{s}, \hat{t}, \hat{u}) = -\frac{16\hat{t}^2\hat{u}^2(f_1(\hat{t})-1)(\hat{t}-\hat{u})}{3\hat{s}^2 f_1(\hat{t})^2} \quad , \tag{B.6}$$

$$F_{120}(\hat{s}, \hat{t}, \hat{u}) = \frac{6\hat{t}^2\hat{u}^2}{\hat{s} f_1(\hat{s}) f_1(\hat{t})} \quad , \tag{B.7}$$

$$F_{021}(\hat{s}, \hat{t}, \hat{u}) = \frac{2\hat{t}^2\hat{u}^2(f_1(\hat{u})-1)(\hat{t}-\hat{u})}{3\hat{s}^2 f_1(\hat{t}) f_1(\hat{u})} \quad , \tag{B.8}$$

$$F_{110}(\hat{s}, \hat{t}, \hat{u}) = -\frac{6\hat{t}\hat{u}(f_1(\hat{t})-1)(\hat{t}-\hat{u})}{\hat{s} f_1(\hat{s}) f_1(\hat{t})} \quad , \tag{B.9}$$

$$F_{011}(\hat{s}, \hat{t}, \hat{u}) = -\frac{\hat{t}\hat{u}(f_1(\hat{t}) - 1)(f_1(\hat{u}) - 1)(3\hat{t}^2 - 2\hat{t}\hat{u} + 3\hat{u}^2)}{3\hat{s}^2 f_1(\hat{t})f_1(\hat{u})} \quad , \tag{B.10}$$

$$F_{100}(\hat{s}, \hat{t}, \hat{u}) = -\frac{6\hat{t}\hat{u}}{\hat{s}f_1(\hat{s})} \left[f_1(\hat{t}) + f_1(\hat{u}) + \frac{1}{f_1(\hat{t})} + \frac{1}{f_1(\hat{u})} - \frac{8}{f_1(\hat{s})} + 4 \right] \quad , \tag{B.11}$$

$$F_{010}(\hat{s}, \hat{t}, \hat{u}) = \frac{1}{3\hat{s}^2} \left[8\hat{u}(2\hat{t}^2 - \hat{t}\hat{u} + \hat{u}^2) \left(f_1(\hat{t}) - \frac{1}{f_1(\hat{t})^2} \right) + \left(\frac{1}{f_1(\hat{t})} - 1 \right) \right.$$
$$\times \left[\hat{t}(\hat{t}^2 - \hat{t}\hat{u} + 2\hat{u}^2) \left(\frac{1}{f_1(\hat{u})} + f_1(\hat{u}) \right) + 2(\hat{t}^3 - 9\hat{t}^2\hat{u} + 6\hat{t}\hat{u}^2 - 4\hat{u}^3) \right. \tag{B.12}$$
$$\left. \left. + \frac{36\hat{t}\hat{u}(\hat{t} - \hat{u})}{f_1(\hat{s})} \right] \right] \quad ,$$

$$F_{020}(\hat{s}, \hat{t}, \hat{u}) = \frac{\hat{t}\hat{u}}{6\hat{s}^2} \left[8\left(3\hat{t}^2 - 5\hat{t}\hat{u} + 4\hat{u}^2\right) \left(1 + \frac{1}{f_1(\hat{t})^2} \right) + \frac{1}{f_1(\hat{t})} \right. \tag{B.13}$$
$$\left. \times \left[\hat{t}f_1(\hat{u})(\hat{t} - 3\hat{u}) \left(1 + \frac{1}{f_1(\hat{u})^2} \right) - 2(23\hat{t}^2 + 11\hat{t}\hat{u} + 16\hat{u}^2) + \frac{72\hat{t}\hat{u}}{f_1(\hat{s})} \right] \right] \quad ,$$

$$F_{000}(\hat{s}, \hat{t}, \hat{u}) = \frac{1}{6\hat{s}^2} \left[\frac{288\hat{t}\hat{u}\left(\frac{1}{f_1(\hat{s})} - 1\right)}{f_1(\hat{s})} - \frac{72\hat{t}\hat{u}\left(f_1(\hat{t}) + \frac{1}{f_1(\hat{t})} + f_1(\hat{u}) + \frac{1}{f_1(\hat{u})}\right)}{f_1(\hat{s})} \right.$$

$$+ \frac{4\hat{u}\left(f_1(\hat{t})^2 + \frac{1}{f_1(\hat{t})^2}\right)\left(3\hat{t}^2 + \hat{u}^2\right)}{\hat{t}} + \frac{4\hat{t}\left(f_1(\hat{u})^2 + \frac{1}{f_1(\hat{u})^2}\right)\left(\hat{t}^2 + 3\hat{u}^2\right)}{\hat{u}}$$

$$- \frac{2\left(f_1(\hat{t}) + \frac{1}{f_1(\hat{t})}\right)\left(\hat{t}^3 - 26\hat{t}^2\hat{u} + \hat{t}\hat{u}^2 - 8\hat{u}^3\right)}{\hat{t}} + \frac{2\left(f_1(\hat{u}) + \frac{1}{f_1(\hat{u})}\right)\left(8\hat{t}^3 - \hat{t}^2\hat{u} + 26\hat{t}\hat{u}^2 - \hat{u}^3\right)}{\hat{u}}$$

$$- (\hat{t} - \hat{u})^2 \left(f_1(\hat{t})f_1(\hat{u}) + \frac{f_1(\hat{t})}{f_1(\hat{u})} + \frac{1}{f_1(\hat{t})f_1(\hat{u})} + \frac{f_1(\hat{u})}{f_1(\hat{t})}\right)$$

$$\left. + \frac{4\left(6\hat{t}^4 - \hat{t}^3\hat{u} + 38\hat{t}^2\hat{u}^2 - \hat{t}\hat{u}^3 + 6\hat{u}^4\right)}{\hat{t}\hat{u}} \right] .$$

$$(\text{B.14})$$

B.2 $gg \to gg$ scattering cross section

The scattering cross section $\sigma_{gg\to gg}$ is complicated, but can be summarized via the following decomposition:

$$\hat{\sigma}_{gg\to gg} = \frac{\alpha_s^2}{\hat{s}} \sum_{i,j,k,\ell,m=0}^{4} f_2(0,0)^i f_2(\hat{t},0)^j f_2(\hat{u},0)^k f_3(0,\hat{t},0)^\ell f_3(0,\hat{u},0)^m F_{ijk\ell m}(\hat{s}, \hat{t}, \hat{u}) .$$

$$(\text{B.15})$$

We find that

$$F_{ikjm\ell}(\hat{s}, \hat{t}, \hat{u}) = F_{ijk\ell m}(\hat{s}, \hat{u}, \hat{t}) , \qquad (\text{B.16})$$

that is, there are non-vanishing functions F in addition to those shown below that are obtained by swapping both j and k and ℓ and m, and whose value is obtained from the result shown by swapping $\hat{t} \leftrightarrow \hat{u}$. All other other $F_{ijk\ell m}(\hat{s}, \hat{t}, \hat{u})$ are zero. We find:

$$F_{00020}(\hat{s},\hat{t},\hat{u}) = \frac{9\hat{t}^2\hat{u}^2(3\hat{t}^2 + 10\hat{t}\hat{u} + 10\hat{u}^2)}{4\hat{s}^2} \ , \tag{B.17}$$

$$F_{40000}(\hat{s},\hat{t},\hat{u}) = \frac{9}{256}\left[\frac{2\hat{s}^2}{f_1(\hat{s})^2}(\hat{t}-\hat{u})^2 + \frac{2\hat{t}^2}{f_1(\hat{t})^2}(\hat{t}+2\hat{u})^2 + \frac{2\hat{u}^2}{f_1(\hat{u})^2}(2\hat{t}+\hat{u})^2 \right.$$
$$- \frac{\hat{s}\hat{t}}{f_1(\hat{s})f_1(\hat{t})}(\hat{t}-\hat{u})(\hat{t}+2\hat{u}) + \frac{\hat{s}\hat{u}}{f_1(\hat{s})f_1(\hat{u})}(\hat{t}-\hat{u})(2\hat{t}+\hat{u}) \tag{B.18}$$
$$\left. + \frac{\hat{t}\hat{u}}{f_1(\hat{t})f_1(\hat{u})}(2\hat{t}+\hat{u})(\hat{t}+2\hat{u})\right] \ ,$$

$$F_{04000}(\hat{s},\hat{t},\hat{u}) = \frac{9\hat{t}^2\hat{u}^2(5\hat{t}^2 + 16\hat{t}\hat{u} + 16\hat{u}^2)}{8\hat{s}^2 f_1(\hat{t})^2} \ , \tag{B.19}$$

$$F_{13000}(\hat{s},\hat{t},\hat{u}) = -\frac{9\hat{t}^2\hat{u}^2(\hat{t}+2\hat{u})}{\hat{s}f_1(\hat{t})^2} \ , \tag{B.20}$$

$$F_{03000}(\hat{s},\hat{t},\hat{u}) = -\frac{9\hat{t}\hat{u}^2(\hat{t}^2 + 4\hat{t}\hat{u} + 8\hat{u}^2)}{2\hat{s}^2 f_1(\hat{t})^2} \ , \tag{B.21}$$

$$F_{11010}(\hat{s},\hat{t},\hat{u}) = \frac{9\hat{t}^2\hat{u}^2(\hat{t}+2\hat{u})}{\hat{s}f_1(\hat{t})} \ , \tag{B.22}$$

$$F_{10110}(\hat{s},\hat{t},\hat{u}) = \frac{9\hat{t}^2\hat{u}^2(2\hat{t}+5\hat{u})}{4\hat{s}f_1(\hat{u})} \ , \tag{B.23}$$

$$F_{10010}(\hat{s}, \hat{t}, \hat{u}) = -\frac{9\hat{t}\hat{u}}{8\hat{s}^2} \left[\frac{-2\hat{s}}{f_1(\hat{t})}(\hat{t} - 2\hat{u})(\hat{t} + 2\hat{u}) + \frac{\hat{s}}{f_1(\hat{u})}(2\hat{t}^2 + 3\hat{t}\hat{u} - 3\hat{u}^2) \right. \tag{B.24}$$

$$\left. + \frac{\hat{s}}{f_1(\hat{s})}(\hat{t} - \hat{u})(2\hat{t} + 3\hat{u}) + 2(3\hat{t}^3 + 6\hat{t}^2\hat{u} + 4\hat{t}\hat{u}^2 + 9\hat{u}^3) \right] \ ,$$

$$F_{01010}(\hat{s}, \hat{t}, \hat{u}) = -\frac{9\hat{t}\hat{u}^2 \left(\hat{t}f_1(\hat{t})(\hat{t} + 2\hat{u}) - \hat{t}^2 - 4\hat{t}\hat{u} - 8\hat{u}^2 \right)}{2\hat{s}^2 f_1(\hat{t})} \ , \tag{B.25}$$

$$F_{01001}(\hat{s}, \hat{t}, \hat{u}) = \frac{9\hat{t}\hat{u}^2 \left(\hat{s}\hat{t}f_1(\hat{t}) - \hat{t}^2 + 7\hat{t}\hat{u} + 4\hat{u}^2 \right)}{4\hat{s}^2 f_1(\hat{t})} \ , \tag{B.26}$$

$$F_{20010}(\hat{s}, \hat{t}, \hat{u}) = \frac{9\hat{t}\hat{u}}{32} \left(\frac{2\hat{t}(\hat{t} + 2\hat{u})^2}{\hat{s}f_1(\hat{t})} + \frac{\hat{u}(2\hat{t} + \hat{u})(\hat{t} + 3\hat{u})}{\hat{s}f_1(\hat{u})} - \frac{(\hat{t} - \hat{u})(2\hat{t} + 3\hat{u})}{f_1(\hat{s})} \right) \ , \tag{B.27}$$

$$F_{02010}(\hat{s}, \hat{t}, \hat{u}) = -\frac{9\hat{t}^2\hat{u}^2 \left(5\hat{t}^2 + 16\hat{t}\hat{u} + 16\hat{u}^2 \right)}{4\hat{s}^2 f_1(\hat{t})} \ , \tag{B.28}$$

$$F_{02001}(\hat{s}, \hat{t}, \hat{u}) = -\frac{9\hat{t}^2\hat{u}^2 \left(9\hat{t}^2 + 21\hat{t}\hat{u} + 8\hat{u}^2 \right)}{8\hat{s}^2 f_1(\hat{t})} \ , \tag{B.29}$$

$$F_{00011}(\hat{s}, \hat{t}, \hat{u}) = \frac{9\hat{t}^2\hat{u}^2 \left(5\hat{t}^2 + 12\hat{t}\hat{u} + 5\hat{u}^2 \right)}{4\hat{s}^2} \ , \tag{B.30}$$

106

$$F_{31000}(\hat{s},\hat{t},\hat{u}) = \frac{9\hat{t}\hat{u}}{32 f_1(\hat{t})}\left[-\frac{\hat{s}}{f_1(\hat{s})}(\hat{t}-\hat{u}) + \frac{4\hat{t}}{f_1(\hat{t})}(\hat{t}+2\hat{u}) + \frac{\hat{u}}{f_1(\hat{u})}(2\hat{t}+\hat{u})\right] \ , \qquad \text{(B.31)}$$

$$\begin{aligned}
F_{30000}(\hat{s},\hat{t},\hat{u}) = -\frac{9}{64}&\left[\frac{1}{\hat{s}}\left(\frac{\hat{t}}{f_1(\hat{t})}(\hat{t}+2\hat{u})(3\hat{t}^2+\hat{t}\hat{u}+6\hat{u}^2)\right.\right.\\
&\left.+\frac{\hat{u}}{f_1(\hat{u})}(2\hat{t}+\hat{u})(6\hat{t}^2+\hat{t}\hat{u}+3\hat{u}^2)\right) + \frac{(\hat{t}-\hat{u})}{f_1(\hat{s})}\left(\frac{\hat{t}}{f_1(\hat{t})}(\hat{t}+2\hat{u})\right.\\
&\left.-\frac{\hat{u}}{f_1(\hat{u})}(2\hat{t}+\hat{u})\right) + \frac{3\hat{s}\hat{t}\hat{u}}{f_1(\hat{t})f_1(\hat{u})} - \frac{4\hat{t}^2}{f_1(\hat{t})^2}(\hat{t}+2\hat{u}) - \frac{4\hat{u}^2}{f_1(\hat{u})^2}(2\hat{t}+\hat{u})\\
&\left.-\frac{\hat{s}(\hat{t}-\hat{u})}{f_1(\hat{s})}\left((\hat{t}-\hat{u})\left(3+\frac{4}{f_1(\hat{s})}\right) - \frac{\hat{t}}{f_1(\hat{t})} + \frac{\hat{u}}{f_1(\hat{u})}\right)\right] \ ,
\end{aligned} \qquad \text{(B.32)}$$

$$\begin{aligned}
F_{22000}(\hat{s},\hat{t},\hat{u}) = \frac{9\hat{t}\hat{u}}{64 f_1(\hat{t})}&\left[\frac{1}{f_1(\hat{s})}(\hat{t}-\hat{u})(3\hat{t}+4\hat{u}) - \frac{4\hat{t}}{\hat{s}f_1(\hat{t})}(\hat{t}^2+16\hat{t}\hat{u}+16\hat{u}^2)\right.\\
&\left.-\frac{\hat{u}}{\hat{s}f_1(\hat{u})}(2\hat{t}+\hat{u})(\hat{t}+4\hat{u})\right] \ ,
\end{aligned} \qquad \text{(B.33)}$$

$$F_{02200}(\hat{s},\hat{t},\hat{u}) = \frac{9\hat{t}^2\hat{u}^2(16\hat{t}^2+41\hat{t}\hat{u}+16\hat{u}^2)}{16\hat{s}^2 f_1(\hat{t})f_1(\hat{u})} \ , \qquad \text{(B.34)}$$

$$\begin{aligned}
F_{00010}(\hat{s},\hat{t},\hat{u}) = -\frac{9}{8\hat{s}^2}&\left[\frac{\hat{t}\hat{u}}{f_1(\hat{s})}(\hat{t}-\hat{u})(2\hat{t}+3\hat{u}) + \frac{2\hat{u}}{f_1(\hat{t})}(\hat{t}^3+2\hat{t}^2\hat{u}+4\hat{u}^3)\right.\\
&+\frac{\hat{t}}{f_1(\hat{u})}(2\hat{t}^3+2\hat{t}^2\hat{u}-\hat{t}\hat{u}^2+3\hat{u}^3) - \hat{t}\hat{u}^2(\hat{t}-\hat{u})f_1(\hat{s}) - 2\hat{t}^2\hat{u}(\hat{t}+2\hat{u})f_1(\hat{t})\\
&\left.+\hat{s}\hat{t}\hat{u}^2 f_1(\hat{u}) + 2\hat{t}\hat{u}(\hat{t}+2\hat{u})(3\hat{t}+4\hat{u})\right] \ ,
\end{aligned} \qquad \text{(B.35)}$$

$$F_{21100}(\hat{s}, \hat{t}, \hat{u}) = \frac{9\hat{t}^2\hat{u}^2}{2f_1(\hat{t})f_1(\hat{u})} \ , \tag{B.36}$$

$$F_{21000}(\hat{s}, \hat{t}, \hat{u}) = \frac{9\hat{u}}{32}\left[\frac{8\hat{t}^3 + 2\hat{t}^2\hat{u} - \hat{t}\hat{u}^2 + 2\hat{u}^3}{\hat{s}f_1(\hat{t})f_1(\hat{u})} - \frac{(\hat{t} - \hat{u})(5\hat{t} + 2\hat{u})}{f_1(\hat{s})f_1(\hat{t})} + \frac{\hat{t}(\hat{t} - \hat{u})}{f_1(\hat{s})}\right.$$
$$\left. - \frac{4\hat{t}(3\hat{t}^2 - 5\hat{t}\hat{u} + 6\hat{u}^2)}{\hat{s}f_1(\hat{t})} - \frac{4\hat{t}(5\hat{t}^2 + 2\hat{t}\hat{u} - 4\hat{u}^2)}{\hat{s}f_1(\hat{t})^2} - \frac{\hat{t}\hat{u}(2\hat{t} + \hat{u})}{\hat{s}f_1(\hat{u})}\right] \ , \tag{B.37}$$

$$F_{11200}(\hat{s}, \hat{t}, \hat{u}) = -\frac{9\hat{t}^2\hat{u}^2(8\hat{t} + 3\hat{u})}{8\hat{s}f_1(\hat{t})f_1(\hat{u})} \ , \tag{B.38}$$

$$F_{20000}(\hat{s}, \hat{t}, \hat{u}) = \frac{9}{64}\left[\frac{\hat{t}\hat{u}}{\hat{s}}\left((\hat{t} + 2\hat{u})\frac{f_1(\hat{u})}{f_1(\hat{t})} + (2\hat{t} + \hat{u})\frac{f_1(\hat{t})}{f_1(\hat{u})}\right) + \frac{4(\hat{t} - \hat{u})^2}{f_1(\hat{s})}\left(\frac{3}{f_1(\hat{s})} + 2\right)\right.$$
$$+ \frac{\hat{t} - \hat{u}}{f_1(\hat{s})}\left(\hat{u}f_1(\hat{u}) - \hat{t}f_1(\hat{t}) + \frac{2\hat{t}^3 - \hat{t}^2\hat{u} - 4\hat{t}\hat{u}^2 - 2\hat{u}^3}{\hat{s}\hat{t}f_1(\hat{t})} + \frac{2\hat{t}^3 + 4\hat{t}^2\hat{u} + \hat{t}\hat{u}^2 - 2\hat{u}^3}{\hat{s}\hat{u}f_1(\hat{u})}\right)$$
$$+ \frac{(\hat{t} - \hat{u})f_1(\hat{s})}{\hat{s}}\left(\frac{\hat{t}(\hat{t} + 2\hat{u})}{f_1(\hat{t})} - \frac{\hat{u}(2\hat{t} + \hat{u})}{f_1(\hat{u})}\right) + \frac{2\hat{t}^4 + 2\hat{t}^3\hat{u} + 21\hat{t}^2\hat{u}^2 + 2\hat{t}\hat{u}^3 + 2\hat{u}^4}{\hat{t}\hat{u}f_1(\hat{t})f_1(\hat{u})}$$
$$- \frac{4}{\hat{s}}\left(\frac{3\hat{t}^3 + 4\hat{t}^2\hat{u} + 4\hat{t}\hat{u}^2 + 4\hat{u}^3}{f_1(\hat{t})^2} + \frac{4\hat{t}^3 + 4\hat{t}^2\hat{u} + 4\hat{t}\hat{u}^2 + 3\hat{u}^3}{f_1(\hat{u})^2} + \frac{\hat{t}(3\hat{t}^2 + \hat{t}\hat{u} + 18\hat{u}^2)}{f_1(\hat{t})}\right.$$
$$\left.\left. + \frac{\hat{u}(18\hat{t}^2 + \hat{t}\hat{u} + 3\hat{u}^2)}{f_1(\hat{u})}\right) + \frac{4}{\hat{s}^2}\left(15\hat{t}^4 + 21\hat{t}^3\hat{u} + 44\hat{t}^2\hat{u}^2 + 21\hat{t}\hat{u}^3 + 15\hat{u}^4\right)\right] \ , \tag{B.39}$$

$$F_{12000}(\hat{s}, \hat{t}, \hat{u}) = \frac{9\hat{t}\hat{u}}{16\hat{s}^2 f_1(\hat{t})}\left[\frac{\hat{s}}{f_1(\hat{s})}(\hat{t} - \hat{u})(3\hat{t} + 4\hat{u}) - \frac{4\hat{s}}{f_1(\hat{t})}(\hat{t}^2 + 4\hat{t}\hat{u} - 8\hat{u}^2)\right. \tag{B.40}$$
$$\left. + \frac{s}{f_1(\hat{u})}(4\hat{t}^2 + 7\hat{t}\hat{u} - 4\hat{u}^2) + 9\hat{t}^3 + 13\hat{t}^2\hat{u} + 24\hat{u}^3\right] \ ,$$

$$F_{11100}(\hat{s}, \hat{t}, \hat{u}) = \frac{9\hat{t}\hat{u}}{4\hat{s}} \left[\frac{2}{f_1(\hat{t})f_1(\hat{u})}(2\hat{t}^2 - \hat{t}\hat{u} + 2\hat{u}^2) - \hat{t}\hat{u} \left(\frac{1}{f_1(\hat{t})} + \frac{1}{f_1(\hat{u})} \right) \right] \ , \qquad \text{(B.41)}$$

$$F_{02100}(\hat{s}, \hat{t}, \hat{u}) = \frac{9\hat{t}^3\hat{u}(\hat{u}f_1(\hat{u}) - 10\hat{t} - 19\hat{u})}{8\hat{s}^2 f_1(\hat{t})f_1(\hat{u})} \ , \qquad \text{(B.42)}$$

$$\begin{aligned} F_{11000}(\hat{s}, \hat{t}, \hat{u}) = \frac{9}{8\hat{s}^2} \bigg[& \frac{2\hat{s}^2\hat{u}(\hat{t} - \hat{u})}{f_1(\hat{s})f_1(\hat{t})} - \frac{2\hat{s}(\hat{t}^3 - \hat{t}^2\hat{u} + 3\hat{t}\hat{u}^2 - \hat{u}^3)}{f_1(\hat{t})f_1(\hat{u})} + \frac{\hat{s}\hat{t}\hat{u}(\hat{t} - \hat{u})}{f_1(\hat{s})} \\ & - \frac{4\hat{s}\hat{u}(2\hat{t}^2 - \hat{t}\hat{u} + 2\hat{u}^2)}{f_1(\hat{t})^2} - \frac{\hat{u}(\hat{t}^3 + 11\hat{t}^2\hat{u} - 6\hat{t}\hat{u}^2 + 12\hat{u}^3)}{f_1(\hat{t})} - \frac{\hat{s}\hat{t}\hat{u}^2}{f_1(\hat{u})} \\ & + \frac{\hat{s}\hat{t}\hat{u}}{f_1(\hat{t})} \left((\hat{t} - \hat{u})f_1(\hat{s}) + \hat{u}f_1(\hat{u}) \right) + \hat{t}\hat{u}(3\hat{t}^2 + 5\hat{t}\hat{u} + 6\hat{u}^2) \bigg] \ , \end{aligned} \qquad \text{(B.43)}$$

$$\begin{aligned} F_{01100}(\hat{s}, \hat{t}, \hat{u}) = \frac{9\hat{t}\hat{u}}{4\hat{s}^2} \bigg[& \frac{1}{f_1(\hat{t})f_1(\hat{u})}(2\hat{t}^2 + 13\hat{t}\hat{u} + 2\hat{u}^2) + \frac{\hat{t}}{f_1(\hat{u})}(2\hat{t} + \hat{u}) \\ & + \frac{\hat{u}}{f_1(\hat{t})}(\hat{t} + 2\hat{u}) + \hat{t}\hat{u} \bigg] \ , \end{aligned} \qquad \text{(B.44)}$$

$$\begin{aligned} F_{02000}(\hat{s}, \hat{t}, \hat{u}) = \frac{9}{16\hat{s}^2} \bigg[& \frac{\hat{t}\hat{u}(\hat{t} - \hat{u})(3\hat{t} + 4\hat{u})}{f_1(\hat{s})f_1(\hat{t})} + \frac{\hat{t}(6\hat{t}^3 + 8\hat{t}^2\hat{u} - 3\hat{t}\hat{u}^2 + 4\hat{u}^3)}{f_1(\hat{t})f_1(\hat{u})} \\ & - \frac{\hat{t}^2\hat{u}^2 f_1(\hat{u})}{f_1(\hat{t})} + \frac{4\hat{u}(\hat{t}^3 + 8\hat{t}^2\hat{u} + 8\hat{t}\hat{u}^2 + 16\hat{u}^3)}{f_1(\hat{t})^2} + \frac{\hat{t}^2\hat{u}(\hat{t} - \hat{u})f_1(\hat{s})}{f_1(\hat{t})} \\ & + \frac{4\hat{t}\hat{u}(\hat{t} + 2\hat{u})(3\hat{t} + 4\hat{u})}{f_1(\hat{t})} + 8\hat{t}^2\hat{u}^2 \bigg] \ , \end{aligned} \qquad \text{(B.45)}$$

$$F_{10000}(\hat{s}, \hat{t}, \hat{u}) = -\frac{9}{16\hat{s}^2}\left[\hat{s}(\hat{t}-\hat{u})^2\left(3f_1(\hat{s}) + \frac{1}{f_1(\hat{s})}\right) + \hat{t}f_1(\hat{t})(3\hat{t}^2 + 5\hat{t}\hat{u} + 6\hat{u}^2)\right.$$

$$+\hat{u}f_1(\hat{u})(6\hat{t}^2 + 5\hat{t}\hat{u} + 3\hat{u}^2) + 12\hat{s}(\hat{t}^2 + \hat{t}\hat{u} + \hat{u}^2) + \frac{2\hat{s}^2(\hat{t}-\hat{u})}{f_1(\hat{s})}\left(\frac{\hat{u}}{\hat{t}f_1(\hat{t})} - \frac{\hat{t}}{\hat{u}f_1(\hat{u})}\right)$$

$$-4\hat{s}\left(\frac{(\hat{t}-\hat{u})^2}{f_1(\hat{s})^2} - \frac{\hat{t}^2 + 2\hat{u}^2}{f_1(\hat{t})^2} - \frac{2\hat{t}^2 + \hat{u}^2}{f_1(\hat{u})^2}\right) - \hat{s}(\hat{t}-\hat{u})\left(\frac{\hat{t}f_1(\hat{s})}{f_1(\hat{t})} - \frac{\hat{t}f_1(\hat{t})}{f_1(\hat{s})} - \frac{\hat{u}f_1(\hat{s})}{f_1(\hat{u})}\right. \quad \text{(B.46)}$$

$$\left.+\frac{\hat{u}f_1(\hat{u})}{f_1(\hat{s})}\right) - \hat{s}\hat{t}\hat{u}\left(\frac{f_1(\hat{t})}{f_1(\hat{u})} + \frac{f_1(\hat{u})}{f_1(\hat{t})}\right) + \frac{2\hat{s}(\hat{t}^4 + 5\hat{t}^2\hat{u}^2 + \hat{u}^4)}{\hat{t}\hat{u}f_1(\hat{t})f_1(\hat{u})} - \frac{1}{\hat{t}f_1(\hat{t})}(3\hat{t}^4 + 3\hat{t}^3\hat{u}$$

$$\left.+24\hat{t}^2\hat{u}^2 + 8\hat{t}\hat{u}^3 + 12\hat{u}^4) - \frac{1}{\hat{u}f_1(\hat{u})}(12\hat{t}^4 + 8\hat{t}^3\hat{u} + 24\hat{t}^2\hat{u}^2 + 3\hat{t}\hat{u}^3 + 3\hat{u}^4)\right] \quad ,$$

$$F_{01000}(\hat{s}, \hat{t}, \hat{u}) = -\frac{9}{8\hat{s}^2}\left[\hat{t}\hat{u}(\hat{t}-\hat{u})\left(f_1(\hat{s}) - \frac{1}{f_1(\hat{s})}\right) + \hat{t}\hat{u}^2\left(f_1(\hat{u}) - \frac{1}{f_1(\hat{u})}\right)\right.$$

$$+4\hat{t}^2\hat{u}f_1(\hat{t}) + \frac{2\hat{t}^3}{f_1(\hat{u})} + \frac{\hat{u}}{f_1(\hat{s})f_1(\hat{t})}(\hat{t}-\hat{u})(\hat{t}+2\hat{u}) \quad \text{(B.47)}$$

$$+\frac{1}{f_1(\hat{t})f_1(\hat{u})}(2\hat{t}^3 + 8\hat{t}^2\hat{u} - \hat{t}\hat{u}^2 + 2\hat{u}^3) - \frac{4\hat{u}}{\hat{t}f_1(\hat{t})^2}(\hat{t}^3 - 2\hat{t}^2\hat{u} - 2\hat{t}\hat{u}^2 - 4\hat{u}^3)$$

$$\left.+\frac{\hat{u}}{f_1(\hat{t})}\left(f_1(\hat{s})(\hat{t}-\hat{u})(3\hat{t}+2\hat{u}) + \hat{u}f_1(\hat{u})(\hat{t}+2\hat{u}) + 4(\hat{t}+2\hat{u})(2\hat{t}+3\hat{u})\right)\right] \quad ,$$

$$
\begin{aligned}
F_{00000}(\hat{s}, \hat{t}, \hat{u}) = -\frac{9}{16\hat{s}^2} & \left[\frac{(\hat{t} - \hat{u})}{f_1(\hat{s})} \left(\hat{t} f_1(\hat{t}) - \hat{u} f_1(\hat{u}) + 4(\hat{t} - \hat{u}) - \frac{2(\hat{t} - \hat{u})}{f_1(\hat{s})} \right. \right. \\
& \left. - \frac{\hat{t}^2 + 2\hat{t}\hat{u} + \hat{u}^2}{\hat{t} f_1(\hat{t})} + \frac{2\hat{t}^2 + 2\hat{t}\hat{u} + \hat{u}^2}{\hat{u} f_1(\hat{u})} \right) - 20 \left(\hat{t}^2 + \hat{t}\hat{u} + \hat{u}^2 \right) \\
& + \frac{1}{\hat{t} f_1(\hat{t})} \left[(\hat{t} - \hat{u})(\hat{t}^2 - 2\hat{t}\hat{u} - 2\hat{u}^2) f_1(\hat{s}) + \hat{u}(\hat{t}^2 - 2\hat{u}^2) f_1(\hat{u}) - 4\hat{u}(\hat{t} + 2\hat{u})^2 \right] \\
& + \frac{1}{\hat{u} f_1(\hat{u})} \left[(\hat{t} - \hat{u})(2\hat{t}^2 + 2\hat{t}\hat{u} - \hat{u}^2) f_1(\hat{s}) - \hat{t}(2\hat{t}^2 - \hat{u}^2) f_1(\hat{t}) - 4\hat{t}(2\hat{t} + \hat{u})^2 \right] \quad \text{(B.48)} \\
& - \frac{2}{\hat{t}^2 f_1(\hat{t})^2} \left(\hat{t}^4 + 4\hat{t}^2\hat{u}^2 + 4\hat{t}\hat{u}^3 + 4\hat{u}^4 \right) - \frac{2}{\hat{u}^2 f_1(\hat{u})^2} \left(4\hat{t}^4 + 4\hat{t}^3\hat{u} + 4\hat{t}^2\hat{u}^2 + \hat{u}^4 \right) \\
& - (\hat{t} - \hat{u}) f_1(\hat{s}) \left((\hat{t} - \hat{u})(2f_1(\hat{s}) - 4) + \hat{t} f_1(\hat{t}) - \hat{u} f_1(\hat{u}) \right) - \hat{t}\hat{u} f_1(\hat{t}) f_1(\hat{u}) \\
& \left. - 2 \left(\hat{t}^2 f_1(\hat{t})^2 + \hat{u}^2 f_1(\hat{u})^2 \right) - \frac{1}{\hat{t}\hat{u} f_1(\hat{t}) f_1(\hat{u})} \left(2\hat{t}^4 + 4\hat{t}^3\hat{u} + 13\hat{t}^2\hat{u}^2 + 4\hat{t}\hat{u}^3 + 2\hat{u}^4 \right) \right] .
\end{aligned}
$$

...

References

[1] J. G. Lee, E. G. Adelberger, T. S. Cook, S. M. Fleischer, and B. R. Heckel, "New Test of the Gravitational $1/r^2$ Law at Separations down to 52 μm," *Phys. Rev. Lett.* **124** no. 10, (2020) 101101, `arXiv:2002.11761 [hep-ex]`.

[2] **ATLAS** Collaboration, M. Aaboud *et al.*, "Search for low-mass dijet resonances using trigger-level jets with the ATLAS detector in pp collisions at $\sqrt{s} = 13$ TeV," *Phys. Rev. Lett.* **121** no. 8, (2018) 081801, `arXiv:1804.03496 [hep-ex]`.

[3] M. Gell-mann, *The Eightfold Way*. CRC Press, 2000.

[4] G. Zweig, "An SU(3) model for strong interaction symmetry and its breaking. Version 2," in *Developments in the Quark Theory of Hadrons. Vol. 1. 1964 - 1978*, D. B. Lichtenberg and S. P. Rosen, eds., pp. 22–101. 2, 1964.

[5] D. Goldberg, *The Standard Model in a Nutshell*. Princeton University Press, 2, 2017.

[6] A. Salam, "Weak and Electromagnetic Interactions," *Conf. Proc. C* **680519** (1968) 367–377.

[7] P. W. Higgs, "Broken Symmetries and the Masses of Gauge Bosons," *Phys. Rev. Lett.* **13** (1964) 508–509.

[8] F. Englert and R. Brout, "Broken Symmetry and the Mass of Gauge Vector Mesons," *Phys. Rev. Lett.* **13** (1964) 321–323.

[9] H. Georgi, H. R. Quinn, and S. Weinberg, "Hierarchy of Interactions in Unified Gauge Theories," *Phys. Rev. Lett.* **33** (1974) 451–454.

[10] **Particle Data Group** Collaboration, S. Navas *et al.*, "The review of particle physics," 2024. To be published.

[11] P. Nath and P. Fileviez Perez, "Proton stability in grand unified theories, in strings and in branes," *Phys. Rept.* **441** (2007) 191–317, `arXiv:hep-ph/0601023`.

[12] C. Kounnas, A. Masiero, D. V. Nanopoulos, and K. A. Olive, *Grand Unification With and Without Supersymmetry and Cosmological Implications*. 1985.

[13] **WMAP** Collaboration, G. Hinshaw *et al.*, "Nine-Year Wilkinson Microwave Anisotropy Probe (WMAP) Observations: Cosmological Parameter Results," *Astrophys. J. Suppl.* **208** (2013) 19, `arXiv:1212.5226 [astro-ph.CO]`.

[14] S. Mukhi, "String theory: a perspective over the last 25 years," *Class. Quant. Grav.* **28** (2011) 153001, `arXiv:1110.2569 [physics.pop-ph]`.

[15] A. Ashtekar and E. Bianchi, "A short review of loop quantum gravity," *Rept. Prog. Phys.* **84** no. 4, (2021) 042001, `arXiv:2104.04394 [gr-qc]`.

[16] D. F. Litim, "Renormalisation group and the Planck scale," *Phil. Trans. Roy. Soc. Lond. A* **369** (2011) 2759–2778, `arXiv:1102.4624 [hep-th]`.

[17] L. Modesto, "Super-renormalizable Quantum Gravity," *Phys. Rev. D* **86** (2012) 044005, `arXiv:1107.2403 [hep-th]`.

[18] S. Talaganis, T. Biswas, and A. Mazumdar, "Towards understanding the ultraviolet behavior of quantum loops in infinite-derivative theories of gravity," *Class. Quant. Grav.* **32** no. 21, (2015) 215017, `arXiv:1412.3467 [hep-th]`.

[19] S. Weinberg, "Ultraviolet divergences in quantum theories of gravitation," in *General Relativity: An Einstein centenary survey*, S. W. Hawking and W. Israel, eds., pp. 790–831. Cambridge University Press, 1979.

[20] S. E. Rugh and H. Zinkernagel, "The Quantum vacuum and the cosmological constant problem," *Stud. Hist. Phil. Sci. B* **33** (2002) 663–705, `arXiv:hep-th/0012253`.

[21] R. D. Peccei, "The Strong CP problem and axions," *Lect. Notes Phys.* **741** (2008) 3–17, `arXiv:hep-ph/0607268`.

[22] M. Schmaltz, "Physics beyond the standard model (theory): Introducing the little Higgs," *Nucl. Phys. B Proc. Suppl.* **117** (2003) 40–49, `arXiv:hep-ph/0210415`.

[23] S. P. Martin, "A Supersymmetry primer," *Adv. Ser. Direct. High Energy Phys.* **18** (1998) 1–98, `arXiv:hep-ph/9709356`.

[24] H. E. Haber and L. Stephenson Haskins, "Supersymmetric Theory and Models," in *Theoretical Advanced Study Institute in Elementary Particle Physics: Anticipating the Next Discoveries in Particle Physics*, pp. 355–499. WSP, 2018. `arXiv:1712.05926 [hep-ph]`.

[25] N. Arkani-Hamed, A. G. Cohen, E. Katz, and A. E. Nelson, "The Littlest Higgs," *JHEP* **07** (2002) 034, `arXiv:hep-ph/0206021`.

[26] M. Schmaltz and D. Tucker-Smith, "Little Higgs review," *Ann. Rev. Nucl. Part. Sci.* **55** (2005) 229–270, `arXiv:hep-ph/0502182`.

[27] L. Sartore and I. Schienbein, "PyR@TE 3," *Comput. Phys. Commun.* **261** (2021) 107819, `arXiv:2007.12700 [hep-ph]`.

[28] D. J. Gross and F. Wilczek, "Ultraviolet Behavior of Nonabelian Gauge Theories," *Phys. Rev. Lett.* **30** (1973) 1343–1346.

[29] H. D. Politzer, "Reliable Perturbative Results for Strong Interactions?," *Phys. Rev. Lett.* **30** (1973) 1346–1349.

[30] D. J. Gross, "The discovery of asymptotic freedom and the emergence of QCD," *Proc. Nat. Acad. Sci.* **102** (2005) 9099–9108.

[31] M. Reuter, "Nonperturbative evolution equation for quantum gravity," *Phys. Rev. D* **57** (1998) 971–985, `arXiv:hep-th/9605030`.

[32] D. J. Toms, "Quantum gravitational contributions to quantum electrodynamics," *Nature* **468** (2010) 56–59, `arXiv:1010.0793 [hep-th]`.

[33] U. Harst and M. Reuter, "QED coupled to QEG," *JHEP* **05** (2011) 119, `arXiv:1101.6007 [hep-th]`.

[34] N. Christiansen and A. Eichhorn, "An asymptotically safe solution to the U(1) triviality problem," *Phys. Lett. B* **770** (2017) 154–160, `arXiv:1702.07724 [hep-th]`.

[35] A. Eichhorn and F. Versteegen, "Upper bound on the Abelian gauge coupling from asymptotic safety," *JHEP* **01** (2018) 030, `arXiv:1709.07252 [hep-th]`.

[36] M. Reichert and J. Smirnov, "Dark Matter meets Quantum Gravity," *Phys. Rev. D* **101** no. 6, (2020) 063015, `arXiv:1911.00012 [hep-ph]`.

[37] K. Kowalska and E. M. Sessolo, "Minimal models for g-2 and dark matter confront asymptotic safety," *Phys. Rev. D* **103** no. 11, (2021) 115032, `arXiv:2012.15200 [hep-ph]`.

[38] Z.-W. Wang, F. S. Sage, T. G. Steele, and R. B. Mann, "Asymptotic Safety in the Conformal Hidden Sector?," *J. Phys. G* **45** no. 9, (2018) 095002, `arXiv:1511.02531 [hep-ph]`.

[39] M. E. Peskin and D. V. Schroeder, *An Introduction to quantum field theory.* CRC Press, 1995.

[40] W. Pauli and F. Villars, "On the Invariant regularization in relativistic quantum theory," *Rev. Mod. Phys.* **21** (1949) 434–444.

[41] T. D. Lee and G. C. Wick, "Negative metric and the unitarity of the s-matrix," *Nuclear Physics B9* (1969) .

[42] T. D. Lee and G. C. Wick, "Finite theory of quantum electrodynamics," *Physical Review D* (1970) .

[43] B. Grinstein, D. O'Connell, and M. B. Wise, "The Lee-Wick standard model," *Phys. Rev. D* **77** (2008) 025012, `arXiv:0704.1845 [hep-ph]`.

[44] C. D. Carone and R. F. Lebed, "Minimal Lee-Wick Extension of the Standard Model," *Phys. Lett. B* **668** (2008) 221–225, `arXiv:0806.4555 [hep-ph]`.

[45] C. D. Carone and R. F. Lebed, "A Higher-Derivative Lee-Wick Standard Model," *JHEP* **01** (2009) 043, `arXiv:0811.4150 [hep-ph]`.

[46] T. G. Rizzo, "Searching for Lee-Wick gauge bosons at the LHC," *JHEP* **06** (2007) 070, `arXiv:0704.3458 [hep-ph]`.

[47] **CMS** Collaboration, A. M. Sirunyan *et al.*, "Search for high mass dijet resonances with a new background prediction method in proton-proton collisions at $\sqrt{s} = 13$ TeV," *JHEP* **05** (2020) 033, `arXiv:1911.03947 [hep-ex]`.

[48] **CMS** Collaboration, A. M. Sirunyan *et al.*, "Search for narrow and broad dijet resonances in proton-proton collisions at $\sqrt{s} = 13$ TeV and constraints on dark matter mediators and other new particles," *JHEP* **08** (2018) 130, `arXiv:1806.00843 [hep-ex]`.

[49] **ATLAS** Collaboration, "ATLAS SUSY Searches - 95% CL Lower Limits." 2023.

[50] **ATLAS** Collaboration, "ATLAS Heavy Particle Searches - 95% CL Upper Exclusion Limits." 2023.

[51] R. Cutkosky, P. Landshoff, D. Olive, and J. Polkinghorne, "A non-analytic s-matrix," *Nuclear Physics B* **12** no. 2, (1969) 281–300.

[52] B. Grinstein, D. O'Connell, and M. B. Wise, "Causality as an emergent macroscopic phenomenon: The lee-wick $o(n)$ model," *Phys. Rev. D* **79** (May, 2009) 105019.

[53] D. Anselmi and M. Piva, "A new formulation of Lee-Wick quantum field theory," *JHEP* **06** (2017) 066, `arXiv:1703.04584 [hep-th]`.

[54] D. Anselmi and M. Piva, "Perturbative unitarity of Lee-Wick quantum field theory," *Phys. Rev. D* **96** no. 4, (2017) 045009, `arXiv:1703.05563 [hep-th]`.

[55] D. Anselmi, "Fakeons And Lee-Wick Models," *JHEP* **02** (2018) 141, `arXiv:1801.00915 [hep-th]`.

[56] A. Pais and G. E. Uhlenbeck, "On field theories with non-localized action," *Physical Review* (1950) .

[57] T. Biswas, E. Gerwick, T. Koivisto, and A. Mazumdar, "Towards singularity and ghost free theories of gravity," *Phys. Rev. Lett.* **108** (2012) 031101, `arXiv:1110.5249 [gr-qc]`.

[58] J. Boos, *Effects of Non-locality in Gravity and Quantum Theory.* PhD thesis, Alberta U., 2020. `arXiv:2009.10856 [gr-qc]`.

[59] F. Briscese and L. Modesto, "Non-unitarity of minkowskian non-local quantum field theories," *The European Physical Journal C* **81** no. 8, (Aug., 2021) .

[60] C. D. Carone, "Unitarity and microscopic acausality in a nonlocal theory," *Phys. Rev. D* **95** no. 4, (2017) 045009, `arXiv:1605.02030 [hep-th]`.

[61] J. Berges, N. Tetradis, and C. Wetterich, "Nonperturbative renormalization flow in quantum field theory and statistical physics," *Phys. Rept.* **363** (2002) 223–386, `arXiv:hep-ph/0005122`.

[62] M. Niedermaier and M. Reuter, "The Asymptotic Safety Scenario in Quantum Gravity," *Living Rev. Rel.* **9** (2006) 5–173.

[63] R. Percacci, "A Short introduction to asymptotic safety," in *Time and Matter*, pp. 123–142. 10, 2011. `arXiv:1110.6389 [hep-th]`.

[64] G. Hiller, C. Hormigos-Feliu, D. F. Litim, and T. Steudtner, "Anomalous magnetic moments from asymptotic safety," *Phys. Rev. D* **102** no. 7, (2020) 071901, `arXiv:1910.14062 [hep-ph]`.

[65] G. Domènech, M. Goodsell, and C. Wetterich, "Neutrino masses, vacuum stability and quantum gravity prediction for the mass of the top quark," *JHEP* **01** (2021) 180, `arXiv:2008.04310 [hep-ph]`.

[66] F. Grabowski, J. H. Kwapisz, and K. A. Meissner, "Asymptotic safety and Conformal Standard Model," *Phys. Rev. D* **99** no. 11, (2019) 115029, `arXiv:1810.08461 [hep-ph]`.

[67] J. H. Kwapisz, "Asymptotic safety, the Higgs boson mass, and beyond the standard model physics," *Phys. Rev. D* **100** no. 11, (2019) 115001, `arXiv:1907.12521 [hep-ph]`.

[68] G. Hiller, C. Hormigos-Feliu, D. F. Litim, and T. Steudtner, "Model Building from Asymptotic Safety with Higgs and Flavor Portals," *Phys. Rev. D* **102** no. 9, (2020) 095023, `arXiv:2008.08606 [hep-ph]`.

[69] R. Bause, G. Hiller, T. Höhne, D. F. Litim, and T. Steudtner, "B-anomalies from flavorful U(1)′ extensions, safely," *Eur. Phys. J. C* **82** no. 1, (2022) 42, `arXiv:2109.06201 [hep-ph]`.

[70] C. D. Carone and H. Murayama, "Possible light U(1) gauge boson coupled to baryon number," *Phys. Rev. Lett.* **74** (1995) 3122–3125, `arXiv:hep-ph/9411256`.

[71] C. D. Carone and H. Murayama, "Realistic models with a light U(1) gauge boson coupled to baryon number," *Phys. Rev. D* **52** (1995) 484–493, `arXiv:hep-ph/9501220`.

[72] P. Fileviez Perez and M. B. Wise, "Baryon and lepton number as local gauge symmetries," *Phys. Rev. D* **82** (2010) 011901, `arXiv:1002.1754 [hep-ph]`. [Erratum: Phys.Rev.D 82, 079901 (2010)].

[73] M. Duerr, P. Fileviez Perez, and M. B. Wise, "Gauge Theory for Baryon and Lepton Numbers with Leptoquarks," *Phys. Rev. Lett.* **110** (2013) 231801, `arXiv:1304.0576 [hep-ph]`.

[74] M. Duerr and P. Fileviez Perez, "Baryonic Dark Matter," *Phys. Lett. B* **732** (2014) 101–104, `arXiv:1309.3970 [hep-ph]`.

[75] P. Fileviez Perez, S. Ohmer, and H. H. Patel, "Minimal Theory for Lepto-Baryons," *Phys. Lett. B* **735** (2014) 283–287, `arXiv:1403.8029 [hep-ph]`.

[76] P. Fileviez Pérez, E. Golias, R.-H. Li, C. Murgui, and A. D. Plascencia, "Anomaly-free dark matter models," *Phys. Rev. D* **100** no. 1, (2019) 015017, `arXiv:1904.01017 [hep-ph]`.

[77] P. Fileviez Perez and A. D. Plascencia, "Theory of Dirac dark matter: Higgs boson decays and EDMs," *Phys. Rev. D* **105** no. 9, (2022) 095021, `arXiv:2112.02103 [hep-ph]`.

[78] **Particle Data Group** Collaboration, P. A. Zyla *et al.*, "Review of Particle Physics," *PTEP* **2020** no. 8, (2020) 083C01.

[79] A. Eichhorn and A. Held, "Viability of quantum-gravity induced ultraviolet completions for matter," *Phys. Rev. D* **96** no. 8, (2017) 086025, `arXiv:1705.02342 [gr-qc]`.

[80] G. M. Pelaggi, A. D. Plascencia, A. Salvio, F. Sannino, J. Smirnov, and A. Strumia, "Asymptotically Safe Standard Model Extensions?," *Phys. Rev. D* **97** no. 9, (2018) 095013, `arXiv:1708.00437 [hep-ph]`.

[81] C. Poole and A. E. Thomsen, "Constraints on 3- and 4-loop β-functions in a general four-dimensional Quantum Field Theory," *JHEP* **09** (2019) 055, `arXiv:1906.04625 [hep-th]`.

[82] S. Folkerts, D. F. Litim, and J. M. Pawlowski, "Asymptotic freedom of Yang-Mills theory with gravity," *Phys. Lett. B* **709** (2012) 234–241, `arXiv:1101.5552 [hep-th]`.

[83] N. Christiansen, D. F. Litim, J. M. Pawlowski, and M. Reichert, "Asymptotic safety of gravity with matter," *Phys. Rev. D* **97** no. 10, (2018) 106012, `arXiv:1710.04669 [hep-th]`.

[84] O. Lebedev, "On Stability of the Electroweak Vacuum and the Higgs Portal," *Eur. Phys. J. C* **72** (2012) 2058, `arXiv:1203.0156 [hep-ph]`.

[85] B. A. Dobrescu and F. Yu, "Dijet and electroweak limits on a Z' boson coupled to quarks," *Phys. Rev. D* **109** no. 3, (2024) 035004, `arXiv:2112.05392 [hep-ph]`.

[86] V. Shtabovenko, R. Mertig, and F. Orellana, "FeynCalc 10: Do multiloop integrals dream of computer codes?," `arXiv:2312.14089 [hep-ph]`.

[87] A. Hook, E. Izaguirre, and J. G. Wacker, "Model Independent Bounds on Kinetic Mixing," *Adv. High Energy Phys.* **2011** (2011) 859762, `arXiv:1006.0973` `[hep-ph]`.

[88] J. Boos, C. D. Carone, N. L. Donald, and M. R. Musser, "Asymptotic safety and gauged baryon number," *Phys. Rev. D* **106** no. 3, (2022) 035015, `arXiv:2206.02686` `[hep-ph]`.

[89] Y. Hamada, K. Tsumura, and M. Yamada, "Scalegenesis and fermionic dark matters in the flatland scenario," *Eur. Phys. J. C* **80** no. 5, (2020) 368, `arXiv:2002.03666` `[hep-ph]`.

[90] K. Kowalska, S. Pramanick, and E. M. Sessolo, "Naturally small Yukawa couplings from trans-Planckian asymptotic safety," *JHEP* **08** (2022) 262, `arXiv:2204.00866` `[hep-ph]`.

[91] K. Kowalska, E. M. Sessolo, and Y. Yamamoto, "Flavor anomalies from asymptotically safe gravity," *Eur. Phys. J. C* **81** no. 4, (2021) 272, `arXiv:2007.03567` `[hep-ph]`.

[92] A. Chikkaballi, W. Kotlarski, K. Kowalska, D. Rizzo, and E. M. Sessolo, "Constraints on Z' solutions to the flavor anomalies with trans-Planckian asymptotic safety," *JHEP* **01** (2023) 164, `arXiv:2209.07971` `[hep-ph]`.

[93] A. D. Bond, G. Hiller, K. Kowalska, and D. F. Litim, "Directions for model building from asymptotic safety," *JHEP* **08** (2017) 004, `arXiv:1702.01727` `[hep-ph]`.

[94] D. Barducci, M. Fabbrichesi, C. M. Nieto, R. Percacci, and V. Skrinjar, "In search of a UV completion of the standard model — 378,000 models that don't work," *JHEP* **11** (2018) 057, `arXiv:1807.05584` `[hep-ph]`.

[95] A. D. Bond and D. F. Litim, "Theorems for Asymptotic Safety of Gauge Theories," *Eur. Phys. J. C* **77** no. 6, (2017) 429, `arXiv:1608.00519` `[hep-th]`. [Erratum: Eur.Phys.J.C 77, 525 (2017)].

[96] A. D. Bond and D. F. Litim, "Price of Asymptotic Safety," *Phys. Rev. Lett.* **122** no. 21, (2019) 211601, `arXiv:1801.08527` `[hep-th]`.

[97] P. Gondolo and G. Gelmini, "Cosmic abundances of stable particles: Improved analysis," *Nucl. Phys. B* **360** (1991) 145–179.

[98] R. Mann, J. Meffe, F. Sannino, T. Steele, Z.-W. Wang, and C. Zhang, "Asymptotically Safe Standard Model via Vectorlike Fermions," *Phys. Rev. Lett.* **119** no. 26, (2017) 261802, `arXiv:1707.02942` `[hep-ph]`.

[99] O. Antipin, N. A. Dondi, F. Sannino, A. E. Thomsen, and Z.-W. Wang, "Gauge-Yukawa theories: Beta functions at large N_f," *Phys. Rev. D* **98** no. 1, (2018) 016003, `arXiv:1803.09770` `[hep-ph]`.

[100] E. Molinaro, F. Sannino, and Z. W. Wang, "Asymptotically safe Pati-Salam theory," *Phys. Rev. D* **98** no. 11, (2018) 115007, `arXiv:1807.03669 [hep-ph]`.

[101] T. Alanne, S. Blasi, and N. A. Dondi, "Critical Look at β -Function Singularities at Large N," *Phys. Rev. Lett.* **123** no. 13, (2019) 131602, `arXiv:1905.08709 [hep-th]`.

[102] **Particle Data Group** Collaboration, R. L. Workman *et al.*, "Review of Particle Physics," *PTEP* **2022** (2022) 083C01.

[103] P. Agrawal, Z. Chacko, C. Kilic, and R. K. Mishra, "A Classification of Dark Matter Candidates with Primarily Spin-Dependent Interactions with Matter," `arXiv:1003.1912 [hep-ph]`.

[104] J. M. Cline, G. Dupuis, Z. Liu, and W. Xue, "The windows for kinetically mixed Z'-mediated dark matter and the galactic center gamma ray excess," *JHEP* **08** (2014) 131, `arXiv:1405.7691 [hep-ph]`.

[105] T. Lin, "Dark matter models and direct detection," *PoS* **333** (2019) 009, `arXiv:1904.07915 [hep-ph]`.

[106] **PandaX-II** Collaboration, X. Cui *et al.*, "Dark Matter Results From 54-Ton-Day Exposure of PandaX-II Experiment," *Phys. Rev. Lett.* **119** no. 18, (2017) 181302, `arXiv:1708.06917 [astro-ph.CO]`.

[107] **DARWIN** Collaboration, J. Aalbers *et al.*, "DARWIN: towards the ultimate dark matter detector," *JCAP* **11** (2016) 017, `arXiv:1606.07001 [astro-ph.IM]`.

[108] **XENON** Collaboration, E. Aprile *et al.*, "Dark Matter Search Results from a One Ton-Year Exposure of XENON1T," *Phys. Rev. Lett.* **121** no. 11, (2018) 111302, `arXiv:1805.12562 [astro-ph.CO]`.

[109] E. T. Tomboulis, "Superrenormalizable gauge and gravitational theories," `arXiv:hep-th/9702146`.

[110] A. Ghoshal, A. Mazumdar, N. Okada, and D. Villalba, "Stability of infinite derivative Abelian Higgs models," *Phys. Rev. D* **97** no. 7, (2018) 076011, `arXiv:1709.09222 [hep-th]`.

[111] L. Buoninfante, G. Lambiase, and A. Mazumdar, "Ghost-free infinite derivative quantum field theory," *Nucl. Phys. B* **944** (2019) 114646, `arXiv:1805.03559 [hep-th]`.

[112] A. Ghoshal, A. Mazumdar, N. Okada, and D. Villalba, "Nonlocal non-Abelian gauge theory: Conformal invariance and β-function," *Phys. Rev. D* **104** no. 1, (2021) 015003, `arXiv:2010.15919 [hep-ph]`.

[113] J. Boos and C. D. Carone, "Asymptotic nonlocality," *Phys. Rev. D* **104** no. 1, (2021) 015028, `arXiv:2104.11195 [hep-th]`.

[114] J. Boos and C. D. Carone, "Asymptotic nonlocality in gauge theories," *Phys. Rev. D* **104** no. 9, (2021) 095020, `arXiv:2109.06261 [hep-th]`.

[115] J. Boos and C. D. Carone, "Asymptotic nonlocality in non-Abelian gauge theories," *Phys. Rev. D* **105** no. 3, (2022) 035034, `arXiv:2112.05270 [hep-ph]`.

[116] J. Boos and C. D. Carone, "Asymptotically nonlocal gravity," *JHEP* **06** (2023) 017, `arXiv:2212.00861 [hep-th]`.

[117] G. Dvali, "Black Holes and Large N Species Solution to the Hierarchy Problem," *Fortsch. Phys.* **58** (2010) 528–536, `arXiv:0706.2050 [hep-th]`.

[118] L. Buoninfante, A. Ghoshal, G. Lambiase, and A. Mazumdar, "Transmutation of nonlocal scale in infinite derivative field theories," *Phys. Rev. D* **99** no. 4, (2019) 044032, `arXiv:1812.01441 [hep-th]`.

[119] G. V. Efimov, "Non-local quantum theory of the scalar field," *Commun. Math. Phys.* **5** no. 1, (1967) 42–56.

[120] N. V. Krasnikov, "Nonlocal gauge theories," *Theor. Math. Phys.* **73** (1987) 1184–1190.

[121] Y. V. Kuz'min, "Convergent nonlocal gravity," *Sov. J. Nucl. Phys.* **50** no. 6, (1989) .

[122] C. D. Carone and M. R. Musser, "Note on scattering in asymptotically nonlocal theories," *Phys. Rev. D* **108** no. 9, (2023) 095015, `arXiv:2308.11051 [hep-th]`.

[123] A. S. Koshelev and A. Tokareva, "Unitarity of Minkowski nonlocal theories made explicit," *Phys. Rev. D* **104** no. 2, (2021) 025016, `arXiv:2103.01945 [hep-th]`.

[124] F. Briscese and L. Modesto, "Cutkosky rules and perturbative unitarity in Euclidean nonlocal quantum field theories," *Phys. Rev. D* **99** no. 10, (2019) 104043, `arXiv:1803.08827 [gr-qc]`.

[125] R. Pius and A. Sen, "Cutkosky rules for superstring field theory," *JHEP* **10** (2016) 024, `arXiv:1604.01783 [hep-th]`. [Erratum: JHEP 09, 122 (2018)].

[126] T. Biswas and N. Okada, "Towards LHC physics with nonlocal Standard Model," *Nucl. Phys. B* **898** (2015) 113–131, `arXiv:1407.3331 [hep-ph]`.

[127] I. Bertram and E. H. Simmons, "Dijet mass spectrum limits on flavor universal colorons," *Phys. Lett. B* **443** (1998) 347–351, `arXiv:hep-ph/9809472`.

[128] E. Eichten, I. Hinchliffe, K. D. Lane, and C. Quigg, "Super Collider Physics," *Rev. Mod. Phys.* **56** (1984) 579–707. [Addendum: Rev.Mod.Phys. 58, 1065–1073 (1986)].

[129] C. Schwinn, "Modern methods of quantum chromodynamics," https://www.tep.physik.uni-freiburg.de/lectures/archive/QCD-WS-14/qcd, 2015. Lecture notes.

[130] D. B. Clark, E. Godat, and F. I. Olness, "ManeParse : A Mathematica reader for Parton Distribution Functions," *Comput. Phys. Commun.* **216** (2017) 126–137, `arXiv:1605.08012 [hep-ph]`.

[131] K. Kovarik *et al.*, "nCTEQ15 - Global analysis of nuclear parton distributions with uncertainties in the CTEQ framework," *Phys. Rev. D* **93** no. 8, (2016) 085037, `arXiv:1509.00792 [hep-ph]`.

[132] R. Frederix, S. Frixione, V. Hirschi, D. Pagani, H.-S. Shao, and M. Zaro, "The complete NLO corrections to dijet hadroproduction," *JHEP* **04** (2017) 076, `arXiv:1612.06548 [hep-ph]`.